Final Report

Hybrid Resistojet Development

Contract NAS 5-21080

AVSD-0083-71-RR

Prepared by

Avco Corporation
Systems Division
Lowell Industrial Park
Lowell, Massachusetts 01851

Prepared for

National Aeronautics & Space Administration
Goddard Space Flight Center
Greenbelt, Maryland 20771

Final Report

Hybrid Resistojet Development

Contract NAS 5-21080

AVSD-0083-71-RR

Prepared by

Avco Corporation
Systems Division
Lowell Industrial Park
Lowell, Massachusetts 01851

Prepared for

National Aeronautics & Space Administration
Goddard Space Flight Center
Greenbelt, Maryland 20771

Table of Contents

List of Figures

List of Figures
(concl'd)

List of Figures
(concl'd.)

List of Figures
(concl'd.)

List of Tables

Nomenclature

$\bar{a}$	Sonic velocity, ft/sec
A	Area, ft^2
A_N	Nozzle area, ft^2
C_h	Stanton number
C_p	Heat capacity, Btu/lb ^oR
C^*	Characteristic velocity, ft/sec
C_F	Thrust coefficient
D	Diameter, ft
E	Activation energy, Btu/lb mole
F	Thrust, lb_f
ΔH_f	Heat of formation, Btu/lb mole
ΔH_v	Heat of vaporization, Btu/lb mole
H	Enthalpy Btu/lb
I_{sp}	Specific impulse, sec
h	Heat transfer coefficient, Btu/ft^2-sec-^oR
k	Thermal conductivity, Btu/ft^2-sec-(^oR/ft)
K	First order rate constant, sec^{-1}
K_c	Heterogeneous rate constant
K_h	Homogeneous rate constant
L	Length, ft
L^*	Characteristic length, ft
m	Flow rate, lb/sec
M	Molecular weight, lb/lb mole
Nu	Nusselt number

Nomenclature
(concl'd)

P	Pressure, lb_f/ft^2
Pr	Prandtl number
q	Heat flux, Btu/ft^2-sec
Q	Volumetric heat release rate, Btu/ft^3-sec
r	Radius, ft
R	Gas constant, lb_f-ft/lb mole-^oR
S_u	Burning velocity, ft/sec
t	Time, seconds
T	Temperature, ^oR
V	Volume, ft^3
w	Weight, fraction
x	Axial distance, ft
X	Ammonia dissociation fraction
y	Reacted fraction
α	Thermal diffusivity, ft^2/sec
γ	Specific heat ratio
ϵ	Area ratio
ρ	Density, lb_m/ft^3
χ	Mole fraction
$[Z]$	Concentration of specie Z, $mole/ft^3$

Subscripts

af	Adiabatic flame
b	Boiling point
g	Gas
i	Inlet
l	Liquid
o	Outlet
N	Nozzle

FOREWORD

This is the final report submitted on Contract NAS5-2108 entitled, "Hybrid (Hydrazine) Resistojet Development " The program originated in the Auxiliary Propulsion Branch of the NASA/Goddard Space Flight Center. Mr. Robert A. Callens was the Technical Officer for the NASA/Goddard Space Flight Center. The Project Director at Avco Corporation was Mr. T. K. Pugmire. Other participants in the program were W. Davis, T. O'Connor, R. Olson, and R Shaw

I Summary

This report discusses work performed under NASA Contract NAS5-21080, "Hybrid (Hydrazine) Resistojet Development " The experimental evaluation of several hydrazine thrusters which were ignited by electrical heaters within the thrust chamber indicated that high specific impulse (~240 sec.) could be achieved during steady state operation without power addition, except for that required for ignition purposes Restart capability was demonstrated with the various thrusters investigated

Pulsed operation of preprototype thrusters indicated that the specific impulse obtained for pulses on the order of 1 sec duration decreased much more rapidly than that observed with nominal 5 lb_f catalytic hydrazine thrusters. A limited amount of experimental data for pulse widths of less than 0.1 sec , however, demonstrated that performance comparable to that of catalytic engines can be achieved at duty cycles greater than one percent.

II Conclusions

The experimental data gathered during this study indicate the feasibility of developing a hydrazine thruster in which propellant decomposition is initiated by thermal energy stored within the thruster components or by an electrical heater which would be employed in the initial start-up of the unit Specific impulses well in excess of 200 sec can easily be obtained over a wide range of thrust levels Experimental evidence demonstrates that this type of performance can be achieved even at a thrust level of 5-10 millipounds simply by reduction of heat losses from the thruster

Operation of a hydrazine resistojet thruster at specific impulses on the order of 75 percent of steady state values can be achieved for short pulses The length of the pulse for which this type of performance can be achieved is governed by the ease with which energy can be transferred from thruster components to the propellant

III Analysis

Hydrazine is an unstable chemical compound as is demonstrated by its standard free energy (ΔF^{o}_{f298}=38.02 kcal/mole)[1] which makes it suitable as a monopropellant The decomposition of hydrazine may be written as

$$N_2H_4 \longrightarrow \frac{4}{3} NH_3 + \frac{1}{3} N_2 \qquad -\Delta H = 33\ 8 \text{ k cal/mole} \qquad (1)$$

or

$$N_2H_4 \longrightarrow 2H_2 + N_2 \qquad -\Delta H = 22\ 75 \text{ k cal/mole} \qquad (2)$$

In actual practice, however, the decomposition occurs in accordance with stoichiometric equation

$$N_2H_4 \longrightarrow \frac{4}{3}(1-X) NH_3 + 2X H_2 + \frac{1}{3}(1+2X) N_2 \qquad (3)$$

where the quantity, x, reflects the amount of deviation from the most energetic chemical reaction (eq 1) Experimentally, it has been found that this fraction, x, is a function of the temperature at which the reaction occurs [2].

The actual decomposition of hydrazine occurs by a series of steps which are considerably more complex than the overall stoichiometric relationships (eqs 1-3). For example, Eberstein and Glassman[3], in evaluating their experimental homogeneous reaction rate data gathered over the temperature range of 750 to 1000°K, proposed the following decomposition.

Initiation Reaction.

$$N_2H_4 + M \longrightarrow 2NH_2 + M \qquad K = 10^{19} \exp\left(\frac{-60{,}000}{RT}\right) \qquad (4)$$

Propagation Reactions

$$N_2H_4 + NH_2 \longrightarrow NH_3 + N_2H_3 \qquad K = 10^{12} \exp\left(\frac{-7000}{RT}\right) \qquad (5)$$

$$N_2H_3 + M \longrightarrow N_2 + H_2 + H + M \qquad K = 10^{13} \exp\left(\frac{-20{,}000}{RT}\right) \qquad (6)$$

$$N_2H_4 + H \longrightarrow NH_3 + NH_2 \qquad K = 10^{13} \exp\left(\frac{-7000}{RT}\right) \qquad (7)$$

Branching Reactions

$$N_2H_3 + M \longrightarrow NH + NH_2 + M \qquad K = 10^{12.9} \exp\left(\frac{-18{,}000}{RT}\right) \qquad (8)$$

$$N_2H_4 + NH \longrightarrow NH_2 + N_2H_3 \qquad K = 10^{14} \exp\left(\frac{-10{,}000}{RT}\right) \qquad (9)$$

Termination Reactions

$$NH_2 + N_2H_3 \longrightarrow NH_3 + N_2 + H_2 \qquad K = 10^{12.5} \tag{10}$$

$$N_2H_3 + N_2H_3 \longrightarrow 2NH_3 + N_2 \qquad K = 10^{12} \tag{11}$$

$$N_2H_3 + H \longrightarrow N_2 + 2H_2 \qquad K = 10^{15} \tag{12}$$

$$NH_2 + NH_2 \longrightarrow N_2H_4 \qquad K = 10^{12.5} \tag{13}$$

At low temperatures, the predominant propagation reactions are those described by equations 5 and 7 making the final products formed in the termination reactions mostly ammonia and nitrogen However, at higher temperatures, the propagation reaction which produces nitrogen and hydrogen (eq 6) and the associated termination step (eq 12) become more important leading to larger and larger amounts of hydrogen in the final products. Notice that the reaction scheme above does not involve the homogeneous decomposition of ammonia

$$NH_3 \longrightarrow \frac{1}{2} N_2 + \frac{3}{2} H_2 \tag{14}$$

which has been found to be slow[2]

$$\frac{d[NH_3]}{dt} = -10^{15.64} \exp\left(\frac{-79.5 \text{ kcal/mole}}{RT}\right)[NH_3][M] \tag{15}$$

which implies that in a volume typical of the thrusters considered in this program that a residence time of 3×10^{-2} sec at a temperature of 3000°R would result in only a 5 percent ammonia decomposition.

The overall kinetics which were obtained by Eberstein and Glassman[3]

$$\frac{d}{dt}[N_2H_4] = -K[N_2H_4][M] \tag{16}$$

is second order due to the low hydrazine pressures at which these experiments were performed. However, at high pressures the decomposition of hydrazine is found to be a unimolecular reaction[4] expressed as

$$\frac{d}{dt}[N_2H_4] = -K[N_2H_4] \tag{17}$$

with the transition occurring at pressures in the vicinity of one atmosphere.

Since a hydrazine thruster would operate with chamber pressures in excess of atmospheric, the kinetics of hydrazine decomposition are taken to be first order. The amount of ammonia present in the products of the homogeneous decomposition must, however, be taken to be a function of temperature as shown in Fig. 1 which includes the experimental data of Gray et al,[6] McHale et al[5] and Michel and Wagner[2] It can easily be seen that the amount of ammonia present in hydrazine decomposition products corresponds to $x < 0.5$ in the stoichiometric equation

$$N_2H_4 \longrightarrow \frac{4}{3}(1-x)NH_3 + 2xH_2 + \frac{1}{3}(1+2x)N_2 \qquad (18)$$

for all temperatures less than 2500°R which correspond to the adiabatic flame temperature at x = 0.5

As has been cited previously, the further decomposition of ammonia by dissociation is a slow homogeneous reaction and would not be expected to alter the composition of hydrazine decomposition products. It is well known, however, that many metals act as catalysts for the heterogeneous decomposition of ammonia [7] The list of catalytic metallic surfaces includes iron, molybdenum, tungsten, rhenium, ruthenium, osmium, copper, cobalt, nickel, rhodium and platinum In general, the decomposition rate per unit area of exposed surface is given by

$$r_c = k \exp\left\{\frac{-E}{RT}\right\}[NH_3]^x[H_2]^y \qquad (19)$$

with the exponents x and y varying with material The values of the exponents typically vary from both x and y being zero for tungsten and molybdenum to x = 0.7 and y = 1.4 for rhenium. Typical activation energies (E) required for the process are generally in the range of 40±5 k cal/mole and the frequency factor, A, is on the order of 10^{27} Comparison of the catalytic decomposition rate (equation 10) with the homogeneous reaction rate (equation 15) yields

$$\frac{r_c}{r_h} = \frac{10^{27}}{10^{15.6}} \frac{\exp(-42{,}500/RT)}{\exp(-79{,}500/RT)} \qquad (20)$$

$$= 10^{11.4} \exp(37{,}000/RT) \qquad (21)$$

which clearly demonstrates that, at the temperatures expected within the hydrazine thruster, the heterogeneous decomposition may be considerably more important than homogeneous gas phase reactions.

The amount of hydrazine which can be reacted within a given volume may be easily obtained from data reported in the literature and analysis Kinetic data at pressures in excess of atmospheric pressure and at temperatures greater than 1000°K are illustrated in Fig 2 The data obtained by McHale et al[5] are applicable over the temperature range of 975 to 1540°K while the curve obtained from Eberstein and Glassman[3] is a

FIG 1 AMMONIA DISSOCIATION FRACTION

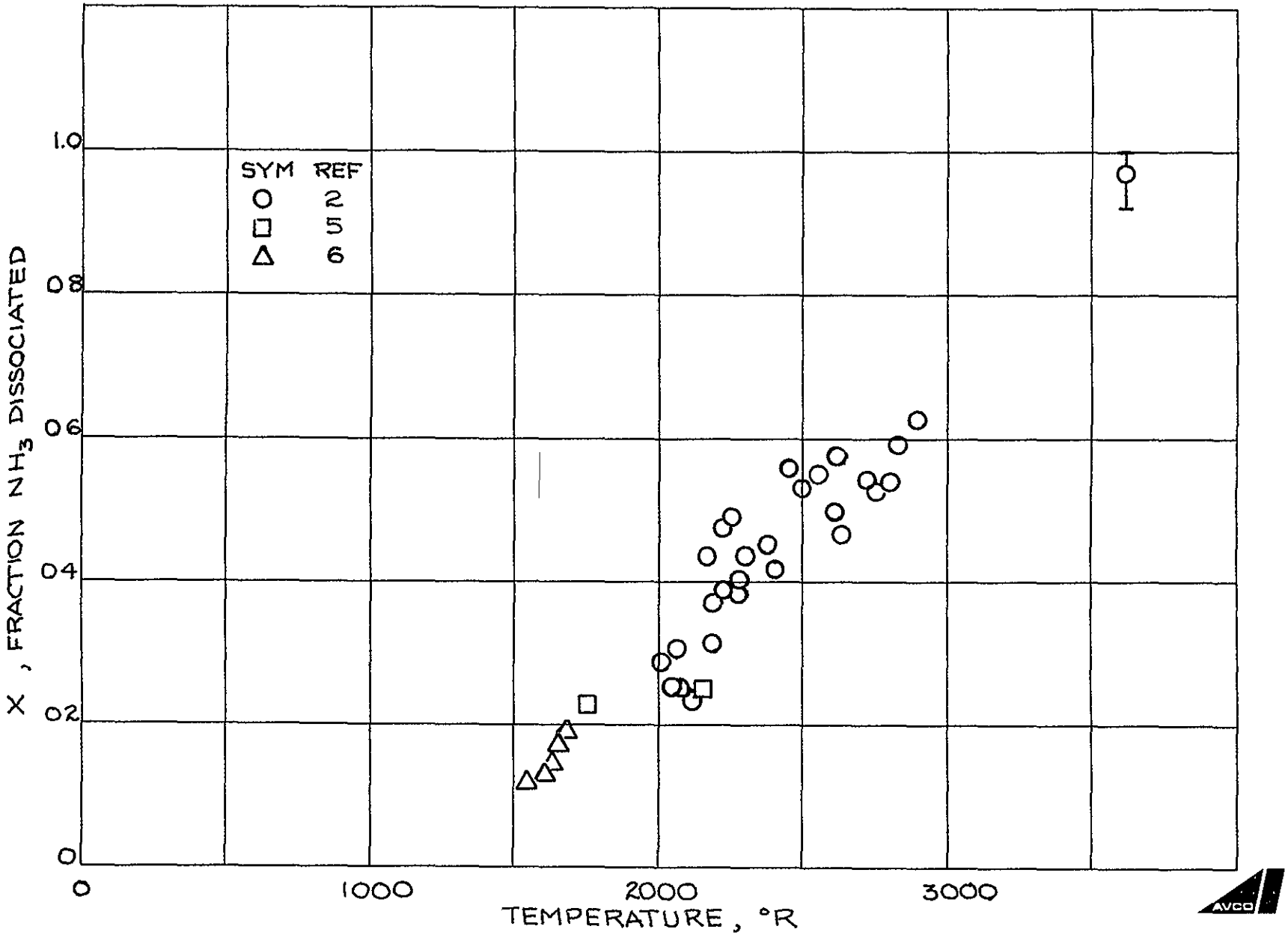

FIG 2 HYDRAZINE DECOMPOSITION KINETICS

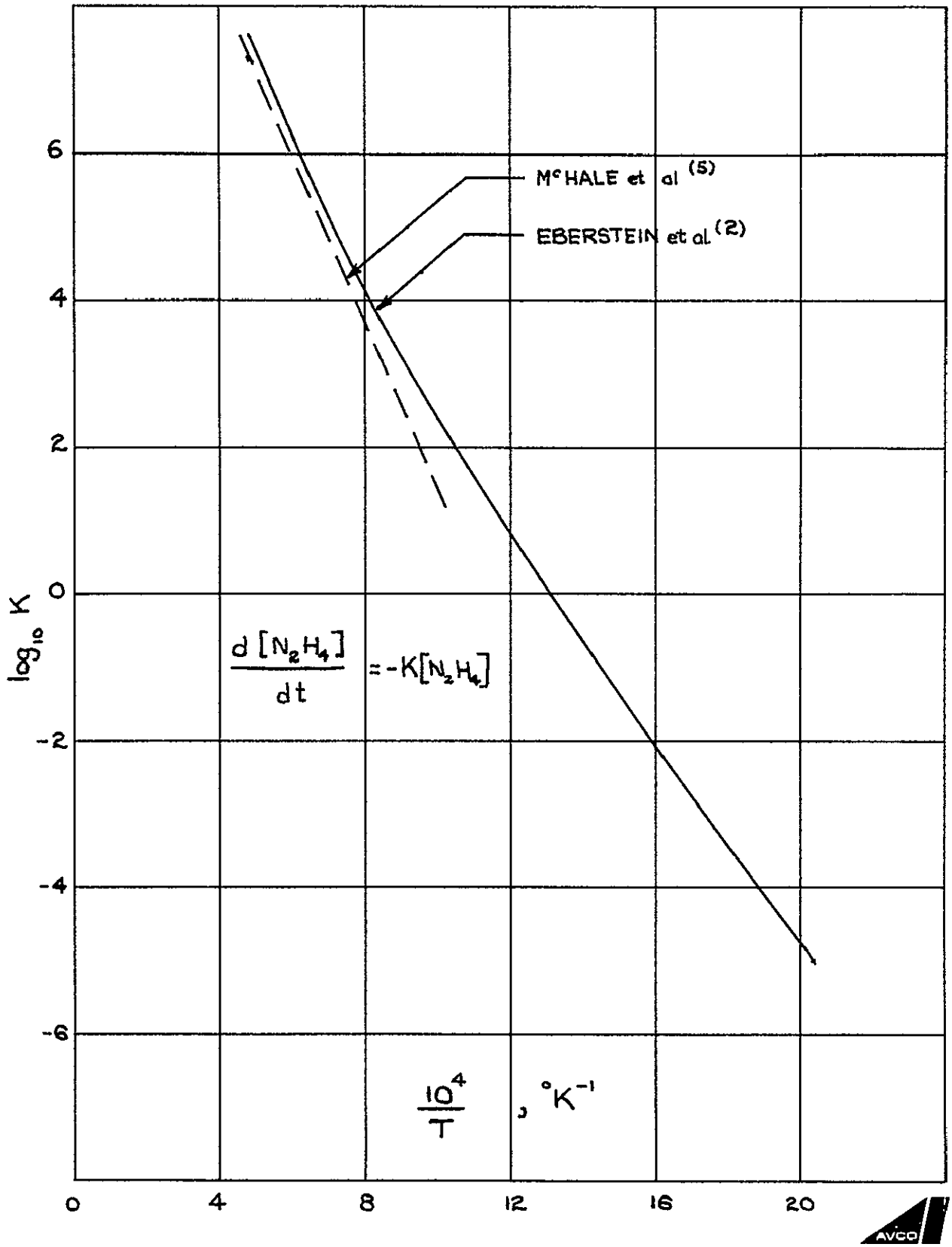

correlation of original data and results published in the literature. Since the latter curve can be applied over a wider temperature range, it will be employed in the subsequent discussions

A material balance for hydrazine contained in any volume may be written as

$$\dot{m}\left(w_i - w_o\right) = -rV \tag{22}$$

where it is assumed that the fluid within the volume is completely mixed with a mass fraction equal to that of the fluid leaving the volume through the exit nozzle The reaction rate of the propellant is given by first order kinetics as

$$r = -k\bar{\rho} w_o \exp\left(-E/RT\right) \tag{23}$$

with $\bar{\rho}$ being the average concentration within the system. Combining these two relationships, we get

$$\frac{w_2}{w_o} - 1 = \frac{k\bar{\rho}V}{\dot{m}} \exp\left(-E/RT\right) \tag{24}$$

with the average density obtained from the equation of state

$$\bar{\rho} = \frac{P\bar{M}}{R\bar{T}} \tag{25}$$

The mass flow leaving the system is simply

$$\dot{m} = PA_N \sqrt{\frac{g\gamma\bar{M}}{R\bar{T}}\left(\frac{2}{\gamma+1}\right)^{\frac{\gamma+1}{\gamma-1}}} \tag{26}$$

Hence,

$$\frac{w_i}{w_o} - 1 = \frac{V}{A_N\left(\frac{g\gamma R\bar{T}}{\bar{M}}\right)^{1/2}} \frac{k\exp\left(-E/RT\right)}{\left[\left(\frac{2}{\gamma+1}\right)^{\frac{\gamma+1}{\gamma-1}}\right]^{1/2}} \tag{27}$$

Since by definition

$$L^* = \frac{V}{A_N} \tag{28}$$

and

$$\bar{a} = \left(\frac{g\gamma R\bar{T}}{\bar{M}}\right)^{1/2} \tag{29}$$

$$\frac{w_i}{w_o} - 1 = \frac{L^* k \exp\left(-E/RT\right)}{\bar{a}\left\{\left(\frac{2}{\gamma+1}\right)\right\}^{\frac{\gamma+1}{2(\gamma-1)}}} \tag{30}$$

Notice that the quantity $L^*/\bar{a}$ is a characteristic "residence time" in the system Equation 30 may be rearranged to give the following relationship for the ratio of outlet and inlet propellant concentrations

$$\frac{W_o}{W_i} = \frac{\left[\frac{2}{\gamma+1}\right]^{\frac{\gamma+1}{2(\gamma-1)}}}{\left[\frac{2}{\gamma+1}\right]^{\frac{\gamma+1}{2(\gamma-1)}} + \frac{L^*}{\bar{a}} k \exp(-E/RT)} \tag{31}$$

From the first order rate expression, we may define a half life for the reactant at any average temperature since

$$\frac{dw}{dt} = w \exp\left(\frac{-E}{R\bar{T}}\right) \tag{32}$$

or upon integrating in the case of a constant temperature system

$$\ln\left(\frac{w}{w_i}\right) = -k\left[\exp\left(\frac{-E}{R\bar{T}}\right)\right] t \tag{33}$$

The time at which the concentration decreased to one-half of its initial value is then

$$t_{1/2} = \frac{0.693}{k \exp\left(\frac{-E}{RT}\right)} \tag{34}$$

which may be substituted into equation 31 to give

$$\frac{W_o}{W_i} = \frac{\left(\frac{2}{\gamma+1}\right)^{\frac{\gamma+1}{2(\gamma-1)}}}{\left(\frac{2}{\gamma+1}\right)^{\frac{\gamma+1}{2(\gamma-1)}} + 0693\left(\frac{L^*}{\bar{a}\, t_{1/2}}\right)}$$

The quantity ($L^*/\bar{a}$ t 1/2) represents a dimensionless time for the system Large dimensionless times imply a large fraction of propellant is decomposed. This can best be accomplished by increasing the temperature of the system since

$$\frac{L^*}{\bar{a}\, t_{1/2}} \propto \frac{L^*}{\bar{T}^{1/2}} \exp\left(-\frac{E}{R\bar{T}}\right) \tag{35}$$

with the exponential increasing much more rapidly than $T^{1/2}$

The ratio of outlet to inlet mass fractions predicted by equation 31 are presented in Fig 3 Over the range of mass fraction ratios less than 0.25 the conversion is well represented by

$$\frac{W_o}{W_i}\left\{\frac{kL^*}{\bar{a}} \exp\left(-\frac{E}{R\bar{T}}\right)\right\}^{095} = 0493 \tag{36}$$

Remembering that

$$\bar{a} = \left\{\frac{g\gamma R\bar{T}}{\bar{M}}\right\}^{1/2} \tag{37}$$

FIG 3 FRACTION N_2H_4 DECOMPOSED

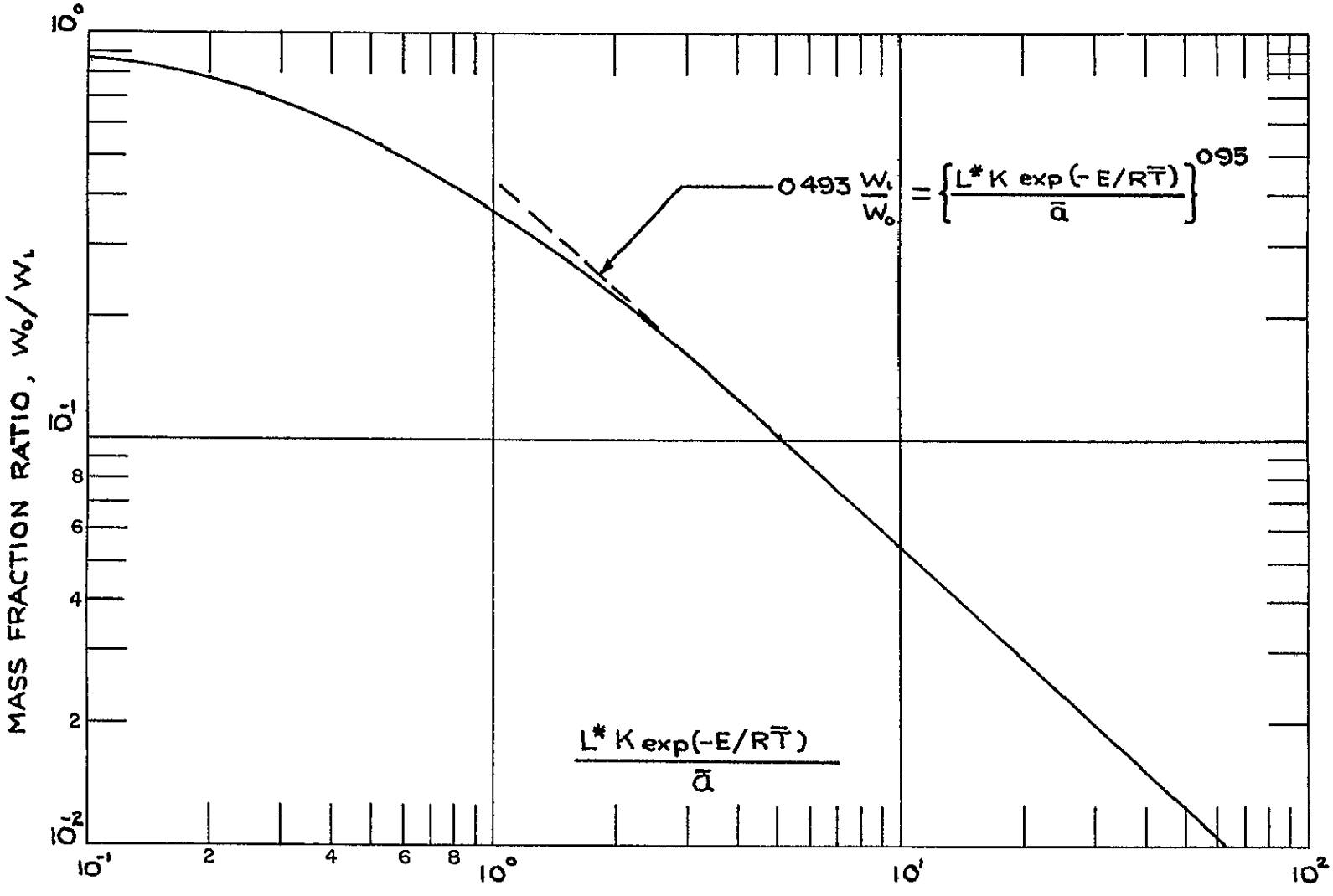

and if it is assumed that the average molecular weight of the combustion products is 15.2 (corresponding to 95 percent conversion), the following relationship is obtained

$$\frac{W_o}{W_i}\left\{\frac{L^* k}{\bar{T}^{1/2}}\exp\left(-\frac{E}{R\bar{T}}\right)\right\}^{0.95} = 711 \tag{38}$$

At a characteristic length of 1 ft. and a temperature of 2000°R, it is found from Fig. 4. that

$$k\exp\left(-\frac{E}{R\bar{T}}\right) = 158\times10^{3} \tag{39}$$

and

$$\left\{\frac{L^* k}{\bar{T}^{1/2}}\exp\left(-\frac{E}{R\bar{T}}\right)\right\}^{0.95} = 295 \tag{40}$$

Thereby indicating that the ratio of outlet to inlet mass fractions for this particular case is 0 242. Since the reaction rate increases exponentially with temperature, increasing the temperature within the volume to 2500°R decreases the mass fraction ratio to a value of 4 2 x 10^{-3} for L^* equal to 1 ft. Increasing the characteristic length to 10 would further reduce the mass fraction ratio, i e , increase the conversion of propellant to reaction products as shown in Fig 4.

Since the concept of a thermally ignited hydrazine resistojet also has the capability of using power addition to enhance the performance of the system, analyses were conducted to evaluate the magnitude of the increase which could be obtained by means of simple energy balance relationships.

The chemical power input to such a thruster is given by

$$P_{CHEM} = m\left(\Delta H_{f_o} + \int_o^{T_i} C_p\, dT\right) \tag{41}$$

For adiabatic operation of the thruster, the power in the exhaust gases is equal to the chemical power input

$$P_{CHEM} = m\sum_i w_i \int_o^{T_a} C_{p_i}\, dT \tag{42}$$

which allows the adiabatic flame temperature to be established for any inlet temperature T_1 since

$$\sum_i w_i \int_o^{T_a} C_{p_i} dT = \Delta H_{f_o} + \int_o^{T_i} C_p\, dT \tag{43}$$

for any set of reaction products

FIG 4 HYDRAZINE DECOMPOSITION DEPENDENCE ON CHARACTERISTIC LENGTH

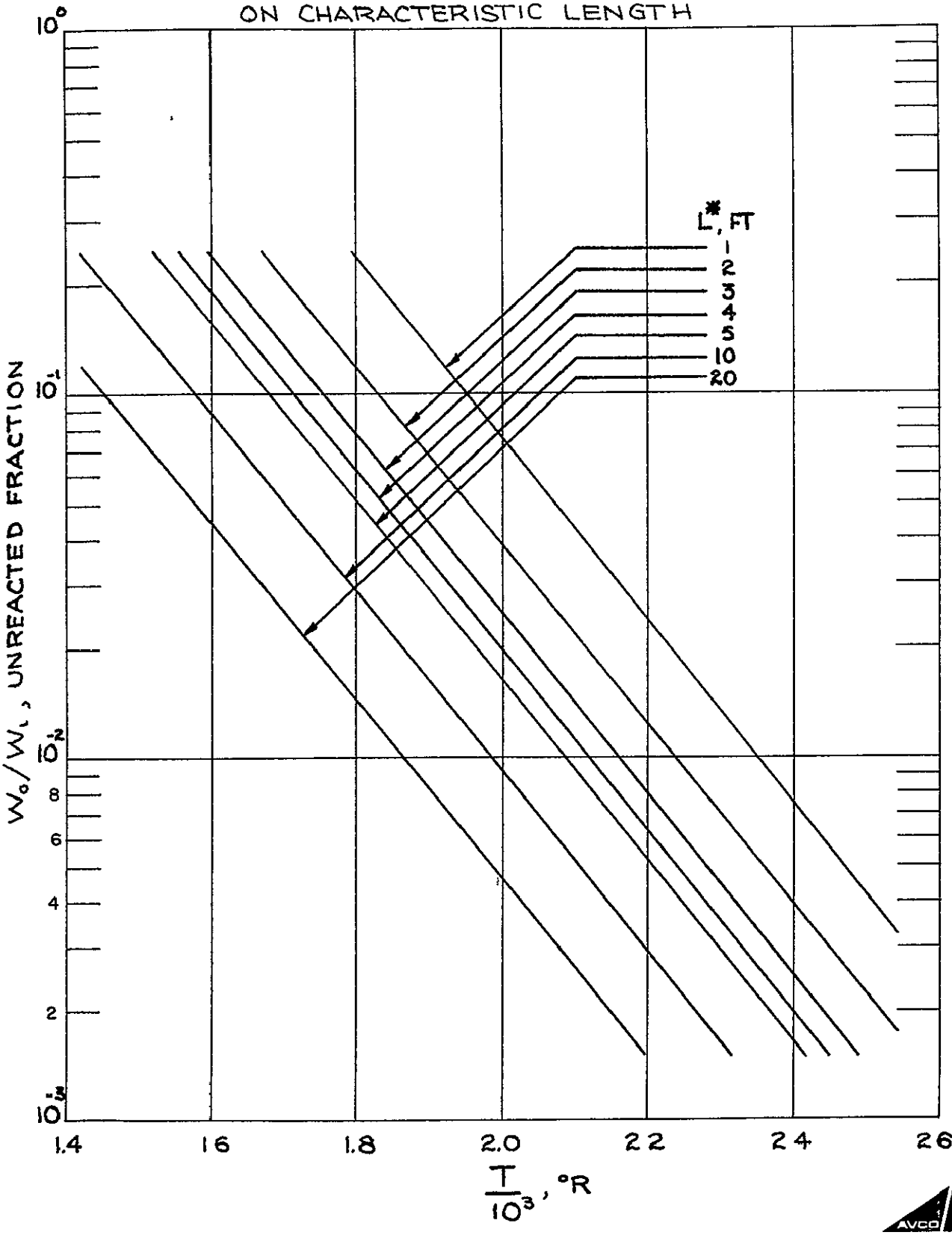

The decomposition reaction of hydrazine is given by

$$N_2H_{4_l} \longrightarrow \frac{4}{3}(1-X)\,NH_{3_g} + 2X\,H_{2_g} + \frac{1}{3}(1+2X)\,N_{2_g} \qquad (44)$$

where X is the fraction of ammonia dissociated. The energy released in this exothermic reaction of liquid hydrazine to gaseous products[8] is

$$\Delta H_{r_{298°K}} = -1503 + 825\,X \qquad BTU/LB\ N_2H_4 \qquad (45)$$

This is equivalent to the energy release of 33 k cal/g-mole reported in the literature[9] for the gas phase reaction with 25 percent of the ammonia dissociated.

Also, the adiabatic flame temperature at various ammonia dissociation fractions was determined by using thermodynamic data for the various chemical species as listed in the JANAF tables[1] and are illustrated in Fig 5 in the form of power addition per unit mass flow (watts-sec /μlb$_m$) as a function of temperature with dissociation fraction as a parameter The adiabatic flame temperature can be determined directly from Fig. 5 since this case corresponds zero power addition The amount of ammonia dissociation as reported in the literature[2, 5, 6] is also included in Fig. 5 In the case where the reaction zone is adiabatic and the decomposition occurs homogeneously, these data indicate that the stoichiometry of the reaction is

$$N_2H_{4_l} \longrightarrow 0.77\,NH_{3_g} + 0.84\,H_{2_g} + 0.61\,N_{2_g} \qquad (46)$$

and the adiabatic flame temperature is 2400°R In practice, however, the amount of dissociation will be less than that indicated by equation 46 (X=0 42) since there will be some energy losses from any actual system, and heterogeneous reactions are expected to play some part in the decomposition

The performance enhancement which can be obtained can be determined from the variation in specific impulse with temperature The specific impulse of a hydrazine thruster was determined analytically from the relationship

$$I_{sp} = \left\{\frac{2RT}{gM}\left(\frac{\gamma}{\gamma-1}\right)\left[1-\left(\frac{P_e}{P_c}\right)^{\frac{\gamma-1}{\gamma}}\right]\right\}^{1/2} \qquad (47)$$

FIG 5 EFFECTS OF POWER ADDITION ON TEMPERATURE AND COMPOSITION OF REACTION PRODUCTS

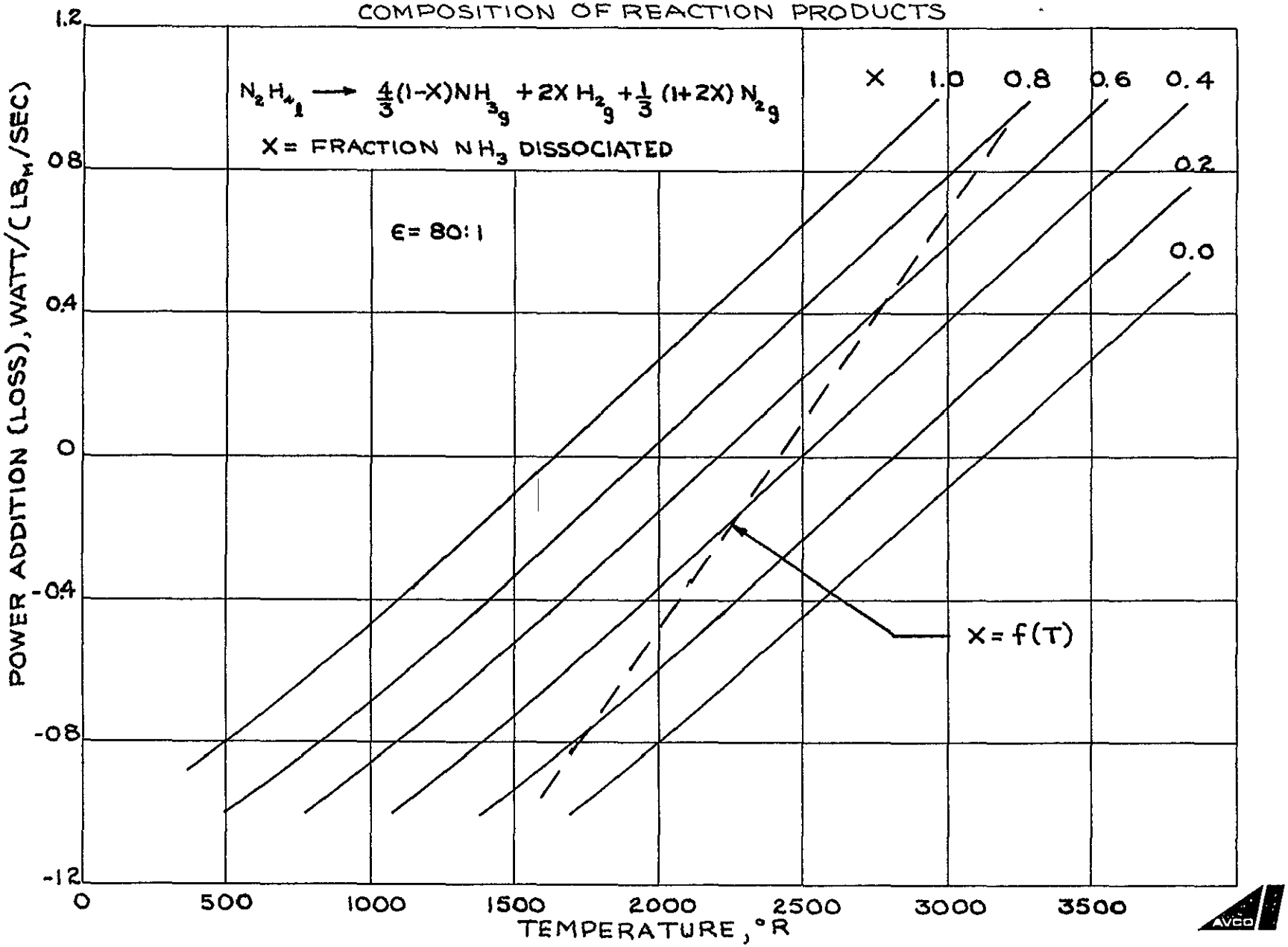

with the molecular weight (M) being a function of the ammonia dissociation fraction and the specific heat ratio as a function of the amount of ammonia present in the decomposition products as presented in Ref 10 The specific impulse for a thruster having an area ratio of 80 1 is shown in Fig 6 for various gas temperatures. The theoretical performance curves demonstrate that for a completely adiabatic system the specific impulse would be in the rate of 250 sec. for x = 0 42 (homogeneous hydrazine decomposition) to 262 sec for x = 0.0 (heterogeneous hydrazine decomposition).

The performance curves can be used to demonstrate the importance of further ammonia decomposition on the efficiency of power addition in increasing specific impulse of a thruster. For example, consider a unit where the decomposition of hydrazine occurred in an adiabatic homogeneous manner (X=0 42) Following the decomposition the thermal losses were such to produce a reduction of the gas temperature to 1800°F and, hence, yield a specific impulse of 220 seconds rather than the theoretical value of 250 seconds If the impulse is to be increased by power addition to 260 seconds and there is no further ammonia decomposition, the total power addition is 0 55 watts/ (μlb_m/sec) However, if in the power addition process all the remaining ammonia decomposes the power requirement is increased to a theoretical value of 0.92 watts/(μlb_m/sec). This simple exercise clearly demonstrates the advisability of limiting the amount of ammonia decomposition within the thruster if power addition is contemplated.

The increase in thrust which is achieved through power addition is shown in Fig. 7 The preparation of this illustration it was assumed that the thruster was capable of operation at a specific impulse of 180 sec and a thrust level of 10 millipounds with no power addition, and that the amount of ammonia in the exhaust was given by the ammonia "dissociation" fraction as a function of temperature A second power addition curve is also presented which depicts the enhancement achieved with no change in composition. In the region where thrust increases linearly with power addition, a 1 millipound thrust enhancement requires 18 5 watts of power for variable composition while the constant composition curve indicates that 14 5 watts of power are necessary to produce the same result

These analyses clearly demonstrate the feasibility of the hybrid hydrazine resistojet concept Reasonable performance would be expected with a device which could operate at a specific impulse of 200 sec. at a thrust level of 20 millipounds This would be achieved with a thrust thermal efficiency on the order of 65 percent at a temperature in the vicinity of 1700°R. Kinetics indicate that with a thruster in which propellant and reaction products were well mixed that 95 percent of the propellant would be reacted in a characteristic length of 10 ft.

FIG 6 EFFECTS OF POWER ADDITION ON THEORETICAL PERFORMANCE

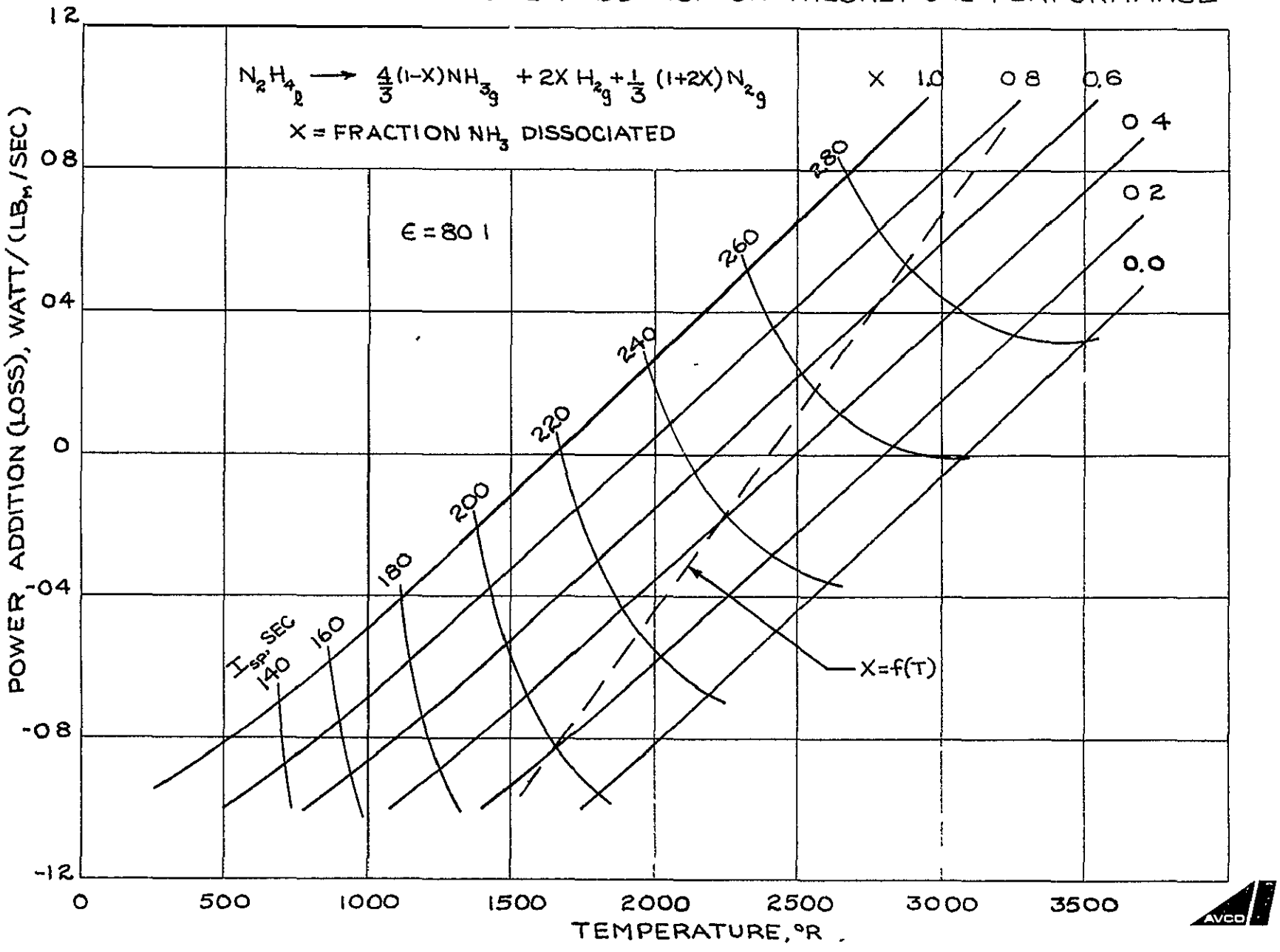

FIG 7 THRUST ENHANCEMENT BY POWER ADDITION

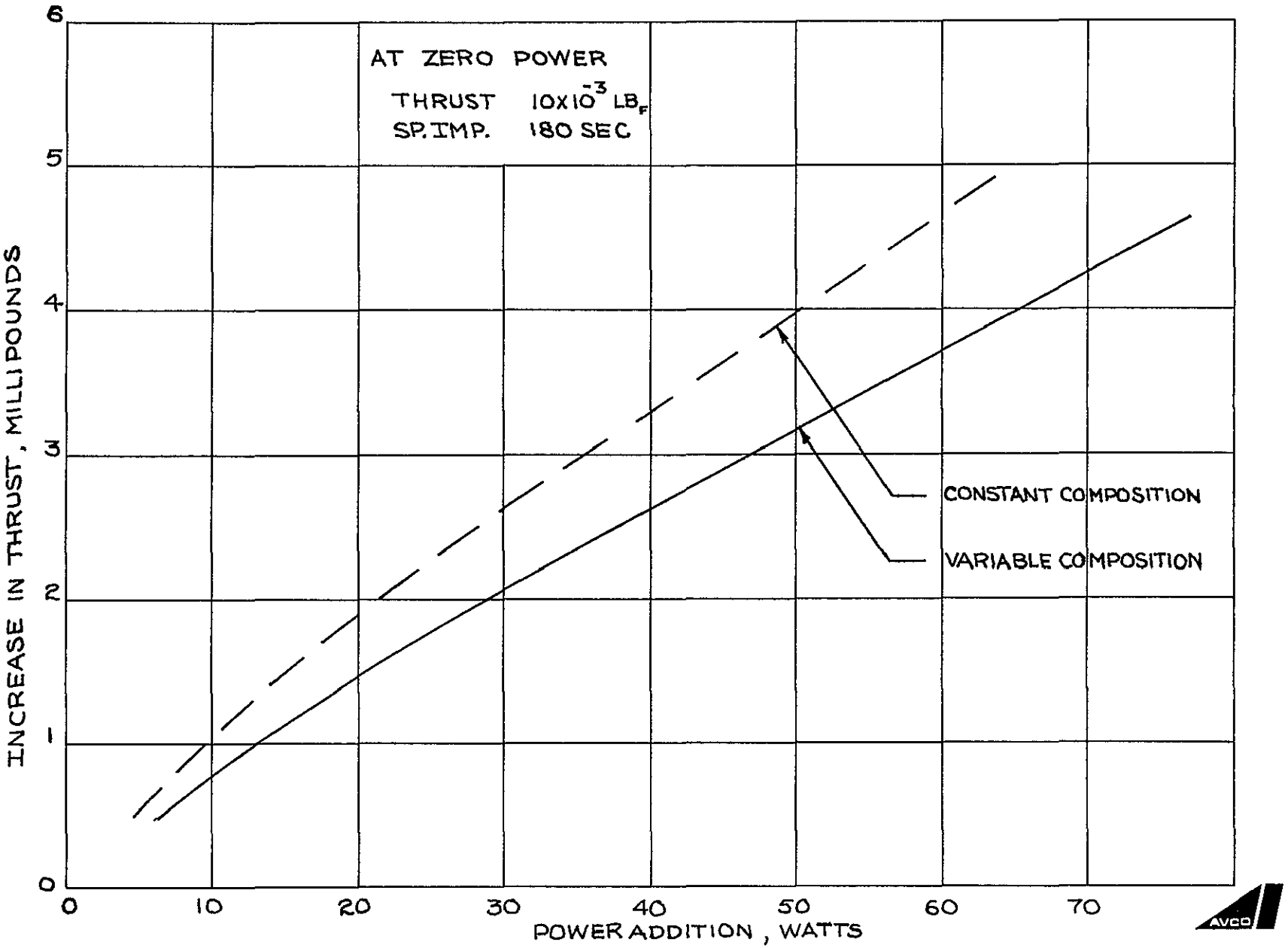

IV Thruster Evaluation

During the course of this study, several thruster configurations were employed to evaluate propellant injection schemes, the effects of power addition and to obtain thruster performance data.

A) Laboratory Thrusters

The devices employed in the earlier phases of the program were relatively simple units as shown schematically in Figs 8-10. Basically, these early thrusters consisted of a quartz tube mounted between a nozzle assembly and base plate assembly A heater coil of molybdenum or rhenium wire was employed as the means of raising the temperature of the thruster to levels sufficient to provide energy for propellant ignition. Several variations in the method of propellant injection were examined with this basic unit. These injection schemes are illustrated in Figs. 8-10.

Injector configurations "A" consists of a simple porous plug mounted in the base plate with the thrust chamber being completely empty This configurations would be expected to have a minimum thermal inertia

Configuration "B" thrusters were essentially identical to configuration "A" with the exception that porous ceramic rod (0 187 in dia x 1 0 in. long) was placed in the thrust chamber The heater coil in this configuration was in close contact with the rod of calcia stabilized zirconia

In the configuration "C" thruster, the ceramic rod was mounted in the base plate and propellant flowed through the calcia stabilized zirconia by means of a 0.030 in dia. passage located on the axis of the rod The ceramic rod had an external diameter of 0 187 in. and a length of 1.00 in. The passage on the axis of the rod extended to approximately 0 090 in. from the downstream end of the rod where it was sealed by ceramic cement.

The last configuration (configuration "D") was nearly identical to "C" except that a 0.025 in o d. by 0 015 in. i d. tube was inserted into the ceramic rod for a distance of 0.8 in from the upstream end,thereby moving the point at which propellant enters the thrust chamber away from the thruster base plate.

A limited amount of exploratory data was gathered with the configurations "A" and "B" while a larger effort was expended in evaluating configurations "C" and "D" Primary stability comparisons were made at zero power addition following the initiation of decomposition. The comparisons were made over a range of flow rates of 10^{-5} to 5×10^{-5} lb/sec (corresponding to a thrust level of 2 to 10 millipounds at a specific impulse of 200 sec) In all cases, the

FIG 8 CONFIGURATION "A" LABORATORY THRUSTER

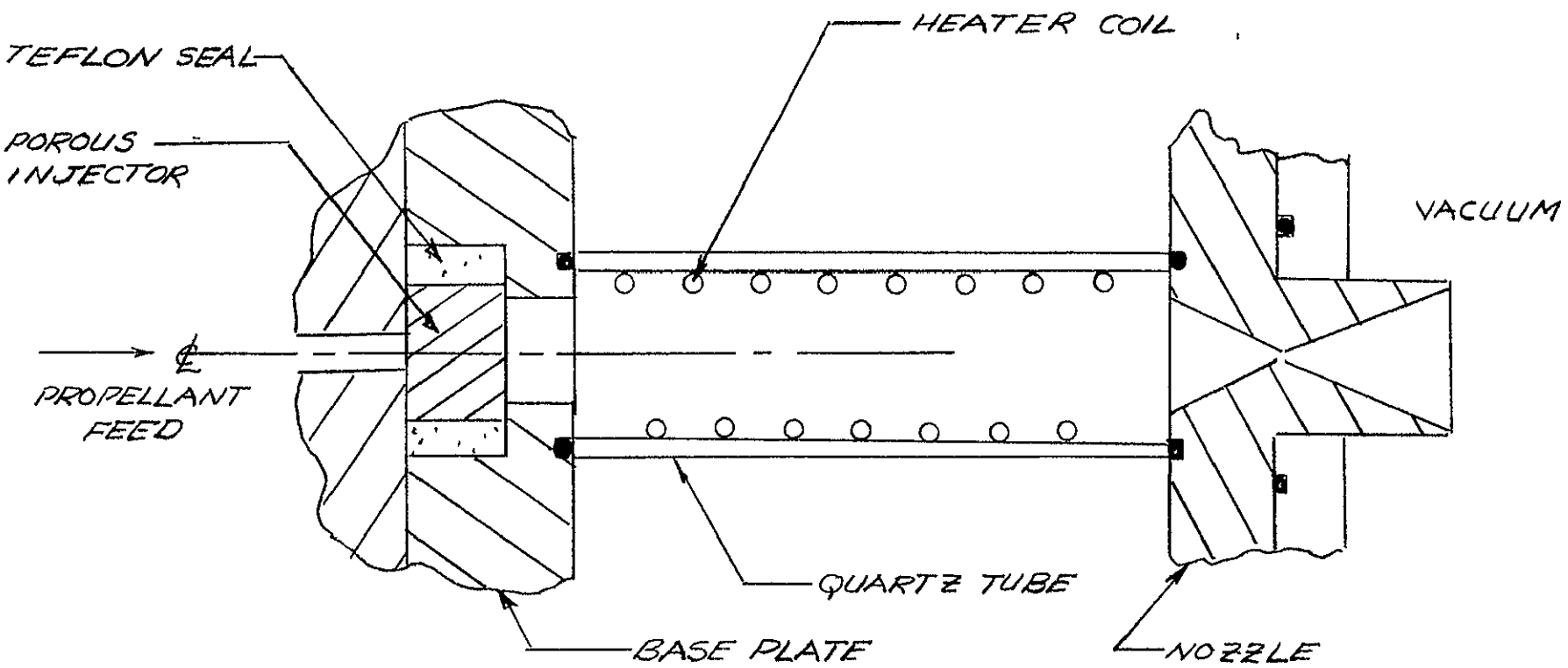

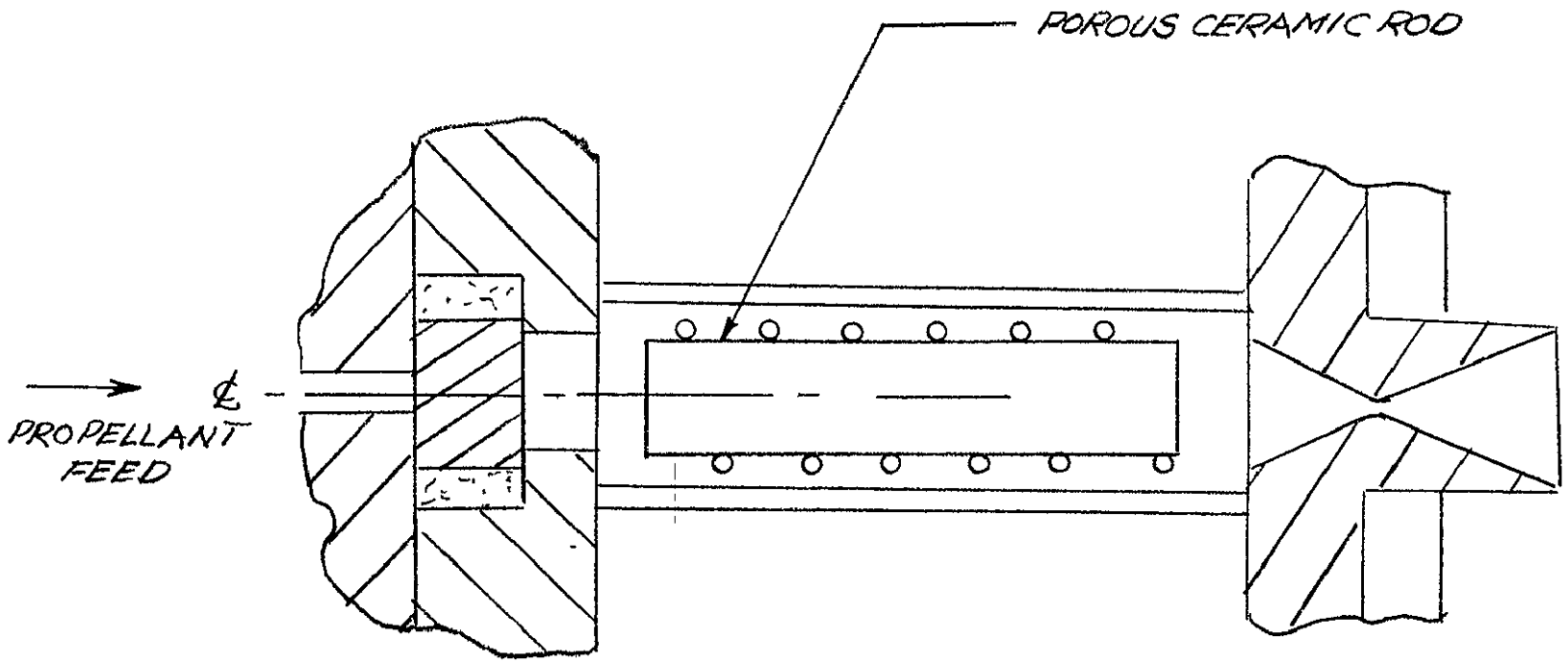

OTHER WISE IDENTICAL TO CONFIGURATION "A"

FIG. 9 CONFIGURATION "B" LABORATORY THRUSTER

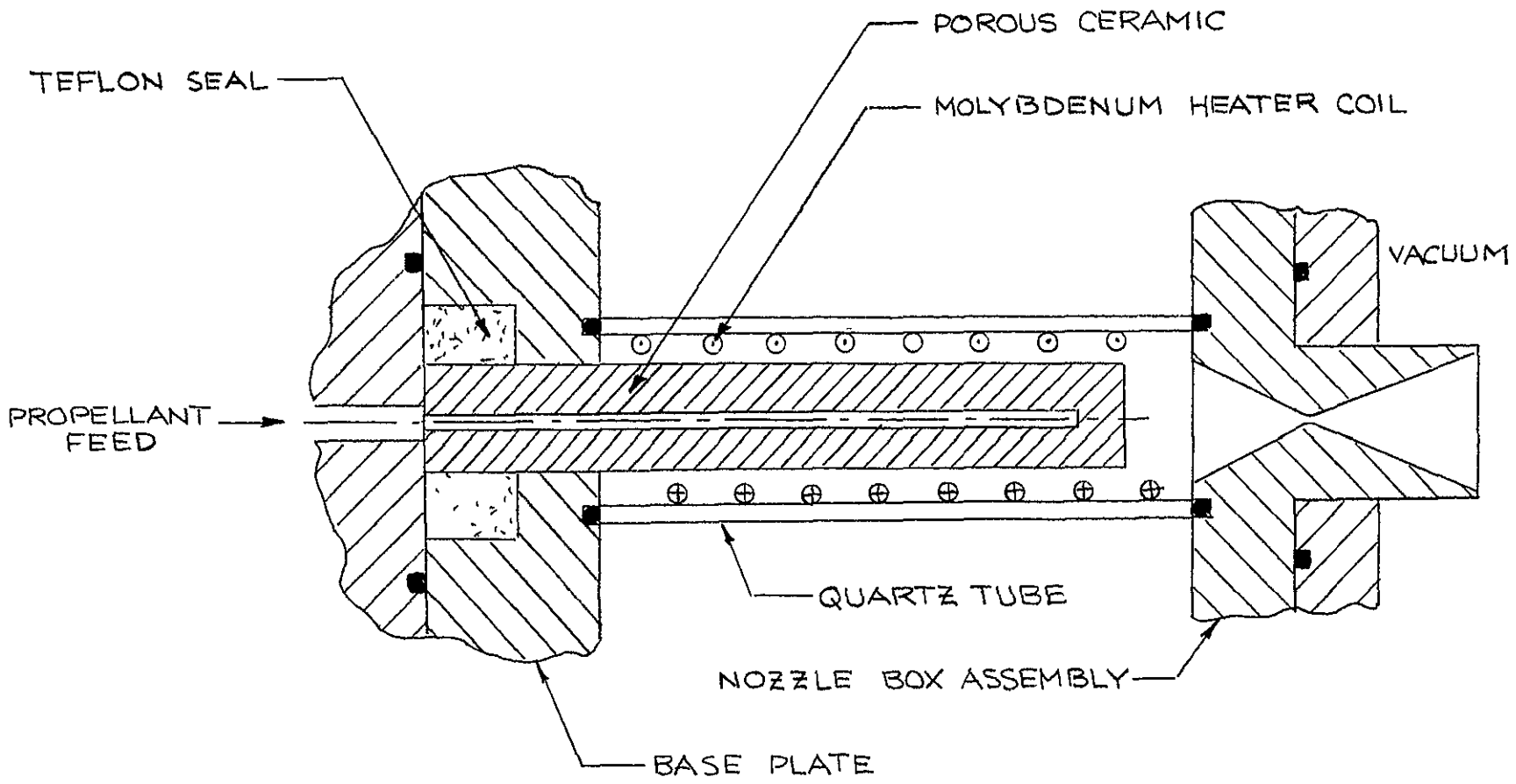

FIG 10 CONFIGURATION "C" LABORATORY THRUSTER

combination of the orifice/porous injector (configuration "C") was superior to configurations "A" and "B" with respect to stable operation and decomposition efficiency as measured by characteristic velocity Samples of nozzle box and injection pressure responses for all configurations are shown in Figs. 11, 12 and 13 at various mass flow rates at zero power input All configurations utilized the same exit nozzle and inlet fixture. The nozzle diameter was 0 017 in. which is a reasonable selection for a 10 millipound thruster In all cases, considerable conductive losses can be expected due to the intimate contact of the inlet and nozzle blocks with large heat sinks. These losses should be the same for all configurations so that good comparisons between competitive configurations may be made

It is immediately obvious that the configuration "A" is extremely unstable at all conditions. The addition of the zirconia flame stabilizer greatly improved performance as can be seen by the pressure responses for configuration "B". When the performance of configuration "C" and "B" are compared, it is noted that the decomposition process for "C" is slightly more stable than "B" and at the highest flow rate, the characteristic velocity is 20% higher for the "C" configuration

The large pressure fluctuations for the "A" configuration were primarily caused by flow variations through the porous injector. Once the thermal decomposition was initiated and the power turned off, the hydrazine was observed reacting on the exposed surface of the porous injector The reaction zone was a small area which was appreciably hotter than the mean temperature of the element. In addition to nonuniform surface temperature, the hot spot was observed to move around the injector, tracing a circle. This phenomenon was accompanied by rapid fluctuations in the temperature of the thruster heater wire presumably caused by hydrazine passing through the porous element without reacting, and then decomposing on the wire. It can be assumed that some fuel was passed through the nozzle without decomposing at all as evidenced by the low mean pressures

A reasonable explanation of the cause of these instabilities is as follows. When hydrazine vapor is entering the thruster at the burning velocity, we may write

$$\bar{\rho} S_u A = \dot{m} \tag{48}$$

where the average density may be taken as that at the normal boiling point of the propellant (238°F).

$$\bar{\rho} = \frac{PM}{RT} \tag{49}$$

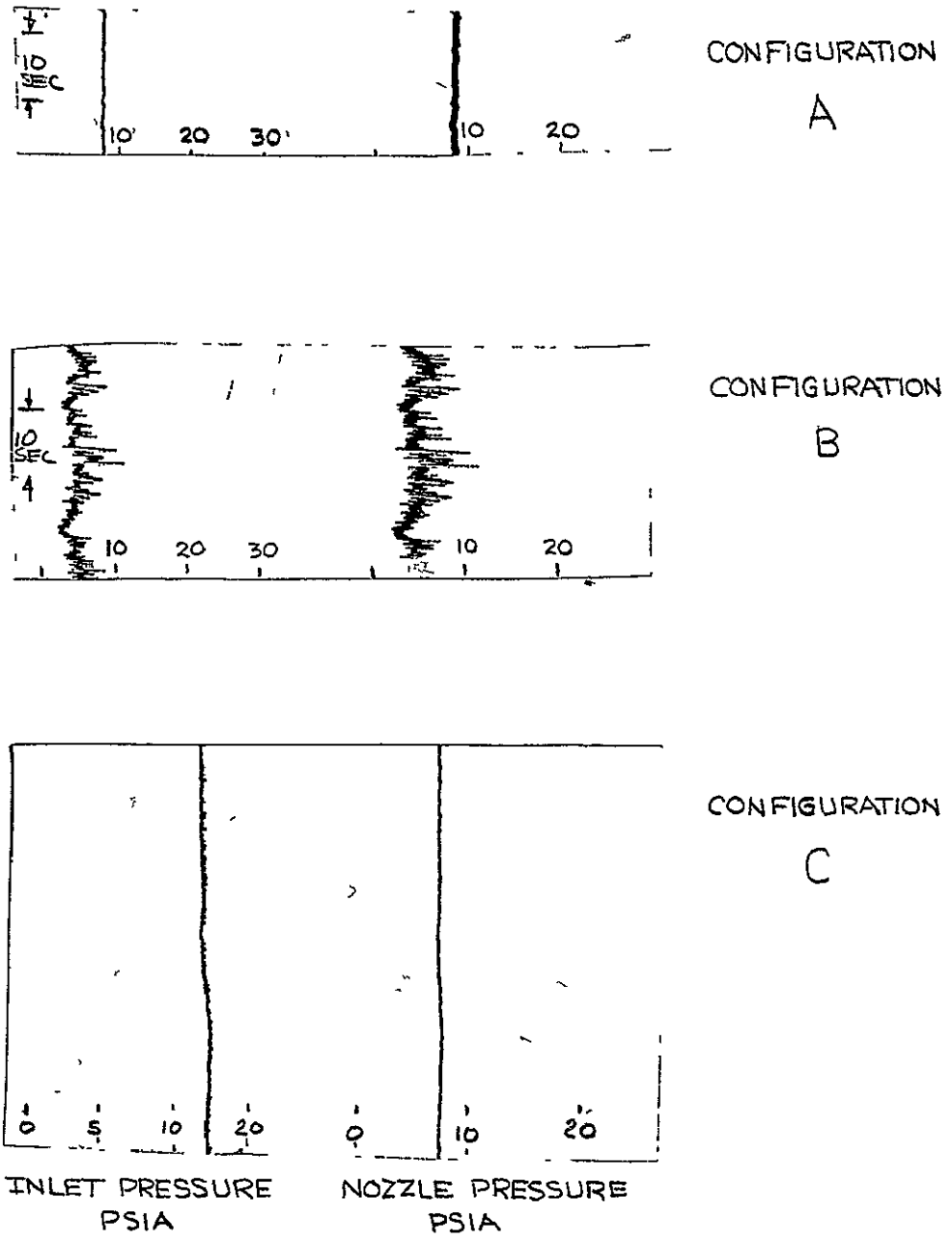

FIG 11 STABILITY COMPARISONS, LABORATORY THRUSTERS

HYDRAZINE FLOW: 1.4×10^{-5} LB_M/SEC

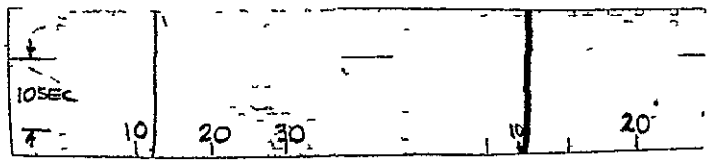

CONFIGURATION
A

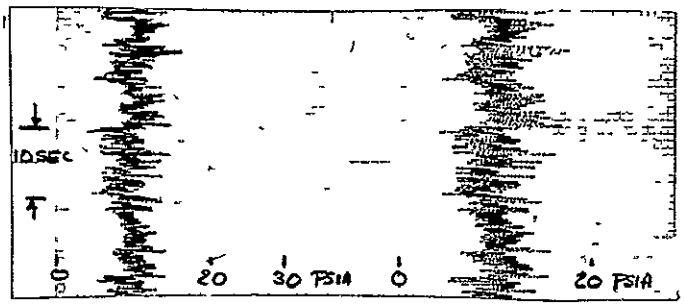

CONFIGURATION
B

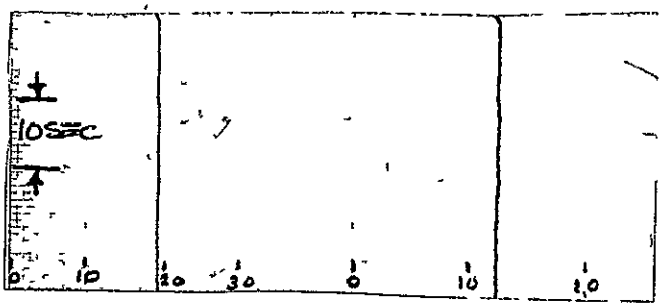

CONFIGURATION
C

INLET PRESSURE
PSIA

NOZZLE PRESSURE
PSIA

FIG 12 STABILITY COMPARISONS, LABORATORY THRUSTERS
HYDRAZINE FLOW : 2.5×10^{-5} LB_H / SEC.

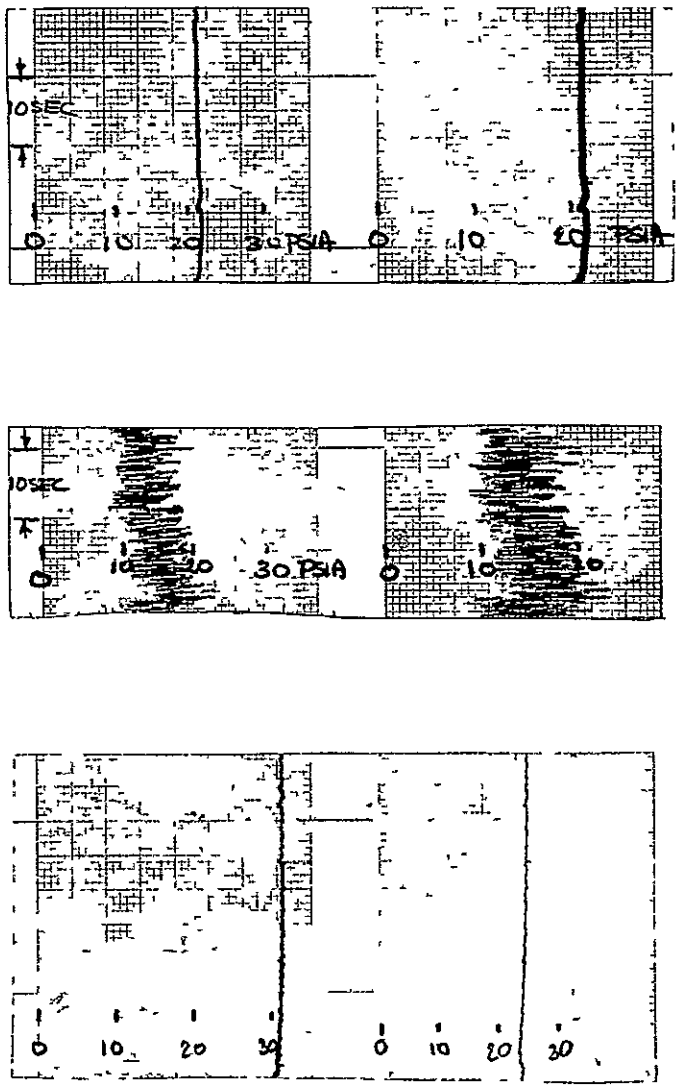

CONFIGURATION

A

CONFIGURATION

B

CONFIGURATION

C

FIG 13 STABILITY COMPARISONS, LABORATORY THRUSTERS, HYDRAZINE FLOW : 4.8×10^{-5} LB_M/SEC.

For a burning velocity of 185 cm/sec[11], and a mass flow rate of 5×10^{-5} lb/sec, the minimum diameter of a cylindrical porous element is

$$D^2 = \frac{4 m R T}{\pi S_u P M} \tag{50}$$

or

$$D = 0.156 \text{ in.}$$

Notice that if the gas temperature is increased to 1250°F with the corresponding decrease in density, the minimum diameter is decreased to a value of 0.024 in.

Since a porous element similar to that used in configuration "A" and "B" thrusters cannot be expected to produce a uniform velocity stream, decomposition of the propellant would occur on those regions of the surface where the velocity is less than the burning velocity. These regions would tend to be localized hot spots due to heat transfer from the reaction zone to the porous element. However, as the temperature increases a critical value is reached when the local velocity is greater than the burning velocity and then the flame lifts off the surface. Furthermore, it is evident that an increase in the temperature of porous element would result in fluctuations in the mass flow through the system if the pressure drop across the element remains constant. This effect is caused strictly through the increase in viscosity with increasing temperature Hence, we may conclude that when the size of the porous element is close to that given by equation 50 than an unstable situation may result, e.g. the large scale pressure fluctuations observed with the configuration "A" prototype thruster. Smaller scale fluctuations are expected with configuration "B" since the ceramic stabilizer would tend to dampen the pressure fluctuations

Stability and performance considerations indicated that configurations "C" and "D" (which was not evaluated in the experiments cited above) to be most satisfactory and further evaluation of these devices was merited Steady state operation of the configuration "C" thruster was examined over a flow rate range of 10^{-5} to 5×10^{-5} lb/sec; experiments were performed in both the powered and unpowered modes of operation These experiments were conducted with the thruster exhausting into vacuum with no provision for direct measurement of thrust, hence, the basic performance parameter employed in these evaluations was the characteristic velocity of the exhaust stream

$$C^* \equiv \frac{g P A_N}{\dot{m}} \tag{51}$$

where the pressure, P_N, is that measured in the thrust chamber, A_t is the nozzle throat area, and m is the mass flow through the system

Propellant was supplied to the thruster by the hydrazine feed system shown schmetically in Fig. 14. The basic components of the feed system were a propellant tank having a capacity of 1000 ml which could be pressurized with inert gas to 180 psig, a flow metering system, a flow regulating valve, and a solenoid control valve. The flow metering device consisted of an orifice having a nominal diameter of 0 0043 in. which was instrumental with a differential pressure transducer (Dynisco Model DPT 69CB-10) which had a linear output over the range of 0-5 psid A schematic diagram of the propellant feed system is shownin Fig. 14 A series of calibration experiments were performed with the system by allowing hydrazine to flow through the orifice for periods ranging from 180 to 240 sec. The total mass flow was collected in a beaker and weighed on an analytical balance having an accuracy of ± 0.0005 grams. The resulting mass flow rate was correlated with the millivolt output of the pressure transducer as shown in Fig. 15 The data are well correlated by the equation

$$\dot{m} = 3.75 \times 10^{-5} \left(E_{mv} \right)^{1/2} \qquad LB_M/SEC \tag{52}$$

with all data falling within 5% of this relationship

Performance data were gathered with a configuration "C" thruster in both powered and unpowered operation over the flow rate range of $1.5\text{-}5.0 \times 10^{-5}$ lb_m/sec. These data are summarized in Figs. 16-18 in the form of characteristic velocity as a function of propellant flow rate with power applied to the heater coils as a parameter. Data obtained at a flow rate of $5 \times 10^{-5} lb_m$/sec are also presented in Fig 19 with characteristic velocity, specific impulse, and thrust as a function of power to the heater coils. The thrust was calculated from the experimental data using an assumed thrust coefficient of 1 65. It is seen from these results that a 50 watt power input increases the thrust level from $7.2 \times 10^{-3} lb_f$ at zero power input to a level of $8.5 \times 10^{-3} lb_f$ This corresponds to a power requirement of 38.4 watts per millipound of thrust. When the experimental value is compared with the theoretical thrust increase (Fig 7), it is found that the power addition process has an efficiency on the order of 50 percent when the variable composition thrust enhancement curve is used as a base A comparison of the calculated specific impulse with the theoretical predictions at an assumed ammonia dissociation fraction corresponding to the exit gas temperature indicates a gas temperature at the nozzle of approximately 900°R whereas a completely adiabatic system would produce gas at 2400°R. The thermal efficiency of the system is also on the order of 50 percent.

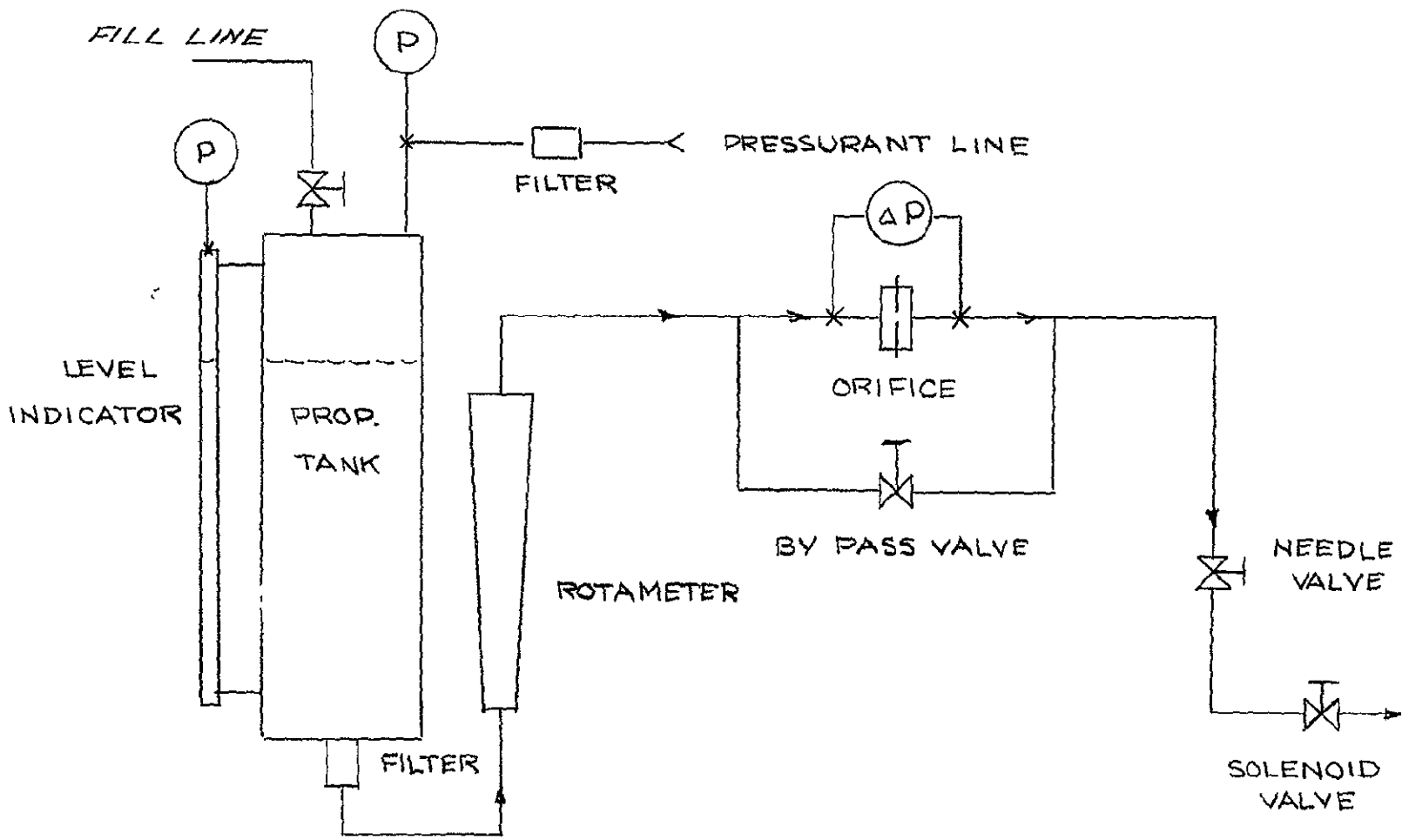

FIG 14. HYDRAZINE FEED SYSTEM SCHEMATIC

FIG 15 CORRELATION OF HYDRAZINE FEED SYSTEM OUTPUT SIGNAL

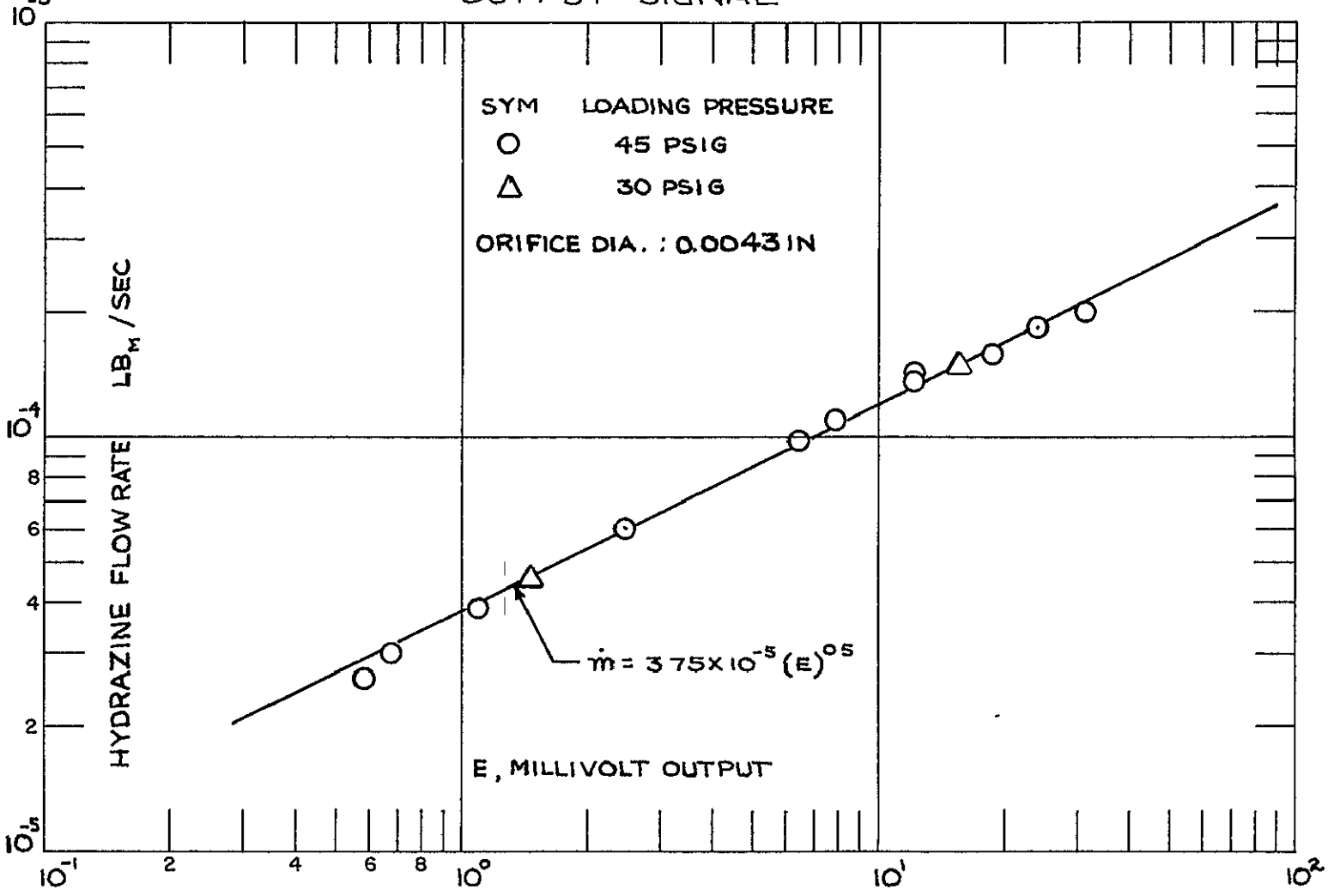

FIG 16 CONFIGURATION "C" THRUSTER DATA

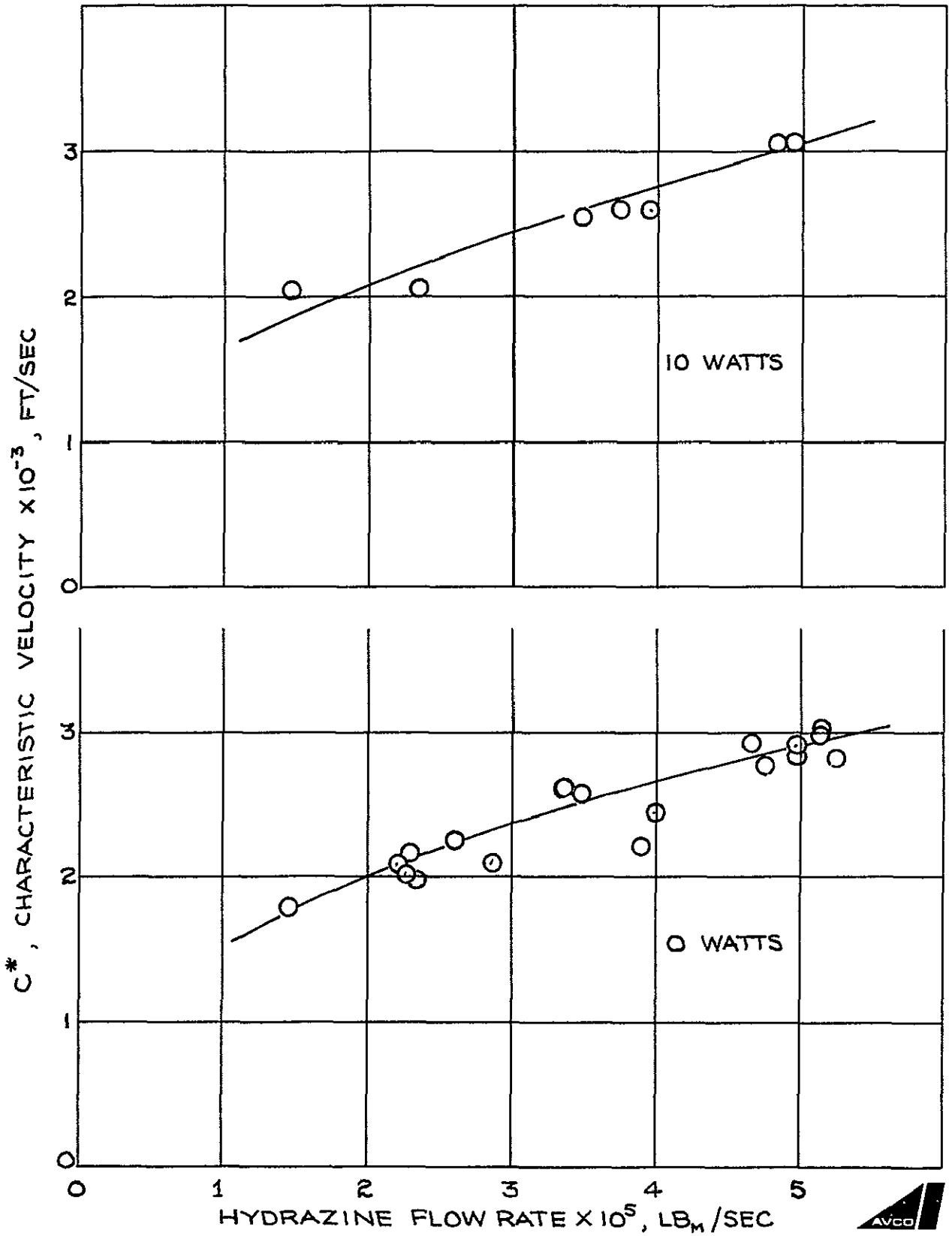

FIG 17 CONFIGURATION "C" THRUSTER DATA

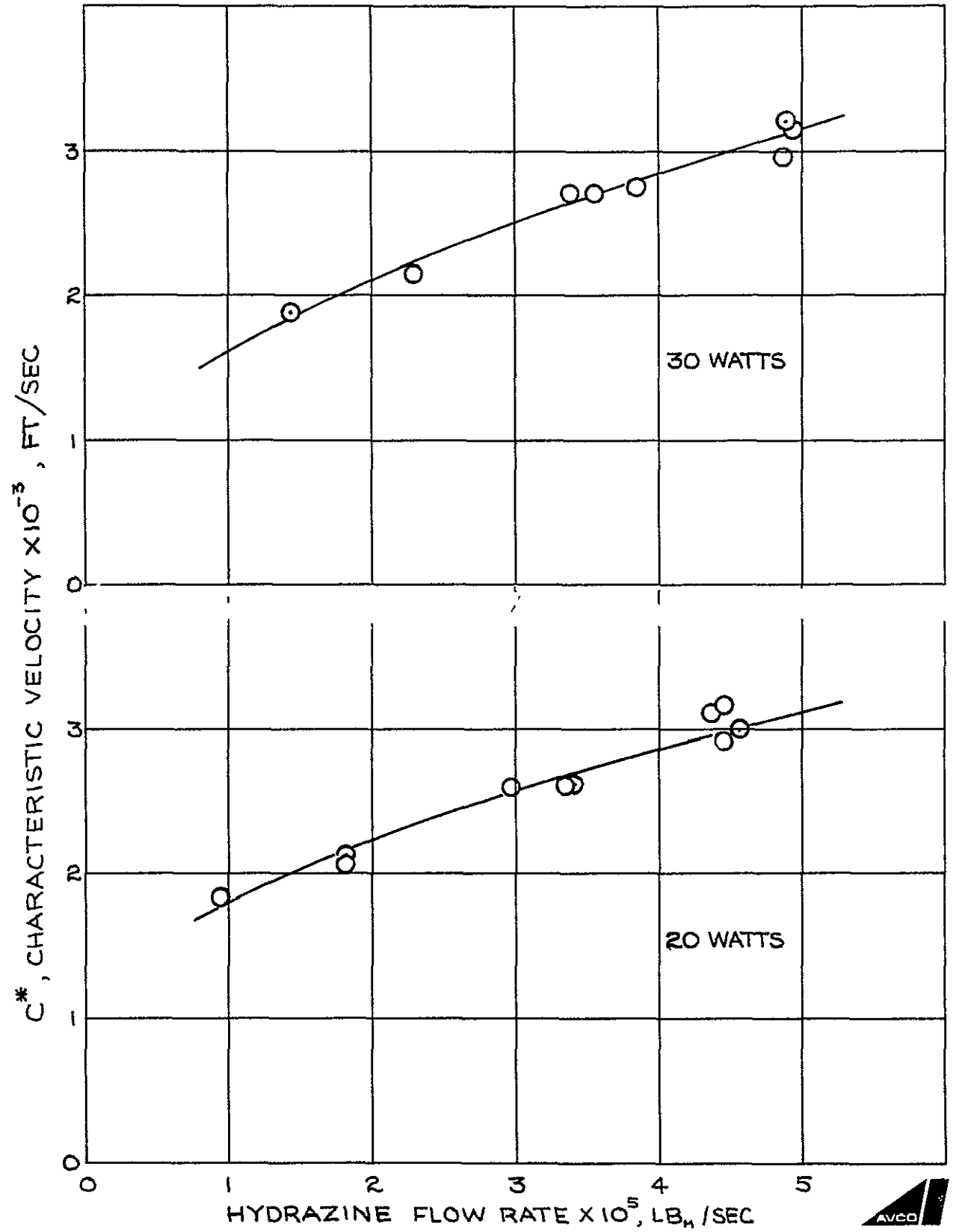

FIG 18 CONFIGURATION "C" THRUSTER DATA

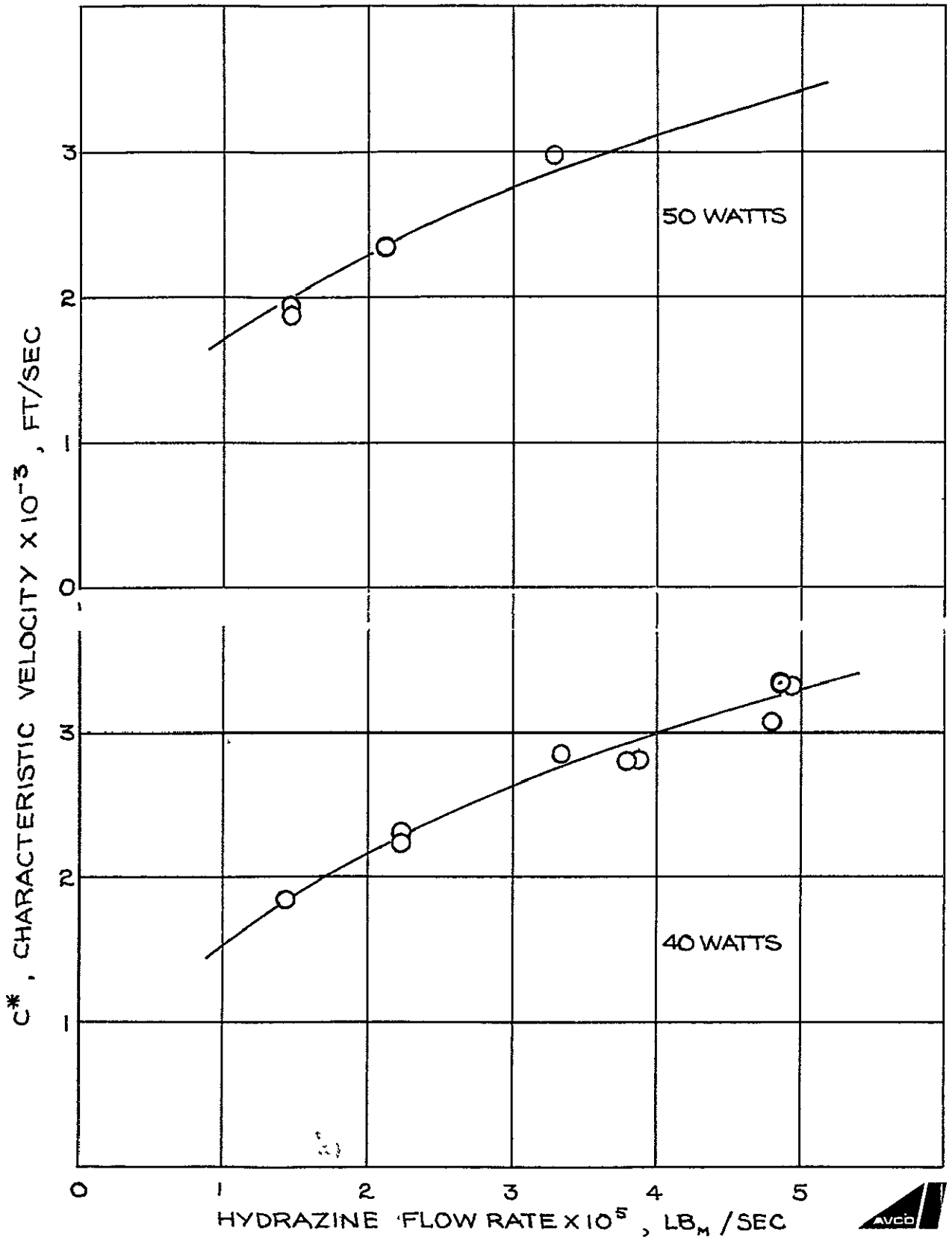

FIG 19 EFFECT OF POWER ADDITION ON CONFIGURATION "C" THRUSTER PERFORMANCE

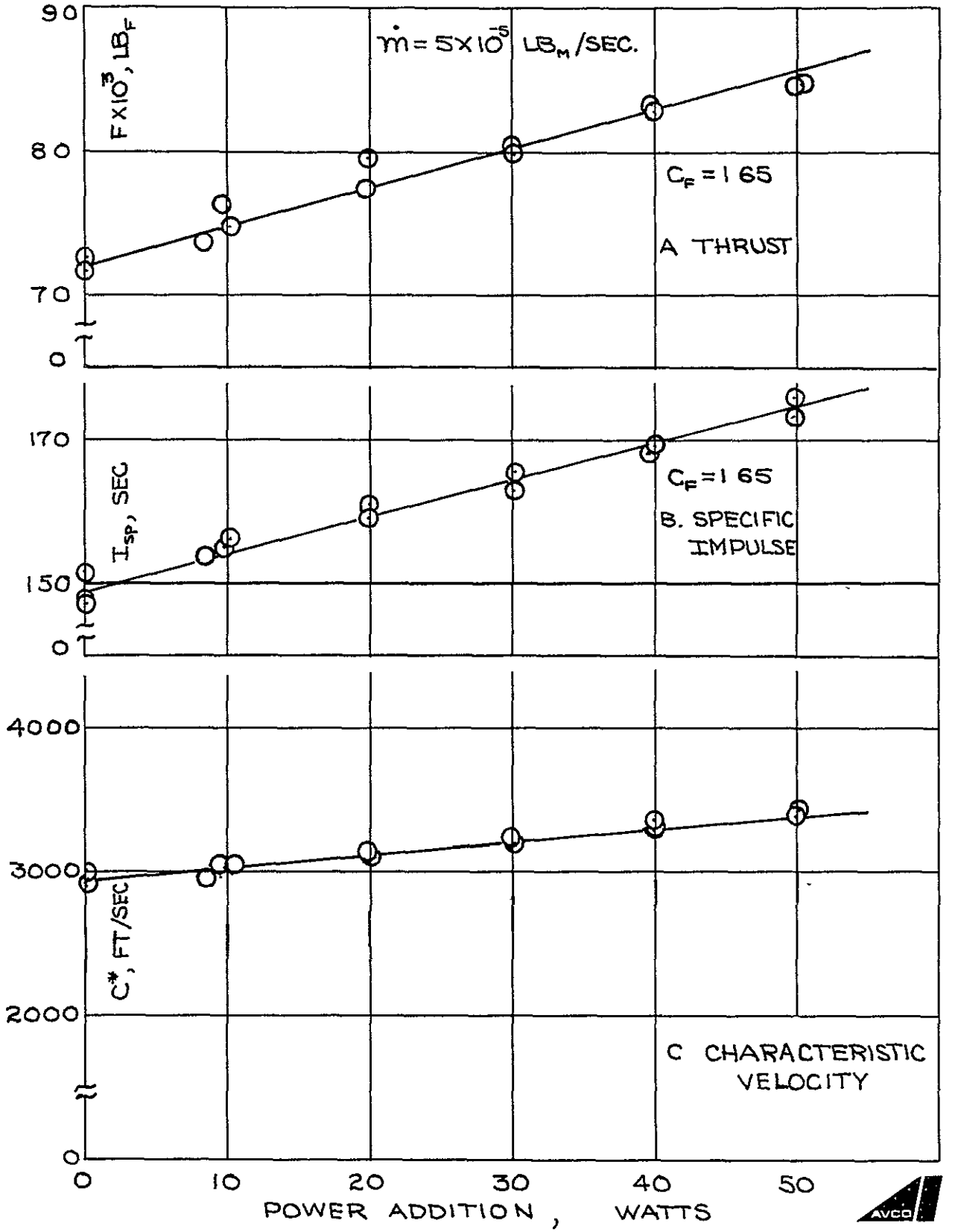

A cursory examination of this system indicates that the thermal efficiency of the entire system would be expected to be quite low. For example, energy released by decomposition within the porous ceramic cylinder can be conducted into the base plate or may be lost by radiation from the external surface of the porous ceramic to the surroundings through the transparent quartz tube. Furthermore, considerable energy may be lost through heat transfer from the decomposition products as they flow through the nozzle box assembly. It would be fortuitous if the system utilized in these preliminary experiments had a thermal efficiency much greater than 0 3-0.4. If a similar estimate is made of the efficiency of energy addition by means of the heater coils, it is immediately obvious that at least 50 percent of the power is lost by radiation to the surroundings.

Visual observation of the thruster through the transparent quartz walls was conducted during all these experiments It was observed that at low propellant flow rates the decomposition of propellant occurred primarily in the region close to the thruster base plate. As the flow rate is increased the reaction zone became more extensive and extended further in the downstream direction.

In spite of the deficiencies noted above, the configuration "C" thruster demonstrated restart capabilities without power application For example, with the thruster operating at steady state, the propellant valve was closed for periods ranging from 30 to 200 sec. Upon reopening the valve, propellant ignition was found to occur The difficulty encountered in the restart was dependent on the length of the off period and the magnitude of the propellant flow rate as is shown by the experimental records obtained in these investigations (Figs. 20-33) At low flow rates, rise times in the range of 5 sec. were achieved for off times on the order of 70 sec.

In several instances, there was evidence of partial flooding of the thruster (Figs. 27, 28) Immediately upon opening the propellant valve, the nozzle pressure was found to rise sharply for a period less than 1 sec. For the next 10 to 15 sec., the propellant flow rate was in excess of the final steady state flow rate, and there is an abrupt change in the slope of the pressure rise curve. After this period, steady state operation was achieved.

Attempts were made to obtain similar data with this configuration thruster mounted entirely within the vacuum system as a means of increasing thruster efficiency by elimination of convective losses from the thrust chamber external surfaces The problems encountered were as follows

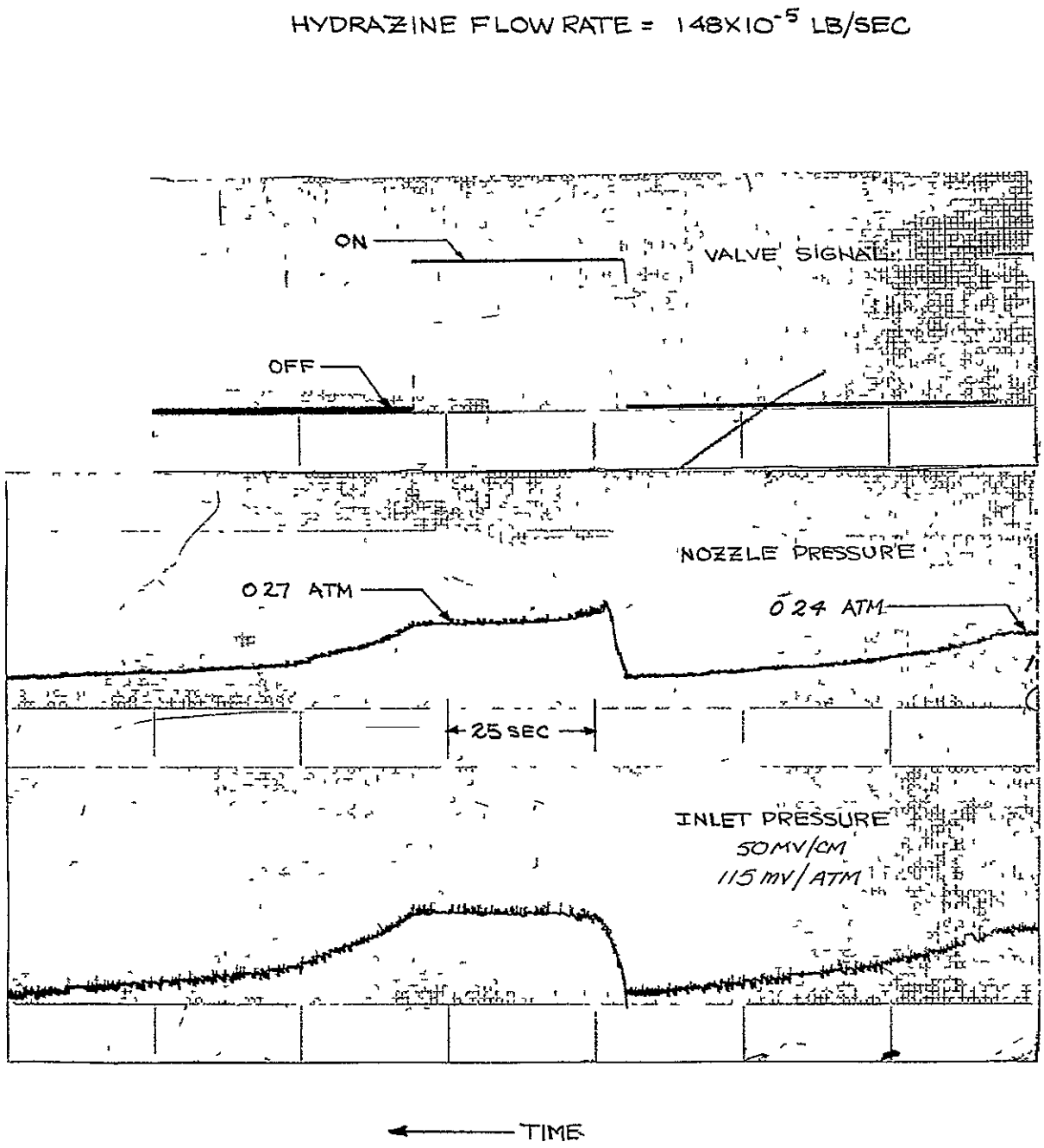

Fig 20 Configuration "C" Laboratory Thruster Transients (No Power)

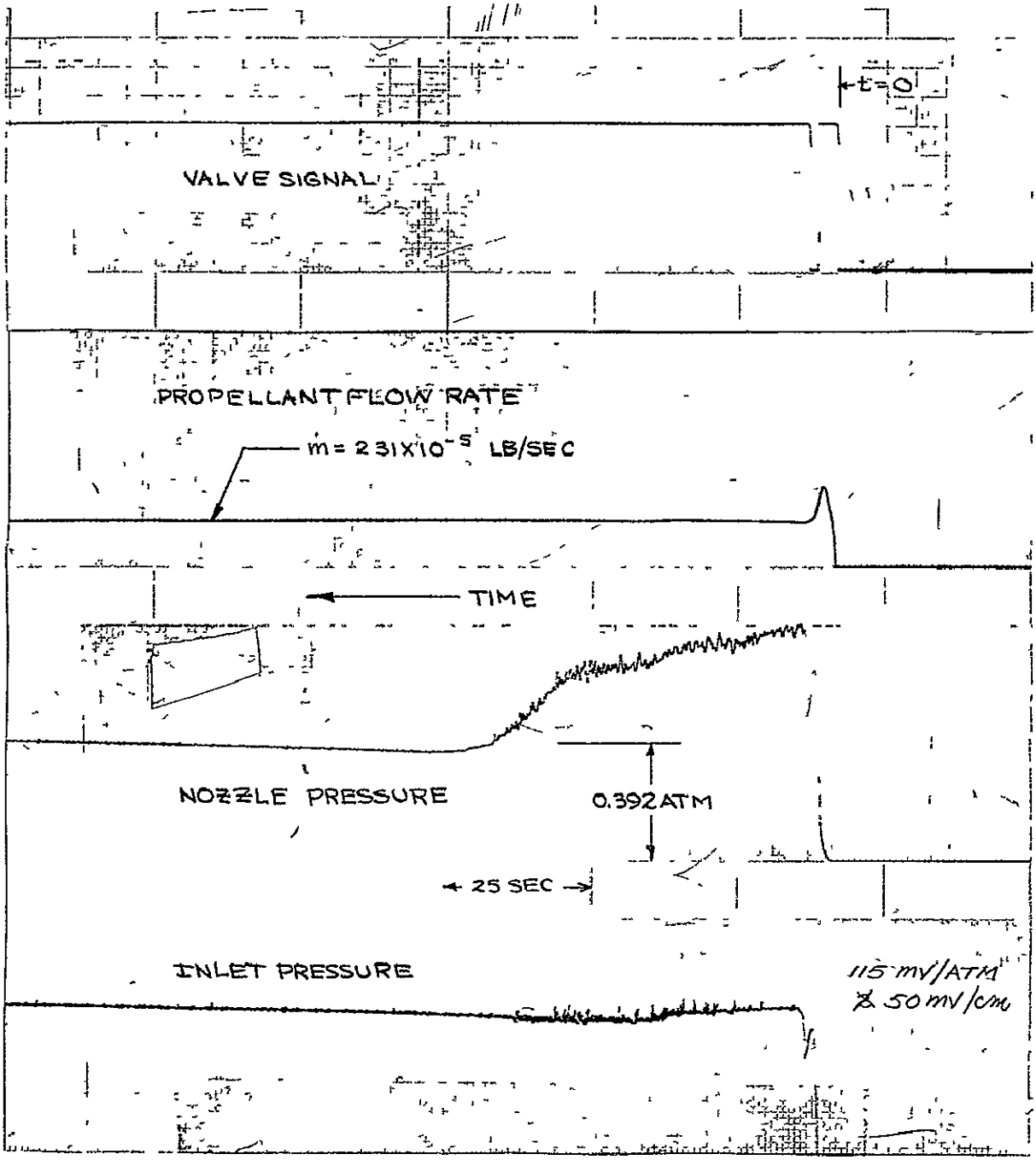

Fig. 21 Configuration "C" Laboratory Thruster Transients (20 watts)

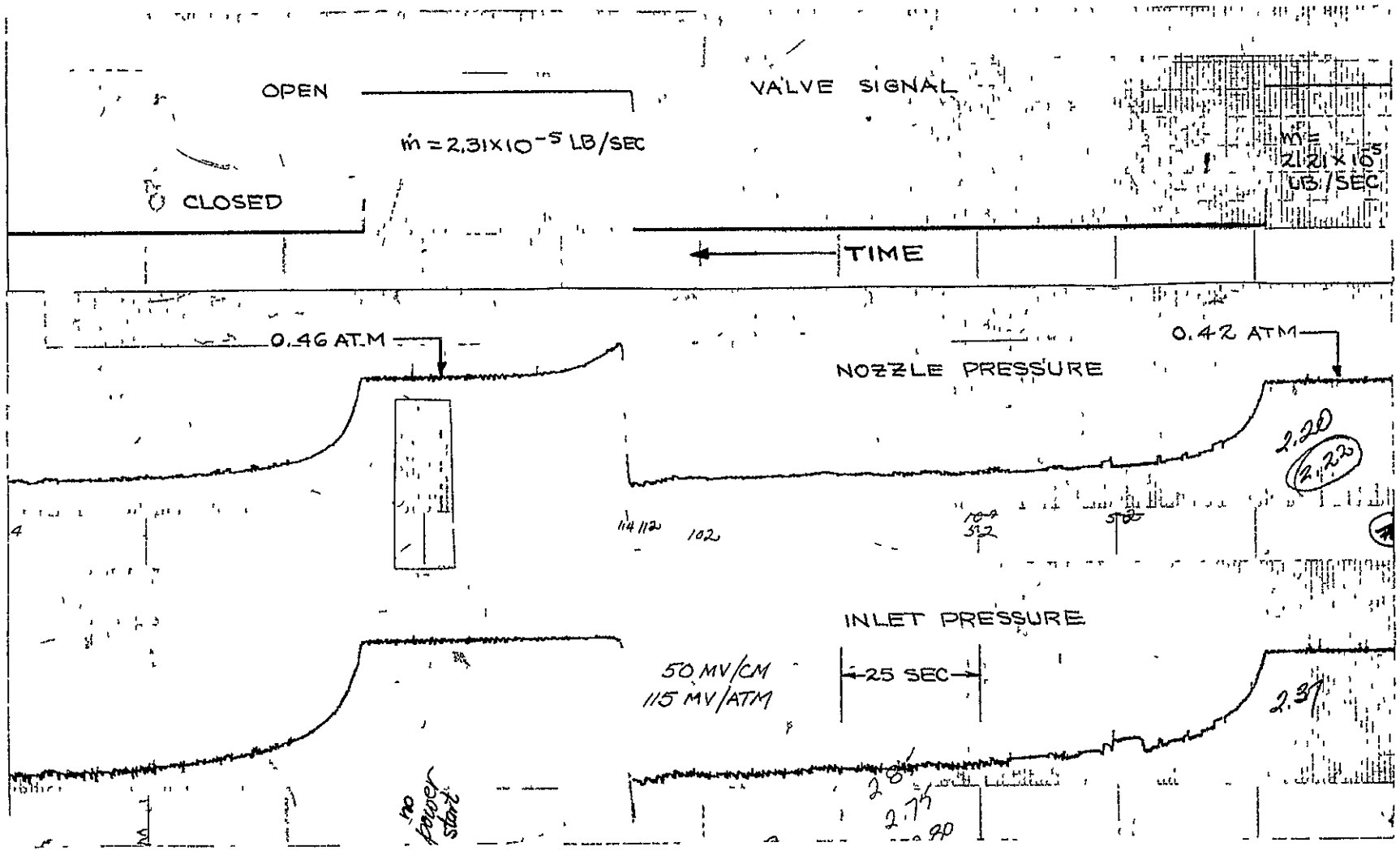

Fig 22. Configuration "C" Laboratory Thruster Transients (No Power)

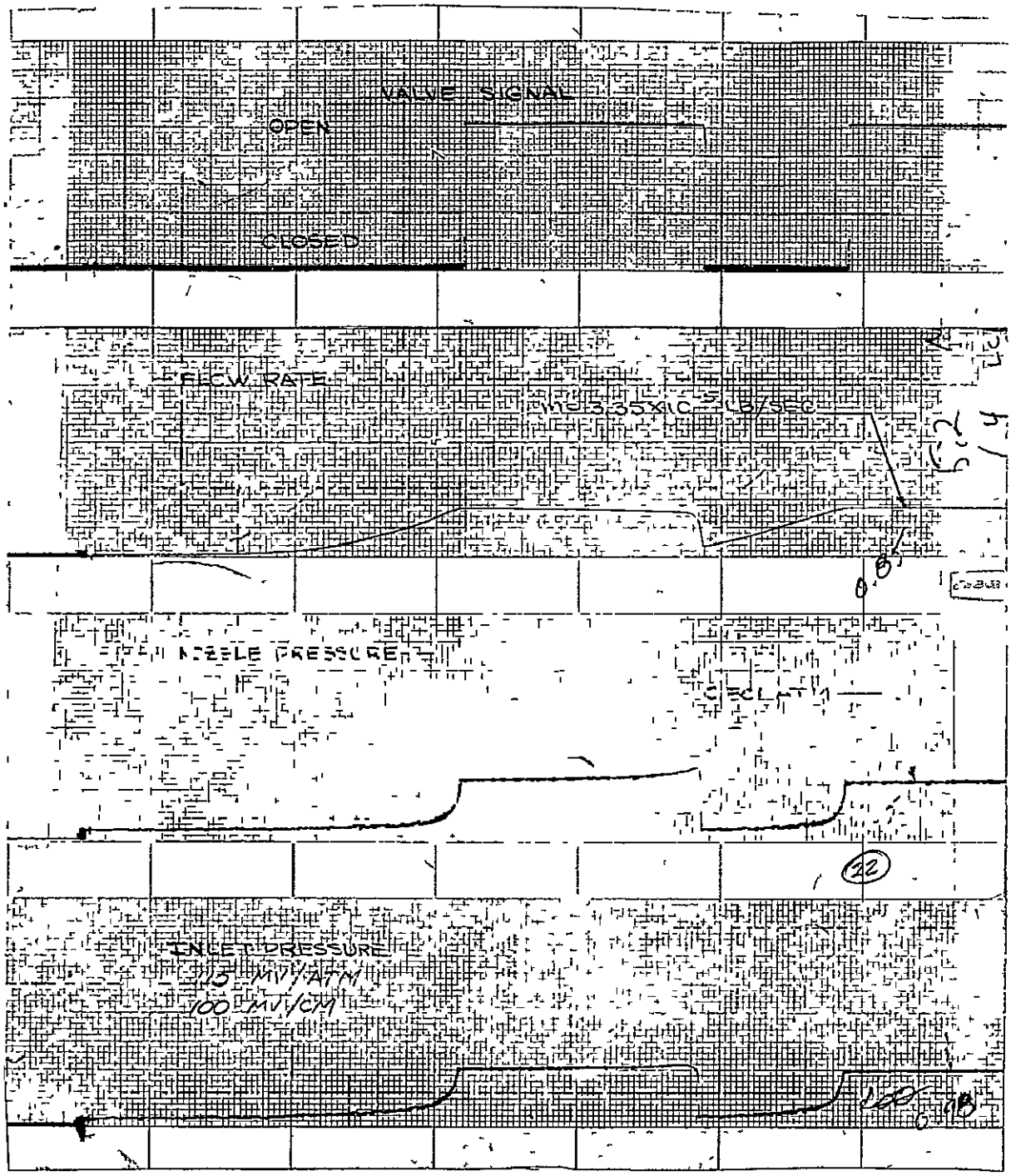

Fig. 23 Configuration "C" Laboratory Thruster Transients (No Power)

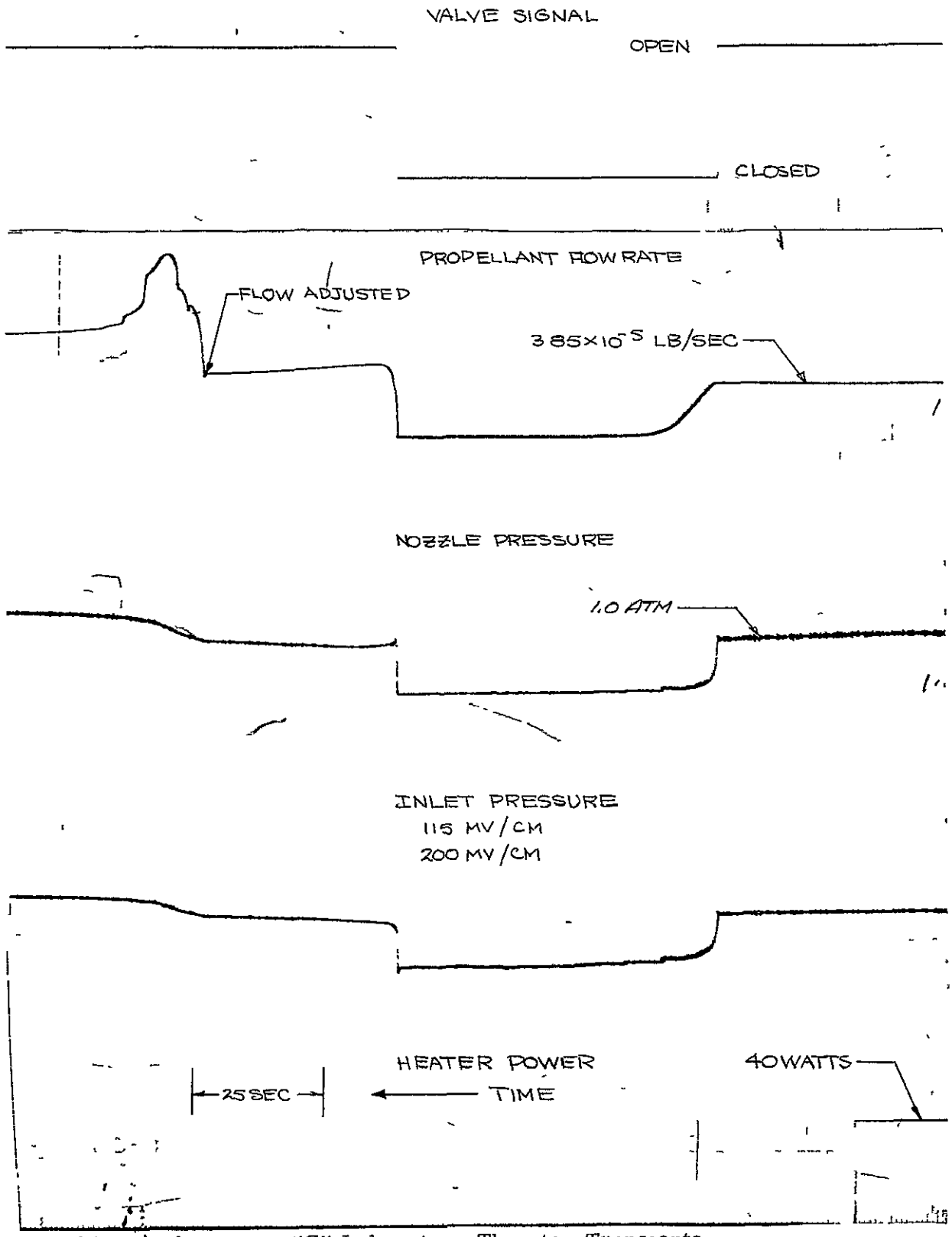

Fig. 24. Configuration "C" Laboratory Thruster Transients

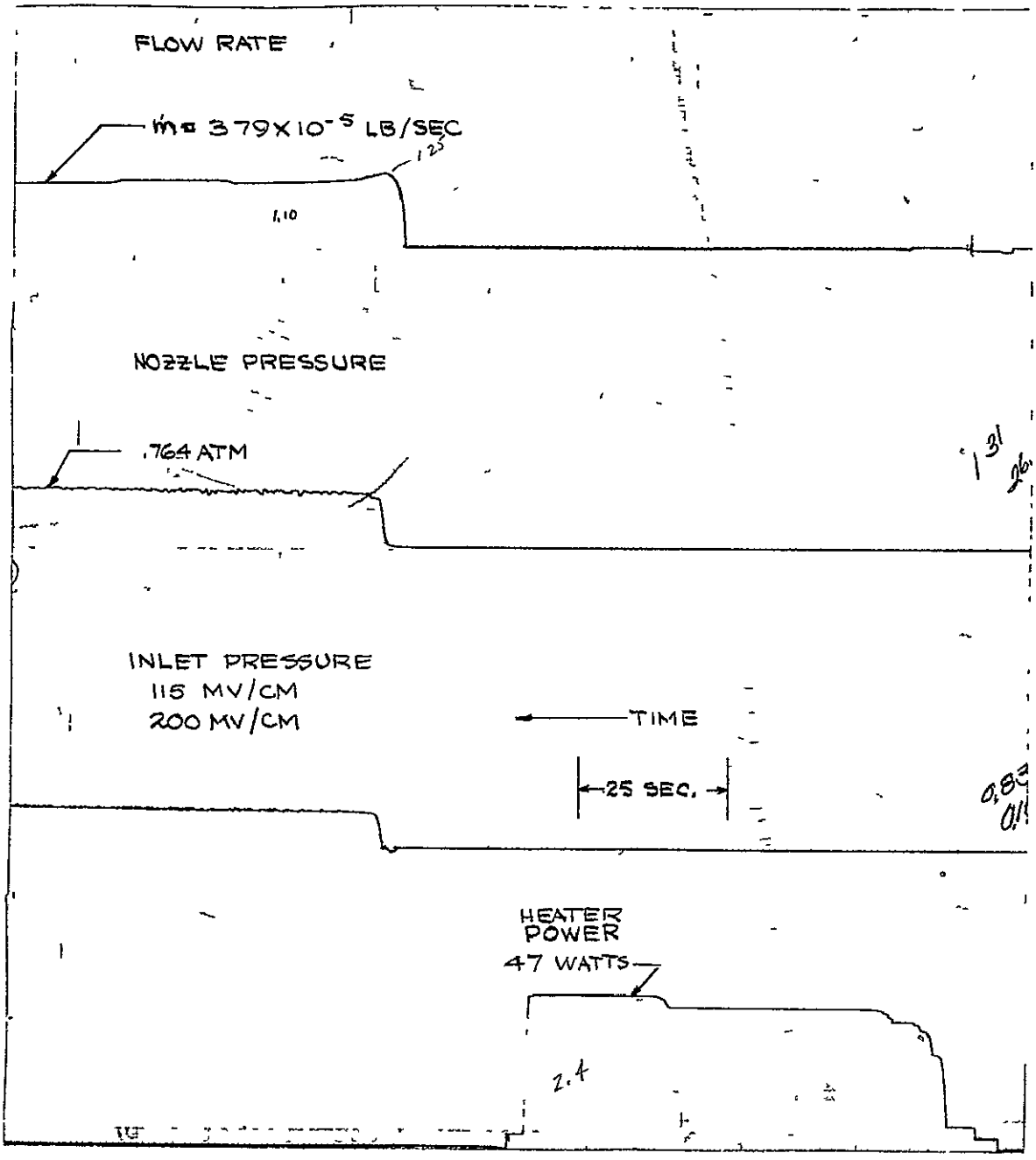

Fig. 25. Configuration "C" Laboratory Thruster Transients

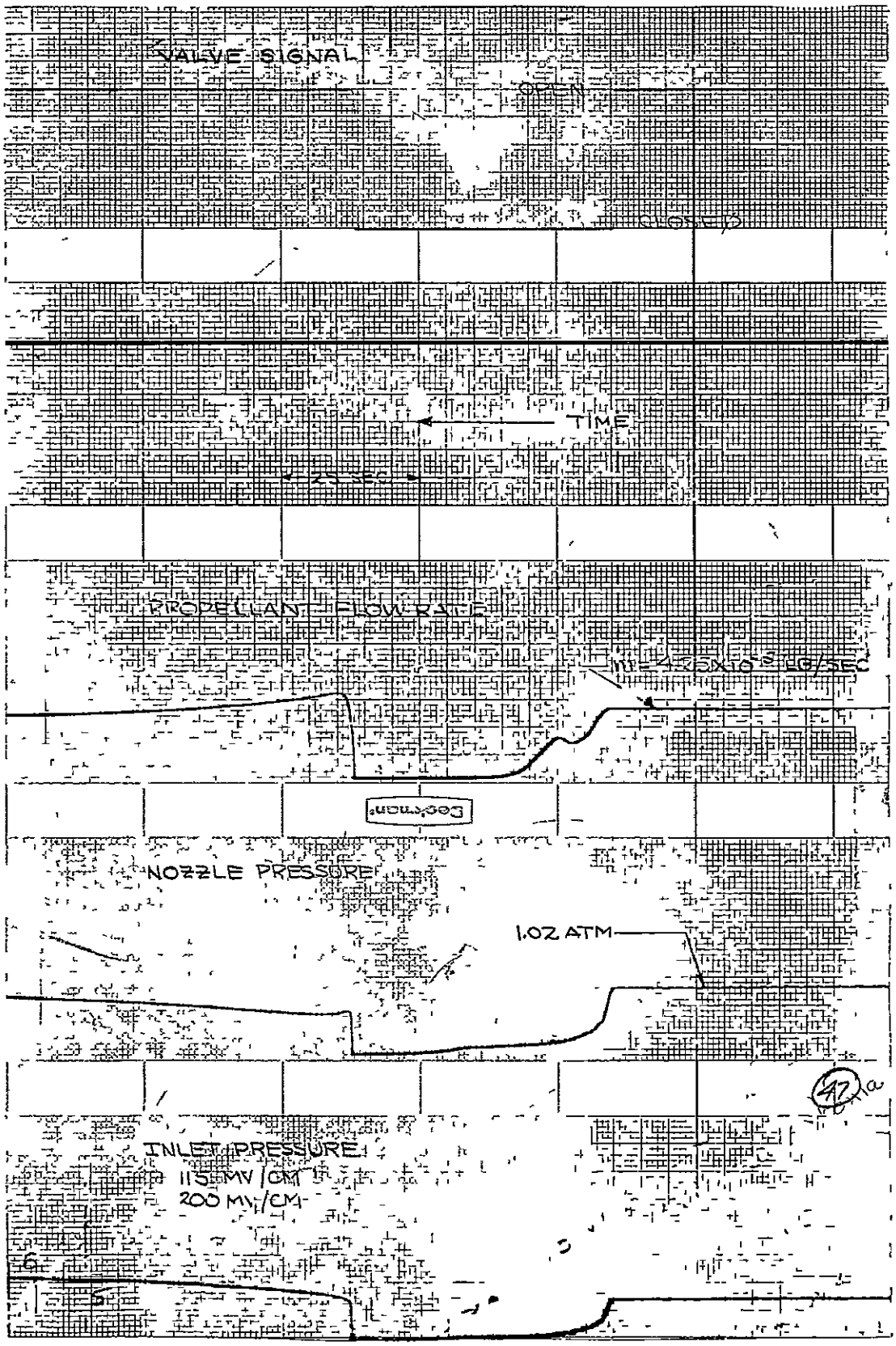

Fig. 26. Configuration "C" Laboratory Thruster Transients (No Power)

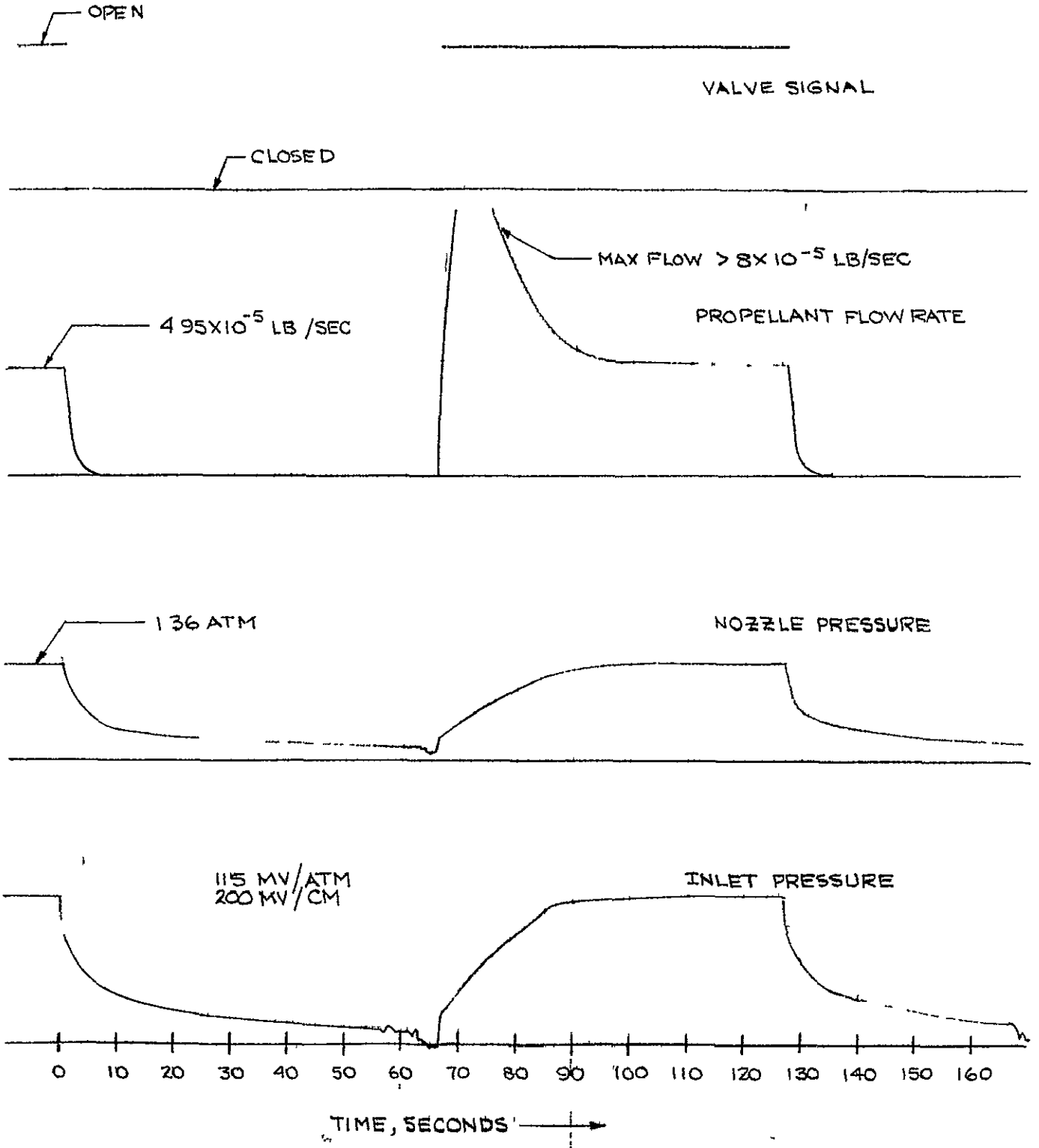

Fig. 27. Configuration "C" Laboratory Thruster Transients (No Power)

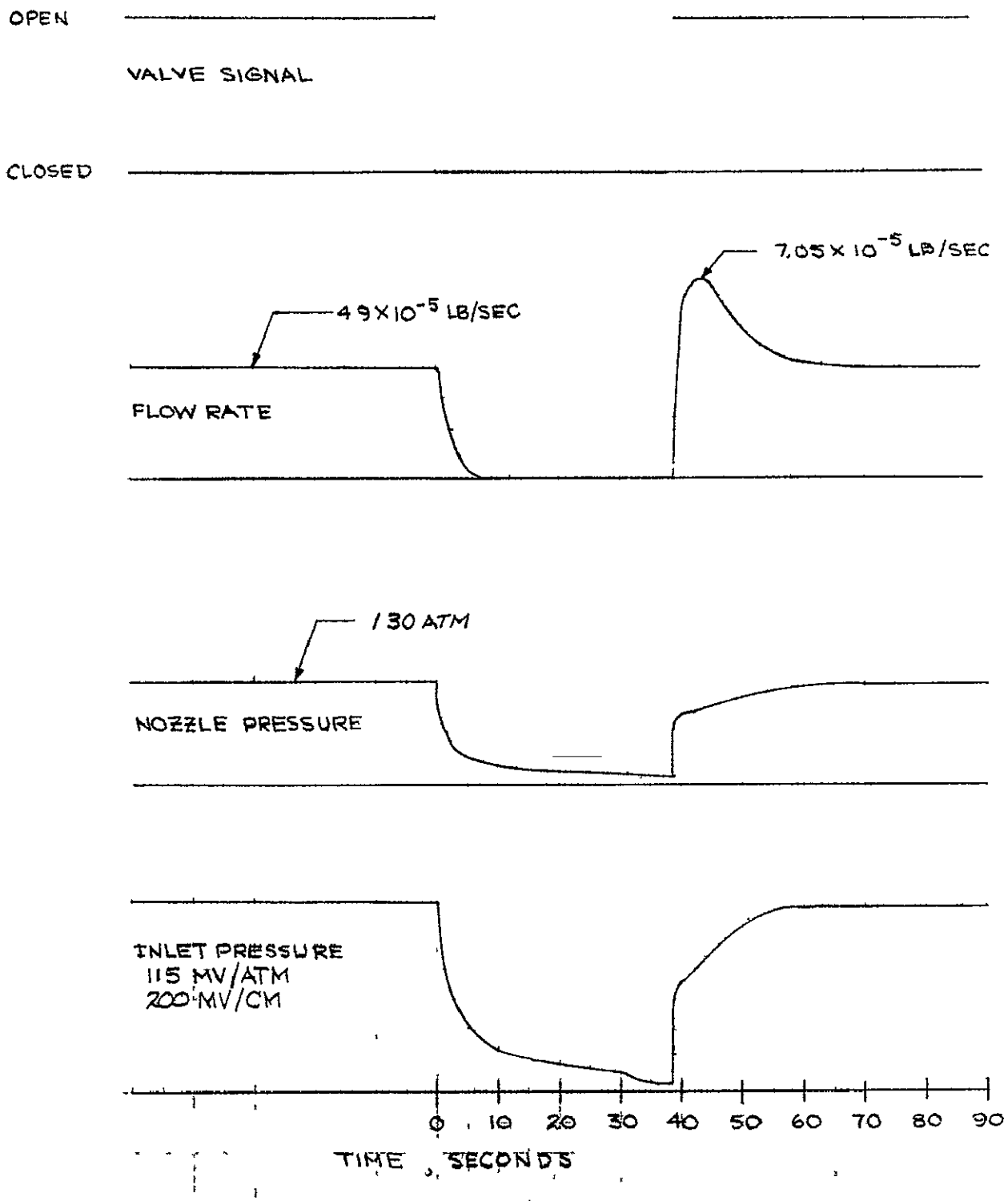

Fig. 28. Configuration "C" Laboratory Thruster Transients (No Power)

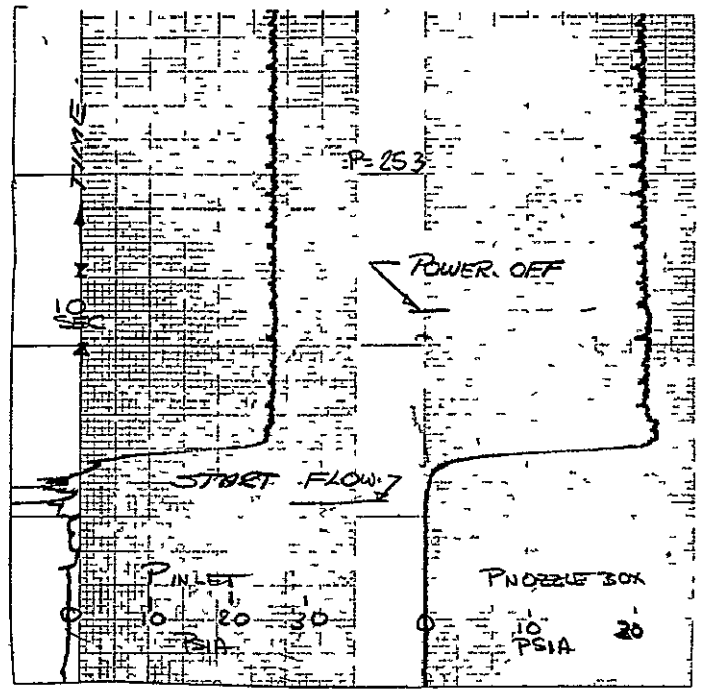

POWER 38 WATTS

OFF TIME 250 SEC

PREHEAT 50 SEC

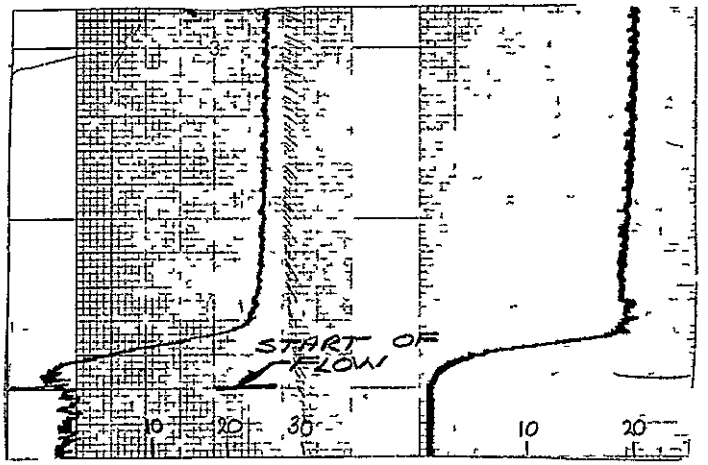

POWER 0 WATT

OFF TIME 150 SEC

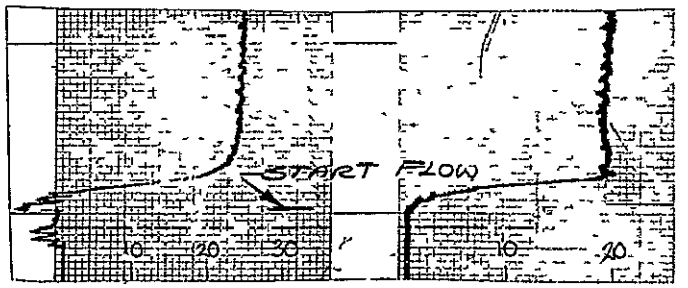

POWER 0 WATT

OFF TIME 100 SEC

FIG 29 INITIATION TRANSIENTS, CONFIGURATION C
LABORATORY THRUSTER (4.9×10^{-5} LB/SEC)

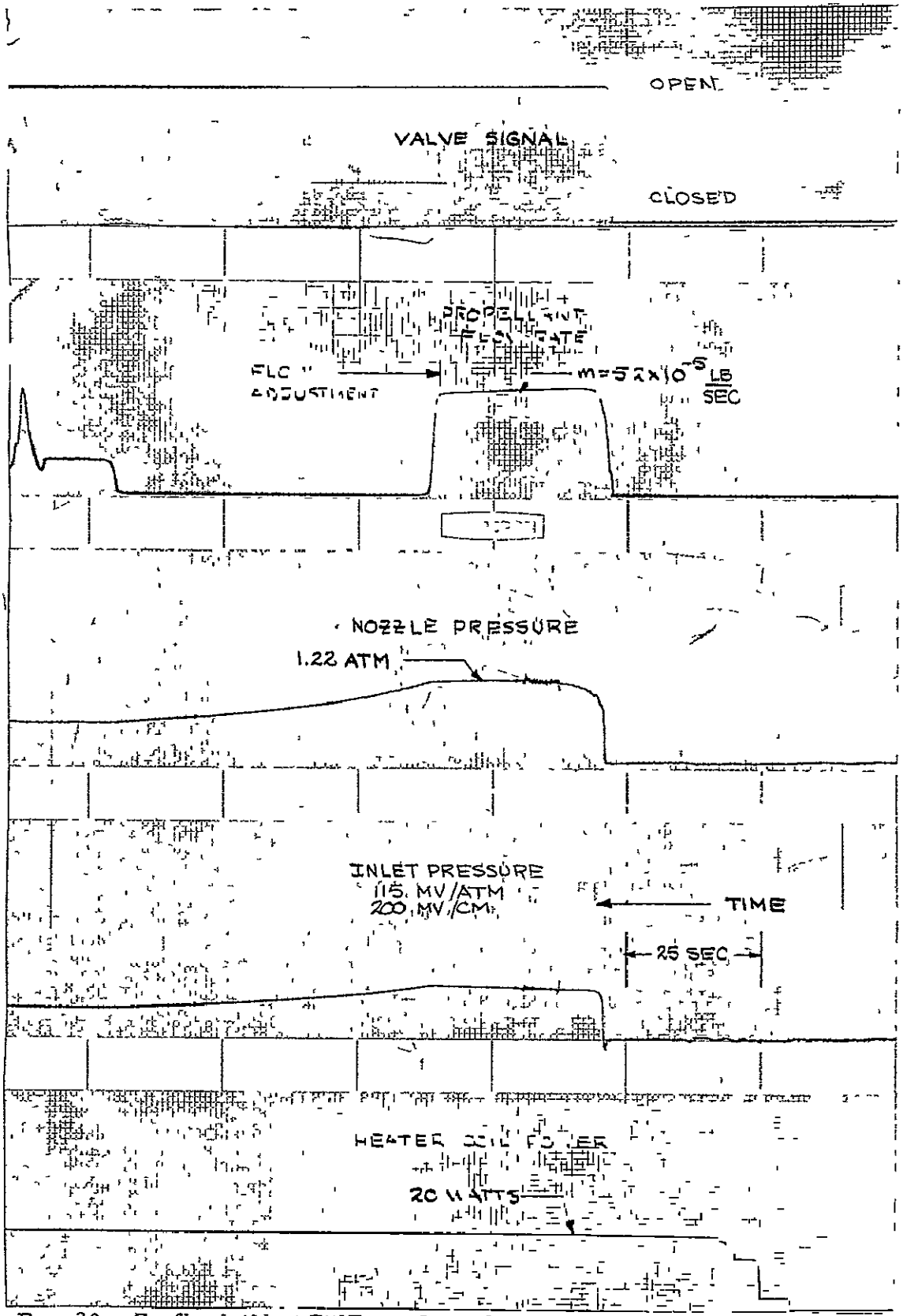

Fig. 30. Configuration [illegible]

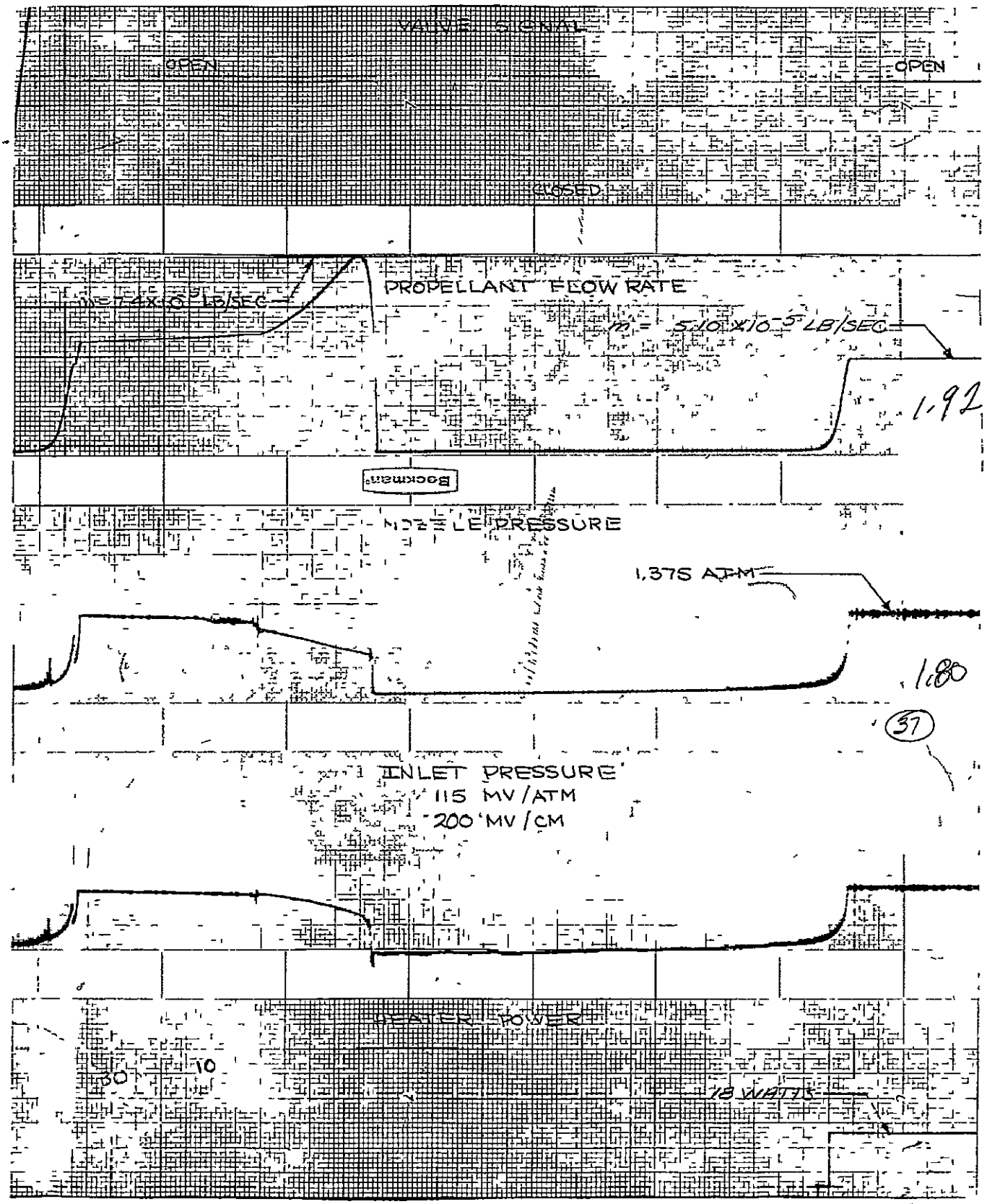

Fig 31. Configuration "C" Laboratory Thruster Transients

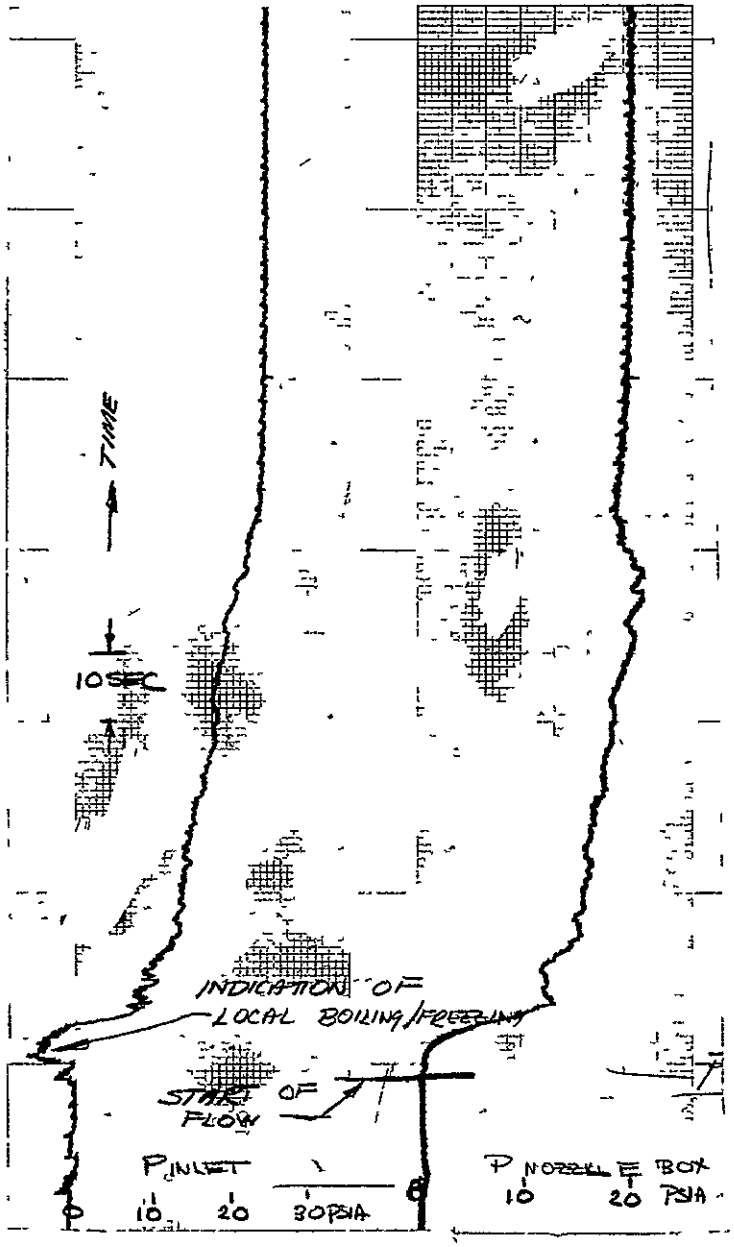

FIG 32. INITIATION TRANSIENTS, CONFIGURATION C
LABORATORY THRUSTER

2⊕

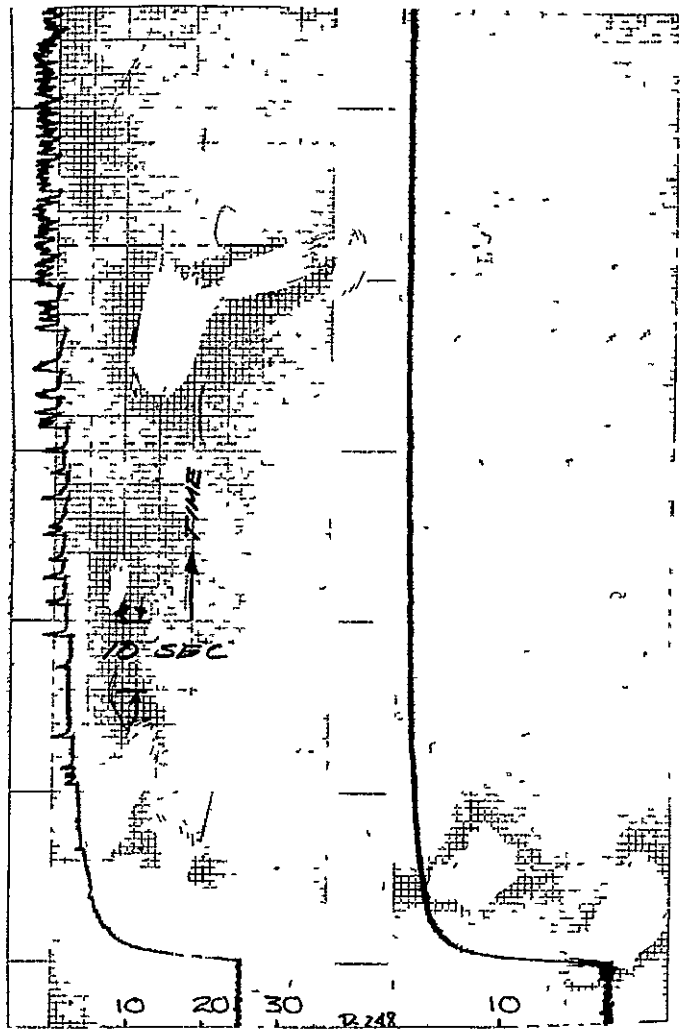

0 WATT

FIG 33 DECAY TRANSIENTS , CONFIGURATION C
LABORATORY THRUSTER

(i) Propellant leakage at the base of the porous zirconia injector, thereby allowing a portion of the propellant to be introduced into the thruster on the external surfaces of the zirconia. This produced fluctuations in the pressure in the thruster nozzle. The area of this leakage is designated as area "A" in Fig. 34 of this report.

(ii) During operation temperatures, the thruster achieved levels sufficient to cause decomposition of the O-ring seals, particularly that seal at the nozzle end of the thrust chamber The area of this problem is designated as area "B" in Fig. 34.

(iii) Increased temperature levels during vacuum operation produced failures in the metal-to-ceramic seals required at the points where the heater coils pass through the quartz outer shell of the prototype. The area of this problem is designated as area "C" in Fig. 34.

B) Preprototype Thruster

As a result of these problems, a second laboratory thruster was fabricated utilizing a metallic external (molybdenum) shell and with elimination of as many seals as possible. In fabricating this device which was denoted as a "preprototype thruster," insulation was placed between the thruster chamber and the external shell, a configuration "D" injector system was incorporated to move the reaction zone away from the thruster base plate, and the device was made sufficiently rugged so as to make it possible for the unit to be disassembled and reassembled without fear of damage A drawing of this device is presented in Fig 35 The stainless steel injection tube employed in this device was a commercially available hypodermic tube (0.025 in o.d. x 0 015 in. i.d.) having an internal diameter less than the quenching distance of hydrazine (0.045 in) as reported by Gerstein.[11]

Experimental performance data (characteristic velocity) were initially obtained with the preprototype thruster over the range of 1×10^{-5} to 5×10^{-5} lb/sec propellant flow rates to provide a direct comparison between this unit and the laboratory devices utilized previously These results are illustrated in Figs. 36 and 37 with the performance shown as characteristic velocity, C*, as a function of power addition at a propellant flow rate of 5×10^{-5} lb/sec It is immediately obvious that the new prototype gives a considerably better performance than the previous prototype. For example, in the unpowered mode of operation, the new thruster had a characterististic velocity of 3400 ft/sec as compared to 2900 ft/sec with the older device. It is also interesting to note that the characteristic velocity during unpowered operation with the new thruster is greater than that obtained with the old device even with the addition of 50 watts of power. During unpowered operation, the new prototype would have a specific impulse of 172 sec and a delivered

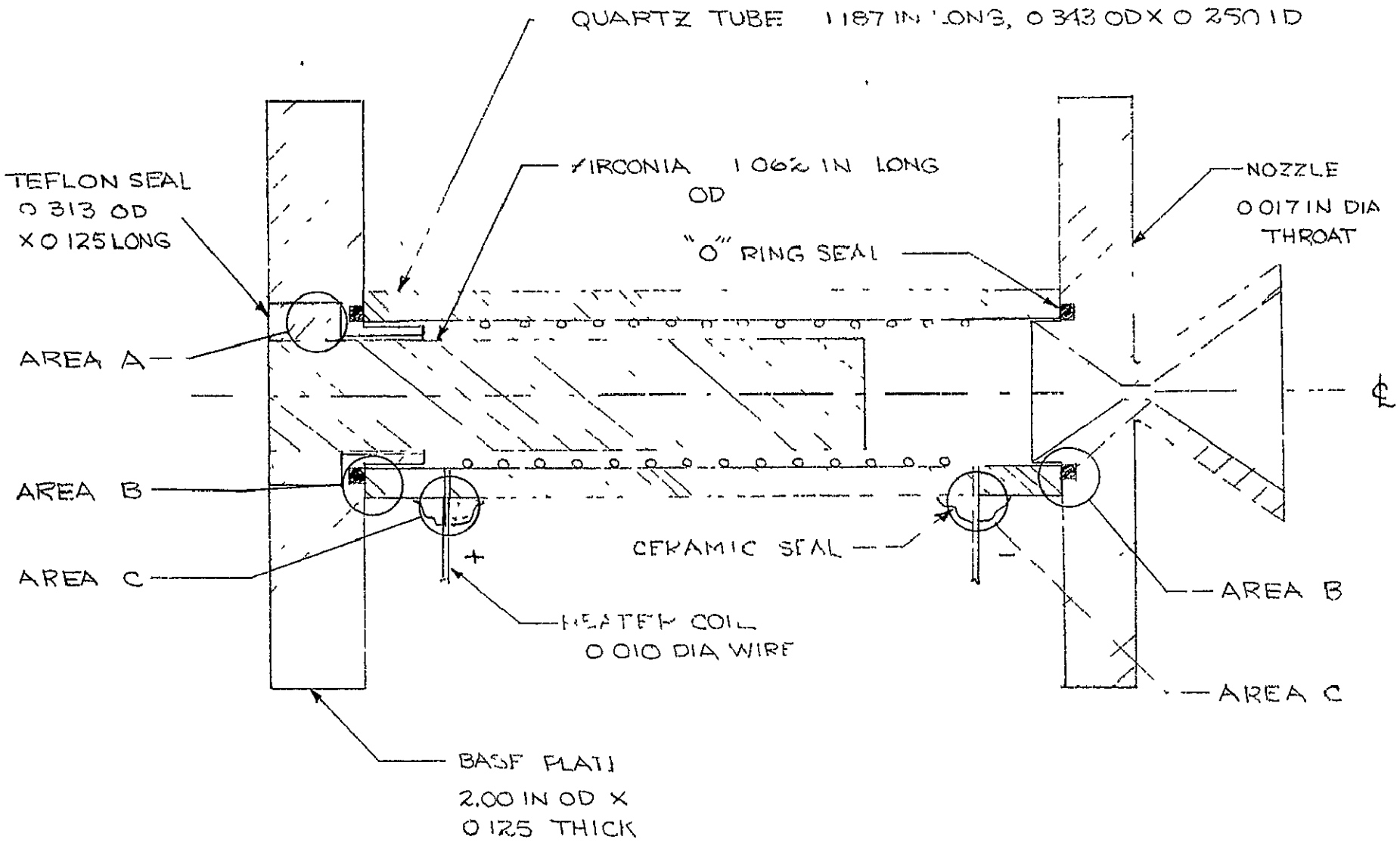

FIG 34 LABORATORY THRUSTER, CONFIGURATION C

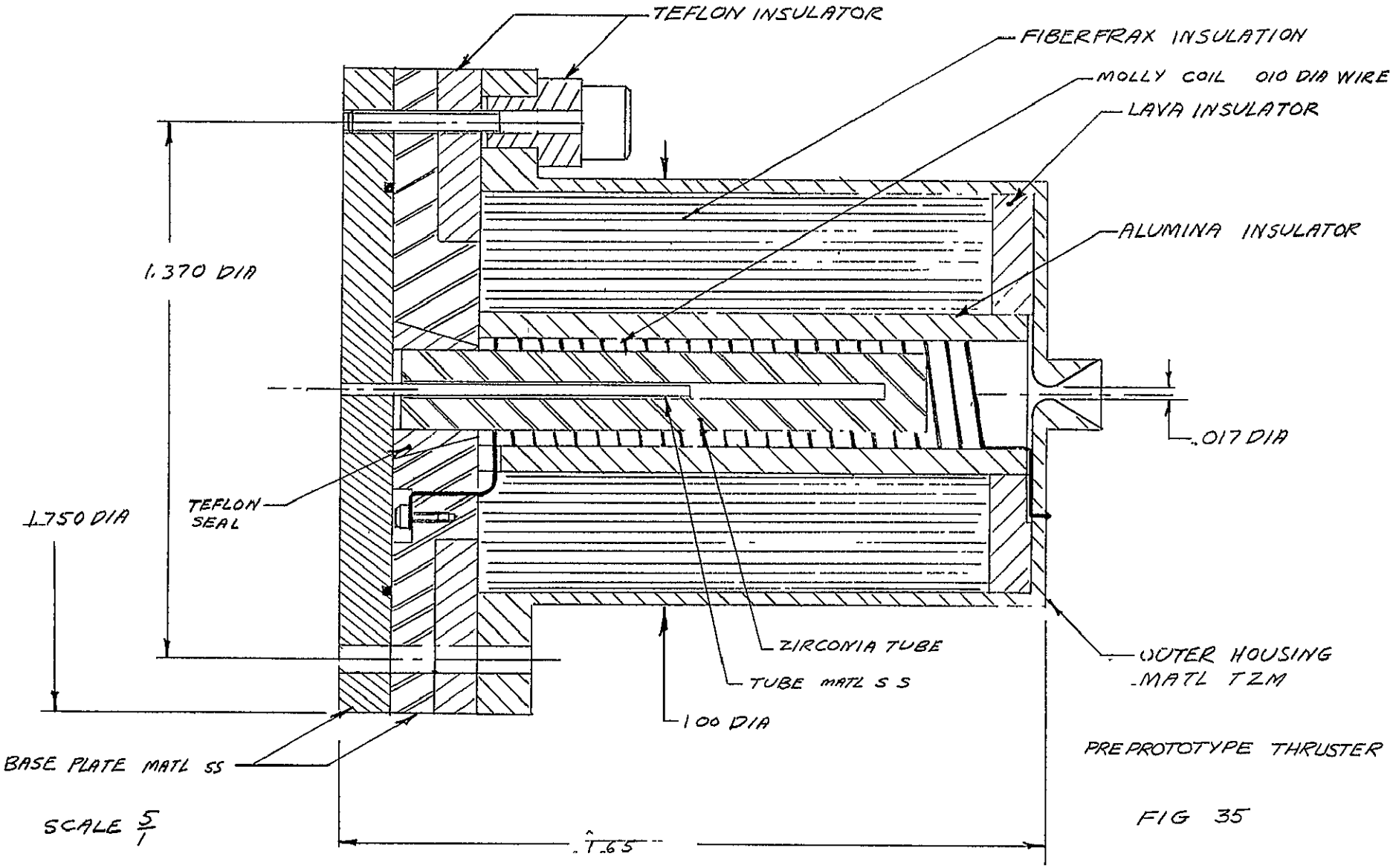

PRE PROTOTYPE THRUSTER

FIG 35

FIG. 36 COMPARISON OF THRUSTER PERFORMANCE

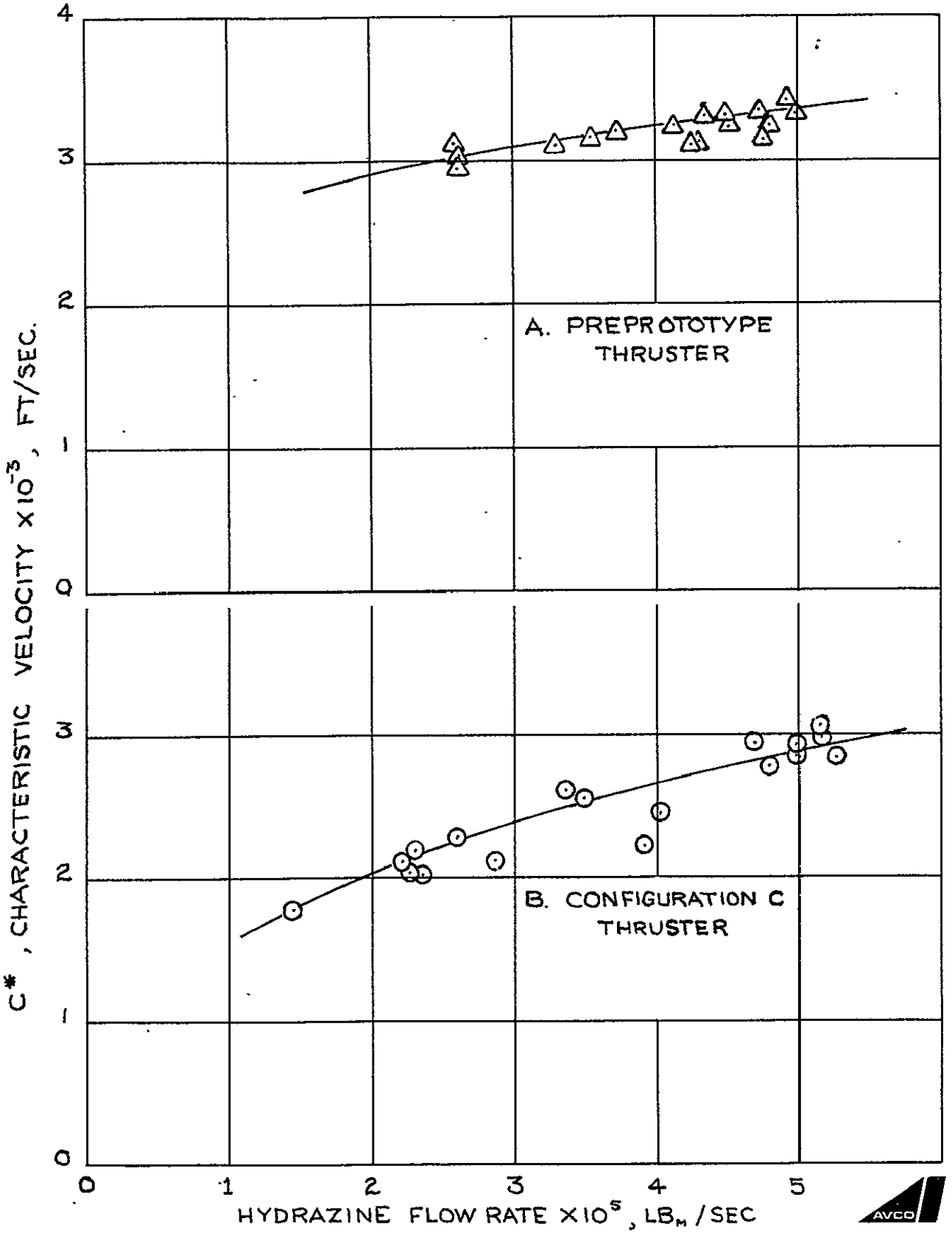

FIG 37 COMPARISON OF THRUSTER PERFORMANCE

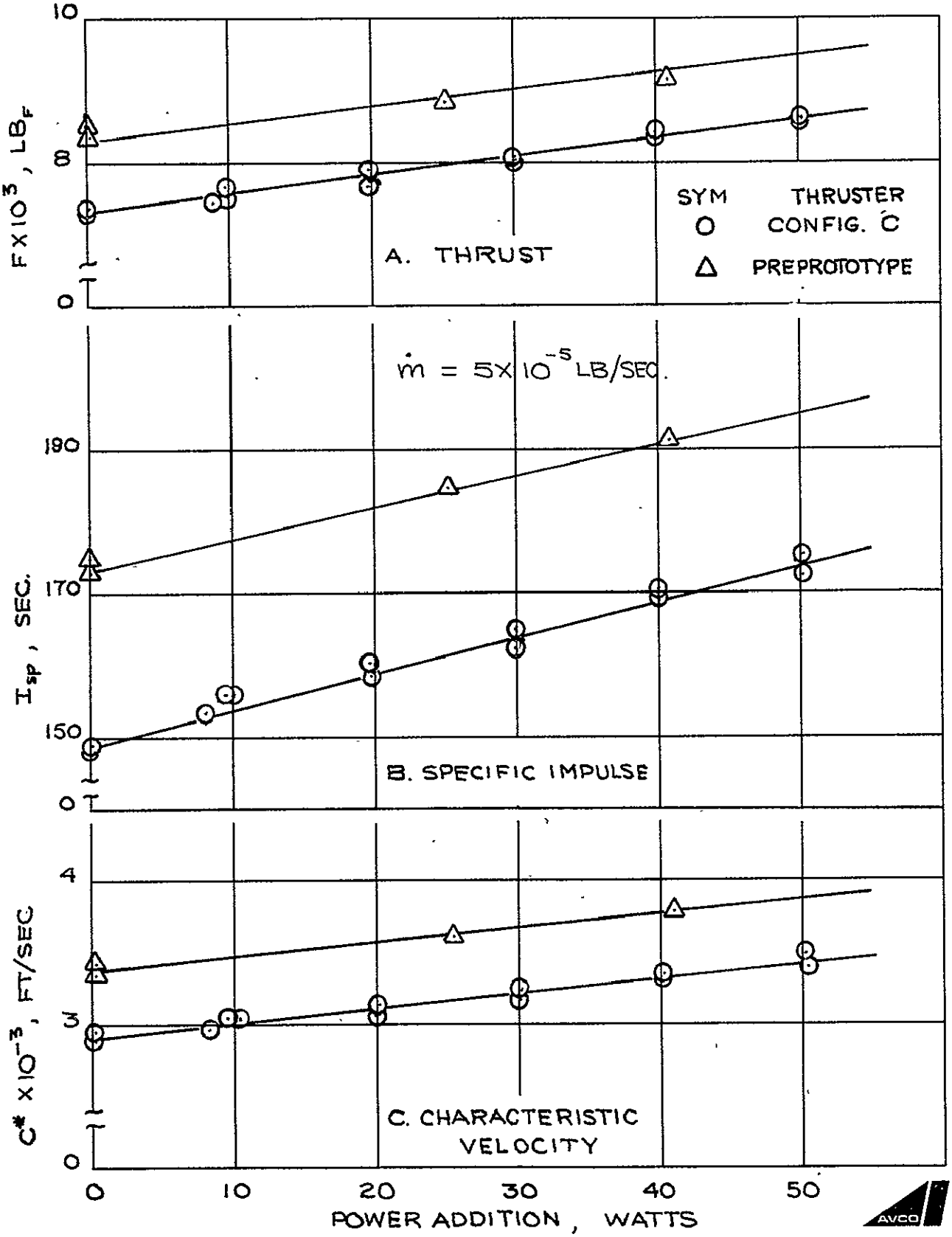

thrust of 8 7 x 10^{-3} lb_f with an assumed thrust coefficient of 1 65 Hence, a thrust level of 10 millipounds could be obtained by increasing the propellant flow to a value of 5 71 x 10^{-5} lb_m/sec

During powered operation, a power addition of 41 watts resulted in an increase in the characteristic velocity from 3400 ft/sec to a value of 3750 ft/sec, and the specific impulse to a value of 192 sec from 172 sec obtained during unpowered operation

Additional data were obtained during unpowered operation at flow rates over the range of 1 5 x 10^{-5} to 10 x 10^{-5} lb/sec as shown in Fig 38 in the form of characteristic velocity as a function of propellant flow rate The characteristic velocity was found to increase monotonically over the entire flow range investigated varying from approximately 2000 ft/sec to 4000 ft/sec at 10 x 10^{-5} lb/sec at feed rates of 1 5 x 10^{-5} and 10 x 10^{-5} lb/sec, respectively This behavior is characteristic of a system with heat losses which are dependent on the propellant flow rate as can be demonstrated by the following analysis. A material balance on the thruster may be written in terms of molar flow rates as

$$n_o - n = r_n V \tag{53}$$

where r_m is the molar generation rate per unit volume (V). For the chemical reaction

$$R \longrightarrow \nu P \tag{54}$$

The molar generation is related to the reaction rate of the reactant·

$$(\nu - 1)\, r = r_m \tag{55}$$

For a first order reaction

$$r = K[C_R] = k[C_R] \exp(-E/RT) \,. \tag{56}$$

with the concentration of the reactants given by

$$C_R = \frac{x_R P}{RT} \tag{57}$$

with the mole fraction (XR) is defined as

$$x_R = \frac{n_R}{n_R + n_P} = \frac{1-y}{1-y+\nu y} \tag{58}$$

where the quantity y is the fraction of reactants converted to products The input and output molar flow rates are also related for any fraction

FIG. 38 PREPROTOTYPE THRUSTER PERFORMANCE

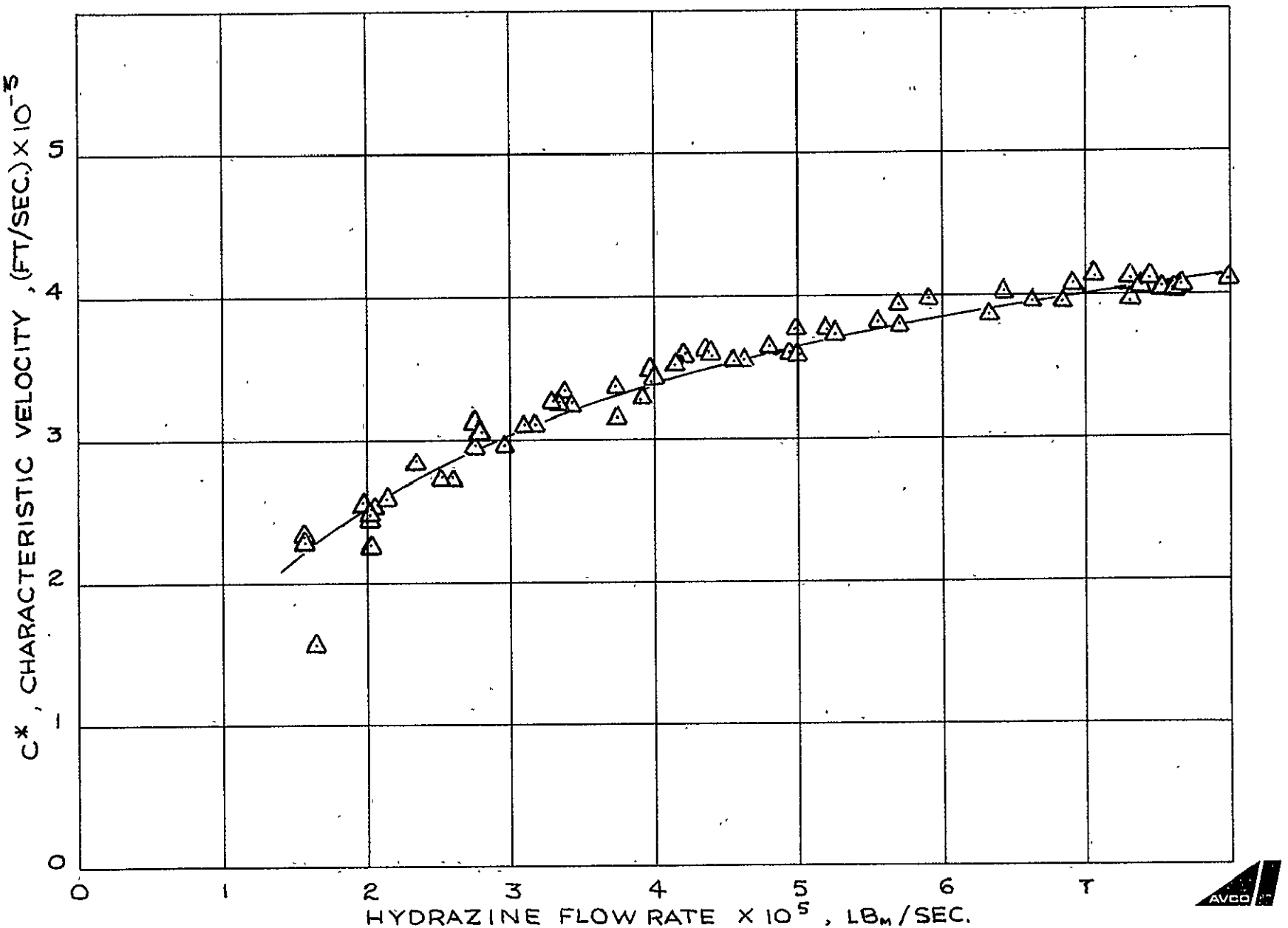

of propellant converted to products since

$$\dot{n}_o = (1 - y + \nu y)\,\dot{n}_i \tag{60}$$

Therefore,

$$y(\nu-1)\,\dot{n}_i = (\nu-1)\,rV \tag{61}$$

$$y\,n_i = rV \tag{62}$$

where

$$r = \left[\frac{1-y}{1-y+\nu y}\right]\frac{P}{RT}\,k\exp\left(-E/RT\right) \tag{63}$$

An energy balance on the thruster may be written in terms of mass flow rates as

$$m\left\{H_i - H\right\} + my\left\{-\Delta H_r\right\} + \frac{hA_w}{C_p}\left\{H_w - H\right\} = m\left\{H - H_o\right\} \tag{64}$$

where the term, $\frac{hA_w}{C_p}\left(H_w - H\right)$, represents the energy losses or addition to the system. Letting

$$H_i = H_o \tag{65}$$

$$my\left\{-\Delta H_r\right\} + \frac{hA_w}{C_p}\left\{H_w - H\right\} = \dot{m}\left\{H - H_o\right\}$$

or

$$y = \left\{\frac{H-H_o}{-\Delta H_r}\right\} - \frac{hA_w}{mC_p}\left\{\frac{H_w - H}{-\Delta H_r}\right\} \tag{66}$$

Substituting equation (62) into the above expression yields

$$\frac{rV}{n_i} = \left\{\frac{H-H_o}{-\Delta H_r}\right\} - \frac{hA_w}{\dot{m}C_p}\left\{\frac{H_w - H}{-\Delta H_r}\right\} \tag{67}$$

where

$$n_i = \dot{m}/M_i \tag{68}$$

with M_1 being the molecular weight of the inlet flow to the system Therefore

$$\frac{rVM_i}{m} = \left\{\frac{H-H_o}{-\Delta H_r}\right\} - \frac{hA_w}{mC_p}\left\{\frac{H_w - H}{-\Delta H_r}\right\} \tag{69}$$

which upon substitution of equation (63) for the reaction rate, r yields

$$\frac{PVM_i}{RTm}\left\{\frac{1-y}{1-y-\nu y}\right\} k \exp\left(\frac{-E}{RT}\right) = \left\{\frac{H-H_o}{-\Delta H_r}\right\} - \frac{hA_w}{\dot{m}C_p}\left\{\frac{H_w-H}{-\Delta H_r}\right\} \tag{70}$$

It is also noted that the mass flow through the system can be related to the pressure and nozzle exit area since

$$m = PA_N\sqrt{\frac{g\gamma M}{RT}\left(\frac{2}{\gamma+1}\right)^{\frac{\gamma+1}{\gamma-1}}} \tag{71}$$

where the molecular weight of the exit gases is

$$M = \frac{M_i}{1-y+\nu y} \tag{72}$$

which implies

$$\frac{PVM_i}{\dot{m}RT} = \frac{V}{A_N}\frac{(1-y+\nu y)^{1/2}}{\sqrt{\left(\frac{2}{\gamma+1}\right)^{\frac{\gamma+1}{\gamma-1}}\frac{g\gamma RT}{M_i}}} \tag{73}$$

A speed of sound a_i may be defined as

$$a_i = \left\{\frac{g\gamma RT}{M_i}\right\}^{1/2} \tag{74}$$

Hence, equation (70) may be written as

$$\frac{V}{A_N}\frac{k\exp(-E/RT)}{a_i\left[\frac{2}{\gamma+1}\right]^{\frac{\gamma+1}{2(\gamma-1)}}}\frac{1-y}{(1-y+\nu y)^{1/2}} = \frac{H-H_o}{-\Delta H_r} - \frac{hA_w}{mC_p}\left\{\frac{H_w-H}{-\Delta H_r}\right\} \tag{75}$$

or by use of equation (66)

$$\frac{V\,k\exp(-E/RT)}{A_N\,a_i\left(\frac{2}{\gamma+1}\right)^{\frac{\gamma+1}{2(\gamma-1)}}} = \frac{y(1-y+\nu y)^{1/2}}{1-y} \tag{76}$$

which relates the fraction of the inlet flow converted to reaction products and the characteristic length of the thruster since

$$L^* \equiv \frac{V}{A_N} \tag{77}$$

The effects of heat losses from the system (Hw < H) can be best seen from equation (75)

$$\frac{L^*\,k\exp(-E/RT)}{a_i\left(\frac{2}{\gamma+1}\right)^{\frac{\gamma+1}{2(\gamma-1)}}}\frac{1-y}{(1-y+\nu y)^{1/2}} = \frac{H-H_o}{-\Delta H_r} + \frac{hA_w}{\dot{m}C_p}\left\{\frac{H-H_w}{-\Delta H_r}\right\} \tag{78}$$

which may be written as

$$\left\{\frac{-\Delta H_r}{H-H_o}\right\}\frac{L^* K \exp(-E/RT)}{a_1\left(\frac{2}{\gamma+1}\right)^{\frac{\gamma+1}{2(\gamma-1)}}}\frac{(1-y)}{(1-y+\gamma y)^{1/2}} = 1+\frac{hA_w}{\dot{m}C_p}\left(\frac{H-H_w}{H-H_o}\right) \quad (79)$$

or

$$[f(T)]\frac{1-y}{(1-y+\gamma y)^{1/2}} = 1+\frac{hA_w}{\dot{m}C_p}\left(\frac{H-H_w}{H-H_o}\right) \quad (80)$$

As the losses increase, the characteristic temperature of the system decreases and f(T) becomes smaller Hence the quantity

$$[f(y)] = \frac{1-y}{(1-y+\gamma y)^{1/2}} \quad (81)$$

must increase. Since f(y) decreases monitonically with increasing values of the fraction of propellant decomposed, increasing heat losses implies a lower conversion of the feed to reaction products.

Equation(80) may also be employed to demonstrate that in a system which experiences heat losses, increasing the flow through the system can result in a greater amount of propellant decomposition thereby producing an increase in the characteristic temperature of the system. For simplicity, consider the system to have a constant wall temperature The non-dimensional heat loss term in equation (80) may be written as

$$\frac{hA_w(H-H_w)}{\dot{m}C_p(H-H_o)} = \frac{A_w}{A_f}\frac{\dot{q}}{\rho u(H-H_i)} = C_h\frac{A_w}{A_f} \quad (82)$$

where C_n is the Stanton number and A_f is the cross-sectional area for fluid flow through the system By definition

$$C_h \equiv \frac{Nu}{Re\,Pr} \quad (83)$$

with

$$Nu = K\,Re^n\,Pr^m \quad (84)$$

with the exponents n and m being less than unity The heat losses may then be expressed as

$$\frac{hA_w(H-H_w)}{\dot{m}C_p(H-H_o)} = \frac{A_w}{A_f}\left\{\frac{K}{Re^{1-n}\,Pr^{1-m}}\right\} \quad (84)$$

Since the Reynolds number is directly proportional to mass flow rate through the system

$$Re = \frac{\rho u D_e}{\mu} = \frac{m D_e}{\mu A_f} \tag{86}$$

For laminar flow through the system (i.e. n=0 50, m=0 33), equation (80) may be written as

$$[f(T)] \frac{1-y}{(1-y+\tau y)^{1/2}} = 1 + K \frac{A_w}{A_f} Pr^{-2/3} \left(\frac{m D_e}{\mu A_f} \right)^{-1/2} \tag{87}$$

This implies that increasing the mass flow decreases the dimensionless heat losses and results in an increase in characteristic temperature and the fraction of propellant converted to reaction products

The characteristic velocity data were utilized to calculate specific impulse and thrust using an assumed value of 1 65 for the thrust coefficient The results of the computations are shown in Fig. 39 Specific impulse is found to vary from 120 sec at 2×10^{-5} lb_m/sec flow rate to 210 sec at 8×10^{-5} lb_m/sec. The thrust level developed by the thruster varied from $2\ 4 \times 10^{-3}$ lb_f to $16\ 8 \times 10^{-3}$ lb_f over the same flow range This is also a considerable increase in performance over that obtained with the configuration "C" thruster as shown in Tables I and II

Data obtained by Schreib and Pugmire[8] with a configuration "C" thruster are included in Table I, whereas, the performance listed in Table II for this type of device is a composite of the two sets of data

A similar series of experiments were conducted to investigate thruster performance with power addition to the thruster heater coil using propellant flow rates of 2×10^{-5} to 5×10^{-5} lb_m/sec, and power inputs of 20 to 80 watts. The results of these tests are illustrated in Figs. 40-42 . At a flow rate of 4×10^{-5} lb_m/sec, power addition amounting to 80 watts was found to produce a 33 percent increase in thruster performance This is equivalent to a power requirement of 34 watts for each millipound of thrust enhancement Comparison of this result with predicted thrust enhancement curves indicates that the power addition process varies from 43 percent efficiency if constant chemical composition is assumed to be 55 percent efficient if the composition of the reaction products is considered variable

The heater current and voltage measurements obtained during the experimental determination of the effects of power addition on thruster performance can be employed to provide some indication as to the average heater coil temperature Since the heater coil is cemented to the internal surface of the alumina cylinder which forms the thrust chamber walls, this average temperature may be a good representative value for the thruster. The average temperature of the thrust chamber wall can be calculated from the resistance of the heater coil since the resistance of the molybdenum heater coil is linear in temperature The average heater coil temperature was then employed to calculate a characteristic velocity of

FIG. 39 PREPROTOTYPE PERFORMANCE, THRUST AND SPECIFIC IMPULSE

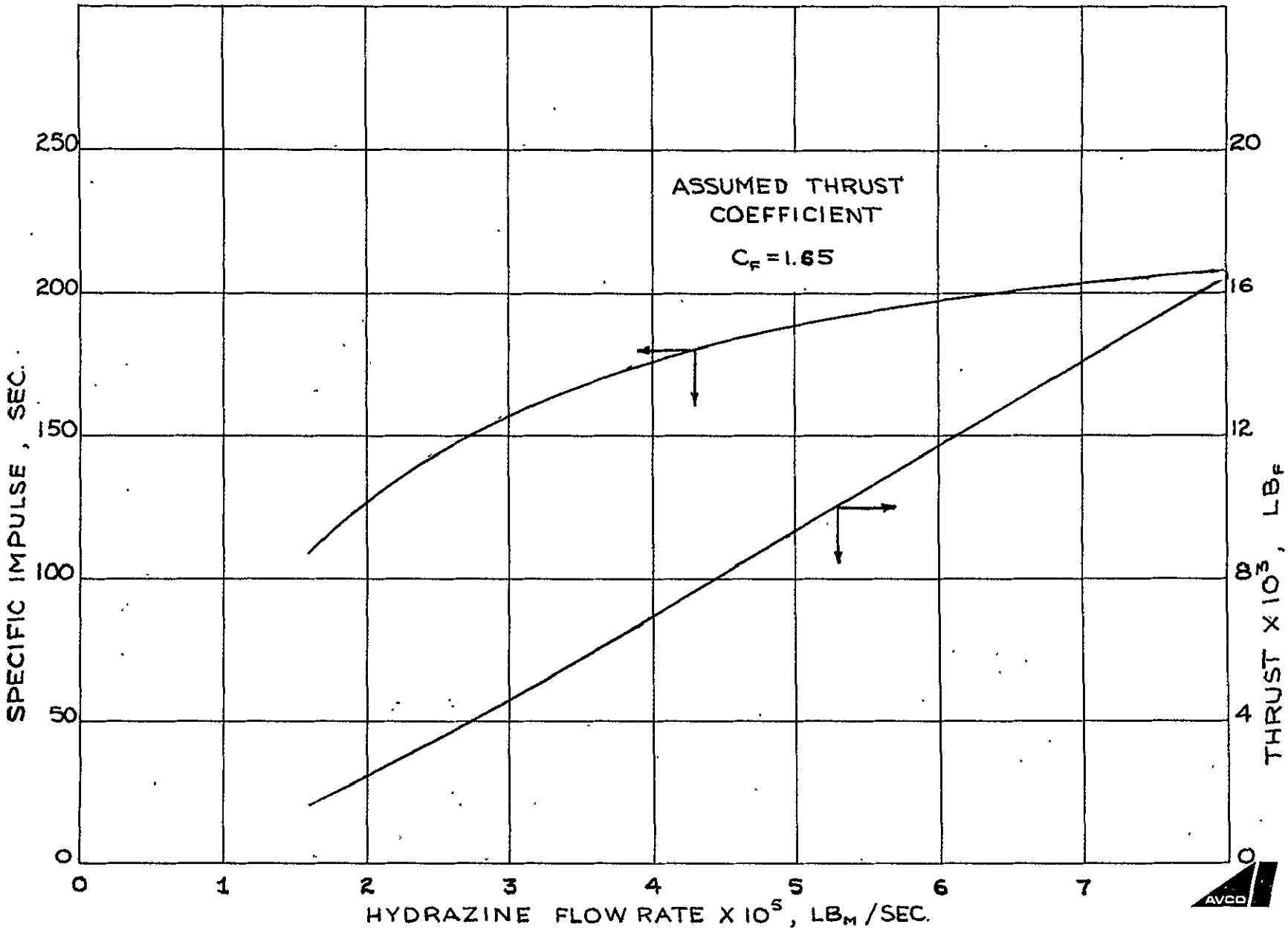

Table I

Comparison of Thruster Performance

Hydrazine Feed Rate lbm/sec	Characteristic Velocity, ft/sec		
	Configuration "c" Thruster Ref 7		Pre-prototype Thruster
2×10^{-5}	1900		2350
3×10^{-5}	2300		3025
4×10^{-5}	2650		3450
5×10^{-5}	2900	2800	3700
6×10^{-5}		2900	3900
7×10^{-5}		3000	4000
8×10^{-5}		3100	4100

Table II

Comparison of Thruster Performance

Hydrazine Flow Rate lbm/sec	Configuration "c" Thruster		Pre-protptype Thruster	
	Isp sec	Thrust lb_f	Isp sec	Thrust lb_f
2×10^{-5}	97	1.9×10^{-3}	120	2.4×10^{-3}
3×10^{-5}	118	3.5×10^{-3}	155	4.6×10^{-3}
4×10^{-5}	136	5.4×10^{-3}	177	7.1×10^{-3}
5×10^{-5}	143	7.2×10^{-3}	190	9.5×10^{-3}
6×10^{-5}	149	8.9×10^{-3}	200	12.0×10^{-3}
7×10^{-5}	154	10.8×10^{-3}	206	14.4×10^{-3}
8×10^{-5}	159	12.7×10^{-3}	210	16.8×10^{-3}

FIG. 40 EFFECT OF POWER ADDITION ON PREPROTOTYPE THRUSTER PERFORMANCE, CHARACTERISTIC VELOCITY

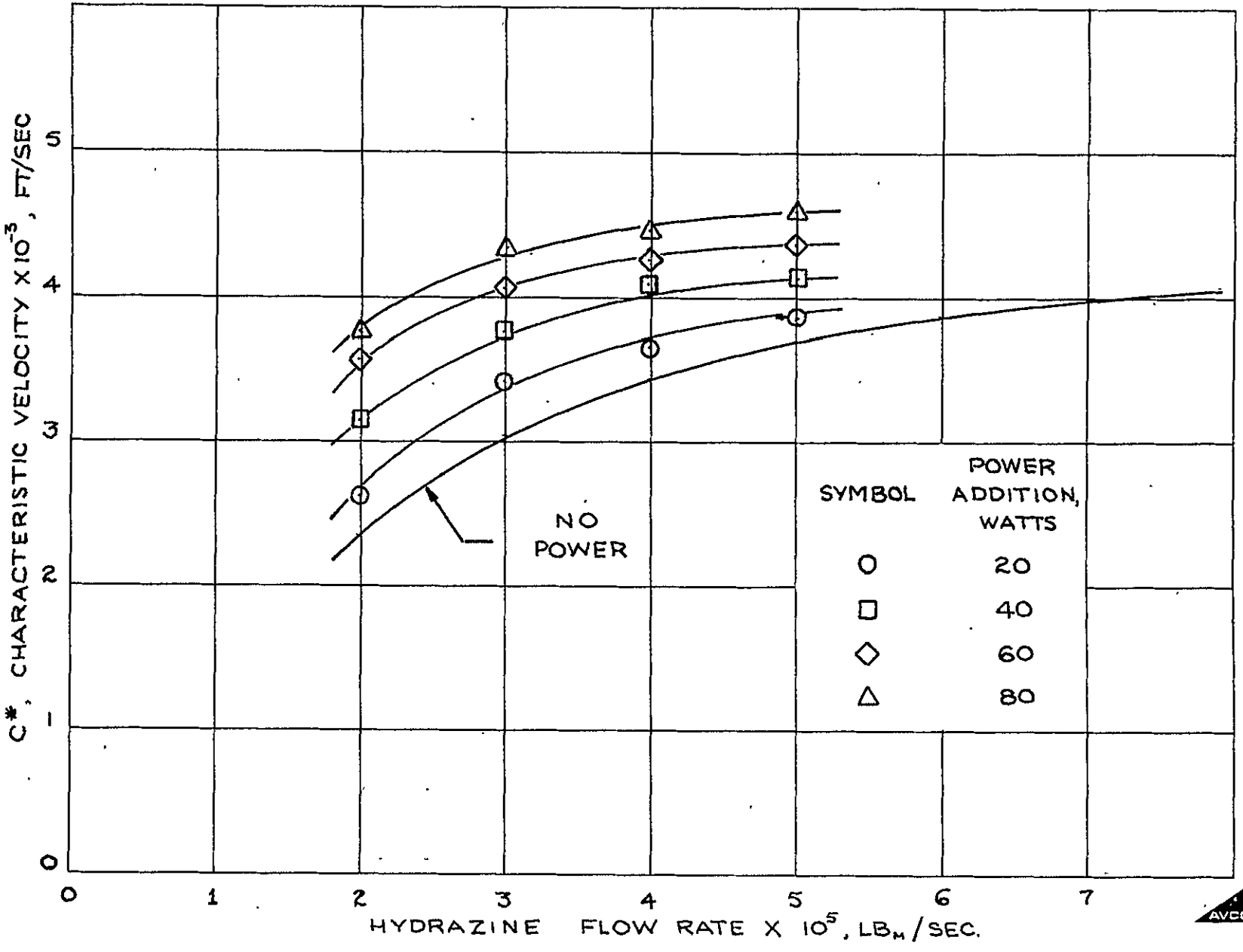

FIG. 41 EFFECT OF POWER ADDITION ON PREPROTOTYPE THRUSTER PERFORMANCE, THRUST

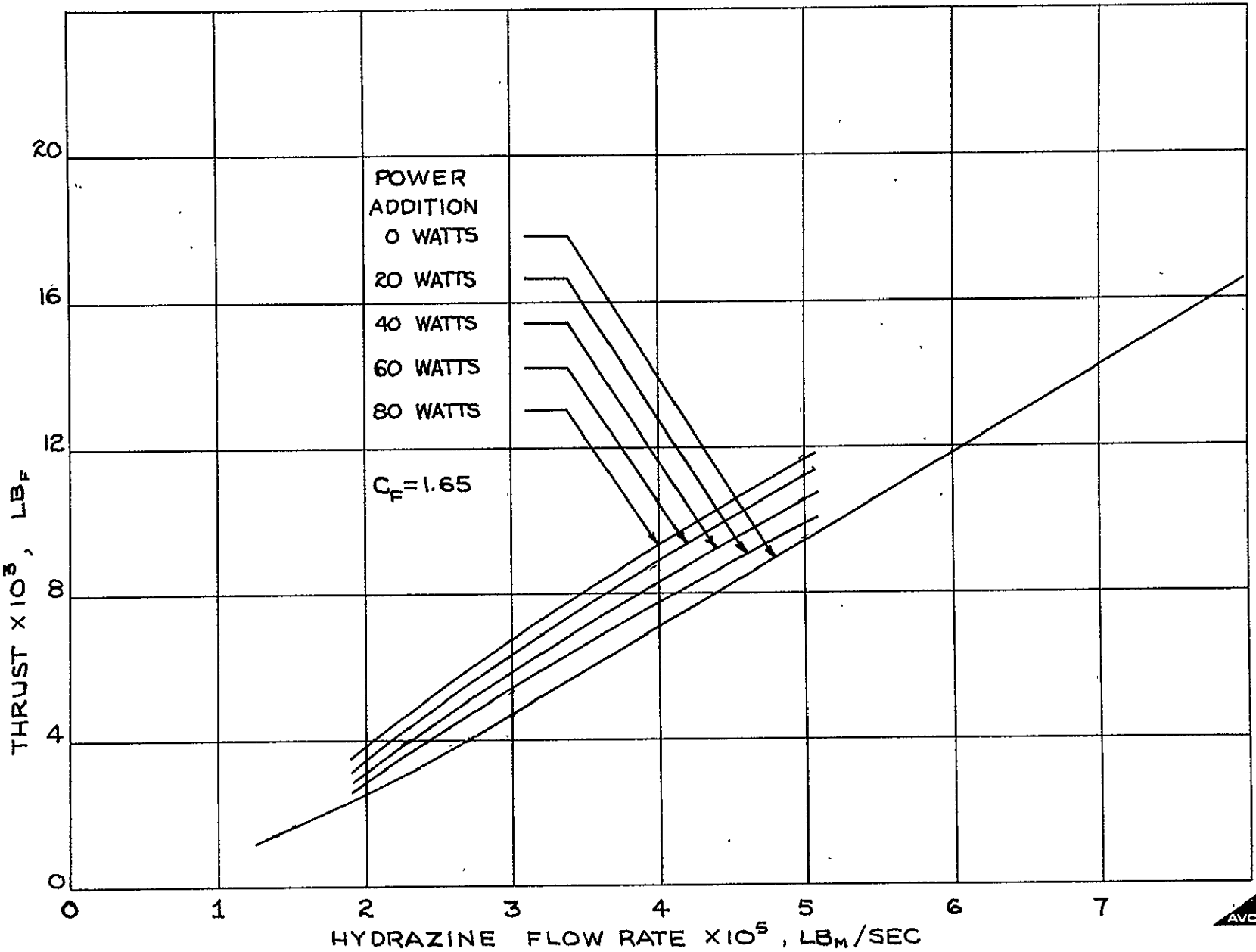

FIG. 42 EFFECT OF POWER ADDITION ON PREPROTOTYPE THRUSTER PERFORMANCE, SPECIFIC IMPULSE

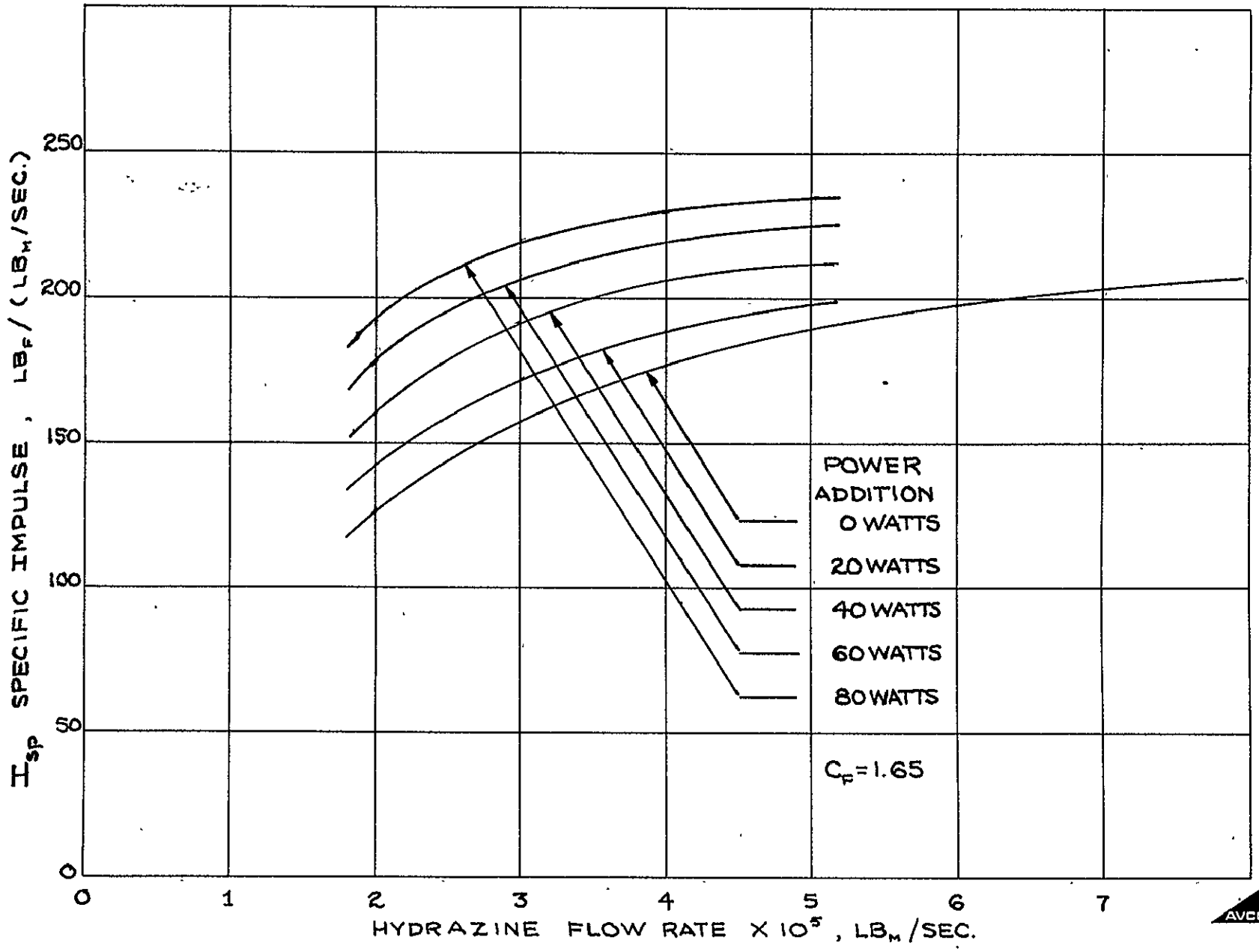

the gas decomposition products The results are illustrated in Fig. 43 which gives a comparison of experimental characteristic velocities

$$C^* = \frac{g P A_N}{\dot{m}} \tag{88}$$

and calculated values obtained from the theoretical relationship

$$C^* = \frac{1}{\gamma}\left\{\frac{g\gamma R\bar{T}}{M\left(\frac{2}{\gamma+1}\right)^{\frac{\gamma+1}{\gamma-1}}}\right\}^{1/2} \tag{89}$$

where T is the average thrust chamber wall temperature obtained from resistance measurements and the specific heat ratio is that for hydrazine decomposition products with 40 percent ammonia dissociation

A somewhat similar procedure was followed to establish average thrust chamber wall temperature in conducting those experiments on which the results listed in Table II of this report were based However, in these tests the voltage to the heater coil was maintained below a level of one volt with the power dissipated in the coil being less than one watt On the basis of the effects of power addition illustrated in Fig 7 , it is evident that this low power dissipation should have little or no effect on characteristic velocity The current and voltage to the coil at various mass flow rates was processed in a manner similar to that discussed above to obtain average thrust chamber wall temperatures and then characteristic velocities which could be compared with experimental data (Fig 44).

The calculated characteristic velocity was found to be in good agreement with the experimental data in the tests which were conducted in what is essentially the unpowered mode of operation (Fig. 44). The maximum deviation between the calculated and experimental characteristic velocities amounts to approximately 250 ft/sec at propellant flow rates in the vicinity of 8 to 10 x 10^{-5} lbm/sec, where the experimental results are nearly constant at a value of 3920 ft/sec. The calculated values are in much poorer agreement with experiment in the powered mode of operation (Fig. 43) and the deviation was found to vary quite strongly with propellant flow rate Closer examination of the r esults indicate that, at the power addition levels considered, the average thrust chamber wall temperature is only slightly dependent on flow rate, i e , the wall temperature appears to be just a function of the power addition level

It is also of interest to consider how much the actual temperature distribution along the interior surface of the thrust chamber wall differs from the mean value For the purposes of this discussion, the thrust chamber wall is considered to be an exterior insulated homogeneous hollow cylinder which is subjected to a uniform heat flux on its interior surface Heat losses from the body were assumed to occur at the surfaces at the two ends of the body The steady state temperature distribution in such a body can be obtained from the solution of the partial differential equation

FIG. 43 COMPARISON OF CALCULATED AND EXPERIMENTAL CHARACTERISTIC VELOCITIES, PREPROTOTYPE THRUSTER, POWERED OPERATION

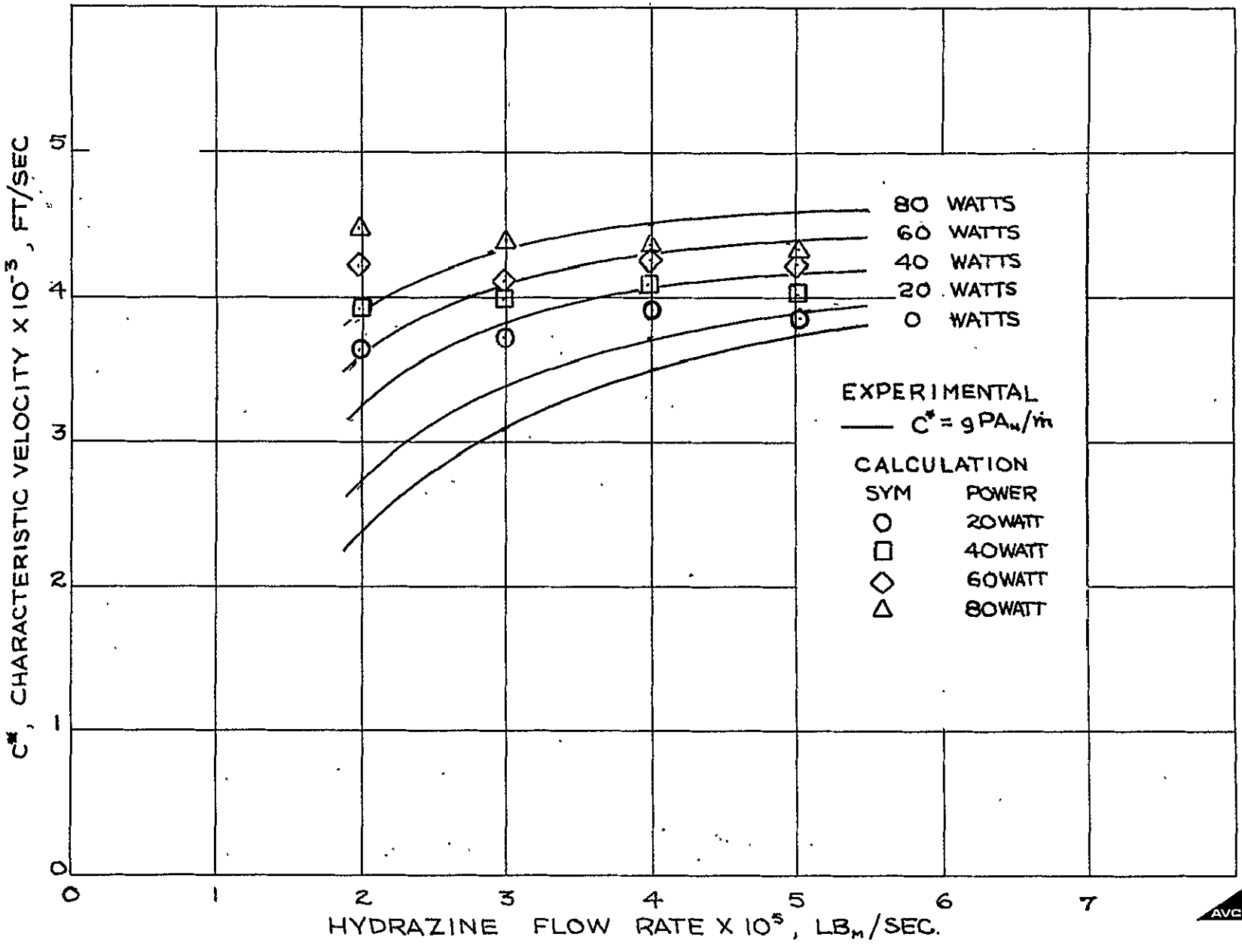

FIG. 44 COMPARISON OF CALCULATED AND EXPERIMENTAL CHARACTERISTIC VELOCITIES, PREPROTOTYPE THRUSTER, UNPOWERED OPERATION

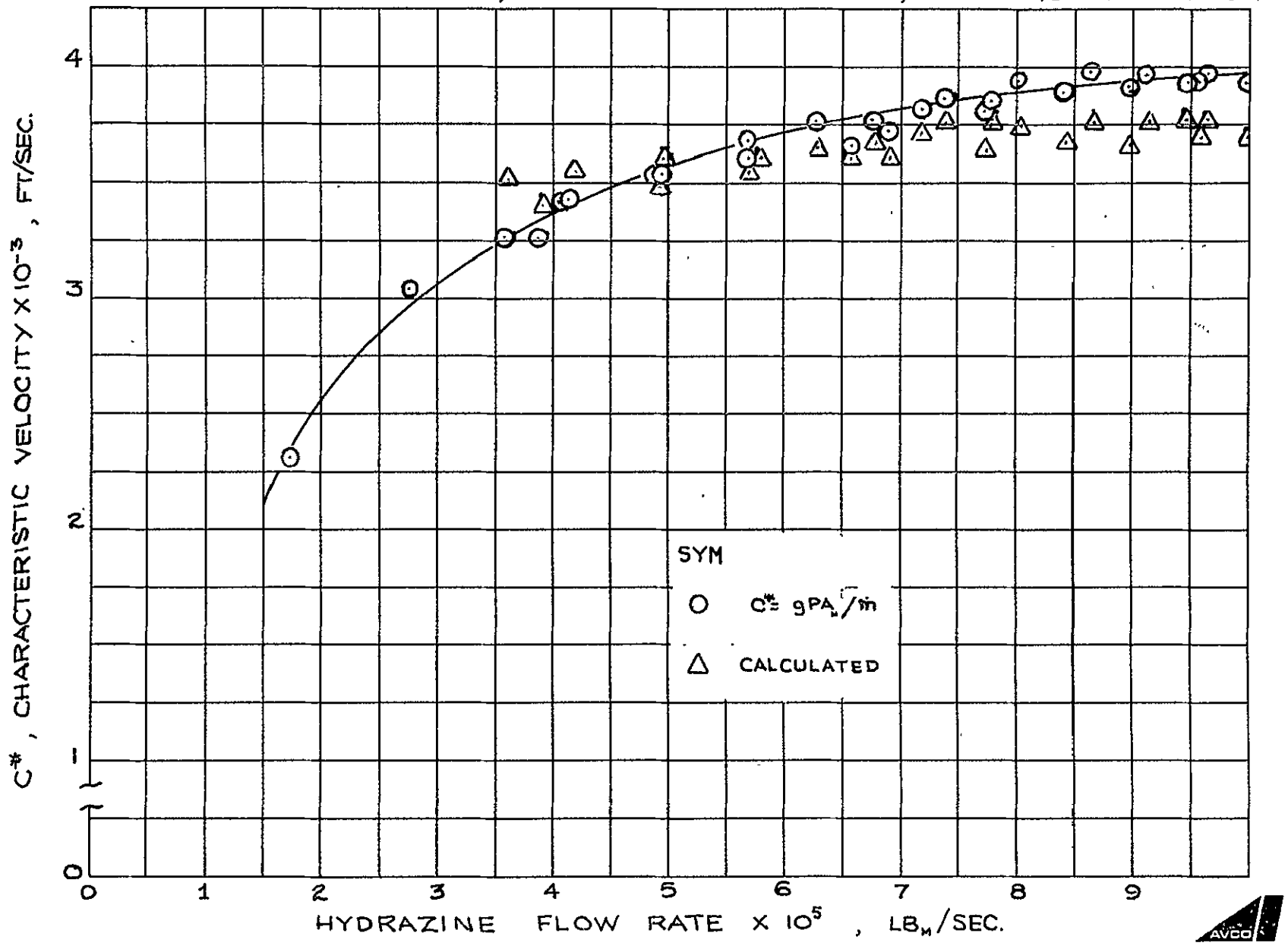

$$\frac{\partial^2 T}{\partial r^2} + \frac{1}{r}\frac{\partial T}{\partial r} + \frac{\partial^2 T}{\partial Z^2} = 0 \tag{90}$$

subject to the boundary conditions

$$\frac{\partial T}{\partial r} = 0 \qquad r = r_o \tag{91}$$

$$-k\frac{\partial T}{\partial r} = \dot{q}_i \qquad r = r_i \tag{92}$$

$$\frac{\partial T}{\partial Z} = 0 \qquad Z = \frac{L}{2}$$

$$-k\frac{\partial T}{\partial Z} = \frac{\dot{q}_i r_i L}{r_o^2 - r_i^2} \qquad Z = 0, L \tag{93}$$

where the boundary condition at the mid-plane of the body reflects the requirement that the temperature distribution by symmetrical The solution to these equations is simply [12]

$$T(r,Z) - T(r_o,0) = \frac{\dot{q}_i r_i L^2}{2k(r_o^2 - r_i^2)}\left\{\left(\frac{r_o}{L}\right)^2\left(\left(\frac{r}{r_o}\right)^2 - 1 + 2\ln\left(\frac{r_o}{r}\right)\right) + 2\frac{Z}{L}\left(1 - \frac{Z}{L}\right)\right\} \tag{94}$$

where the temperature, $T(r_o, 0)$, is the lowest temperature within the body The temperature along the interior surface of the hollow cylinder is then

$$T(r_i,Z) - T(r_i,0) = \frac{\dot{q}_i r_i L^2}{2k(r_o^2 - r_i^2)}\left\{2\frac{Z}{L}\left(1 - \frac{Z}{L}\right)\right\} \tag{95}$$

where

$$T(r_i,0) - T(r_o,0) = \frac{\dot{q}_i r_i L^2}{2k(r_o^2 - r_i^2)}\left\{\left(\frac{r_o}{L}\right)^2\left[\left(\frac{r_i}{r_o}\right)^2 - 1 + 2\ln\left(\frac{r_o}{r_i}\right)\right]\right\} \tag{96}$$

The average temperature under uniform heating conditions may be obtained by integrating equation (96) to give

$$\bar{T}(r_i,Z) - T(r_i,0) = \frac{\dot{q}_i r_i L^2}{2k(r_o^2 - r_i^2)}\int_0^1 2\left(\frac{Z}{L}\right)\left(1 - \frac{Z}{L}\right) d\left(\frac{Z}{L}\right) \tag{97}$$

$$\bar{T}(r_i,Z) - T(r_i,0) = \frac{\dot{q}_i r_i L^2}{6k(r_o^2 - r_i^2)} \tag{98}$$

The maximum temperature within the body occurs at the mid-plane (Z=L/2)

$$T(r_i,z)_{MAX} - T(r_i,0) = \frac{\dot{q}_i r_i L^2}{4k(r_o^2 - r_i^2)} \tag{99}$$

Thereby indicating that

$$\frac{\bar{T}(r_i,z) - T(r_i,0)}{T(r_i,\frac{L}{2}) - T(r_i,0)} = 0667 \tag{100}$$

or

$$\bar{T}(r_i,z) = \frac{1}{3} T(r_i,0) + \frac{2}{3} T(r_i,\frac{L}{2}) \tag{101}$$

The maximum temperature which can occur within the thrust chamber walls during unpowered operation is the adiabatic flame temperature of hydrazine decomposition products. Assuming 40 percent ammonia dissociation in the reaction products, this indicates that the maximum value of $T_{(r_i, L/2)}$ is 2100°R. A reasonable assumption as to the temperature at the end of the thrust chamber walls is 700°R which would imply that the average temperature could vary between 67 percent and 78 percent of the maximum temperature of the tube wall

The exact relationship between average wall temperature and exhaust gas temperature has not been established. However, the experimental data indicates that the average wall temperature gives a reasonable estimate of the temperature of hydrazine decomposition products when the thruster is operated in the unpowered mode.

In the higher portions of the propellant feed range investigated, flow instabilities were observed Typical experimental data obtained which demonstrates this phenomenon are presented in Fig. 45 for the thruster operated in the unpowered mode. Notice that as the flow rate is increased to value of 3×10^{-5} lb_m/sec, short duration pulses are observed in the transducer which monitors the pressure in the propellant feed line immediately upstream of the thruster. No fluctuations are observed, however, in the propellant flow rate or thruster chamber pressure. As the hydrazine feed is increased, however, the inlet line pressure fluctuations become continuous in nature and at high flow rates somewhat random variations in the mean value of the inlet pressure are also observed. At the same time, increasing the mean flow rate results in fluctuations in propellant flow and in the chamber pressure. The maximum pressure fluctuations observed in these experiments amount to approximately ± 3 percent of the mean nozzle pressure while the mass flow rate fluctuations were on the order of ± 5 percent

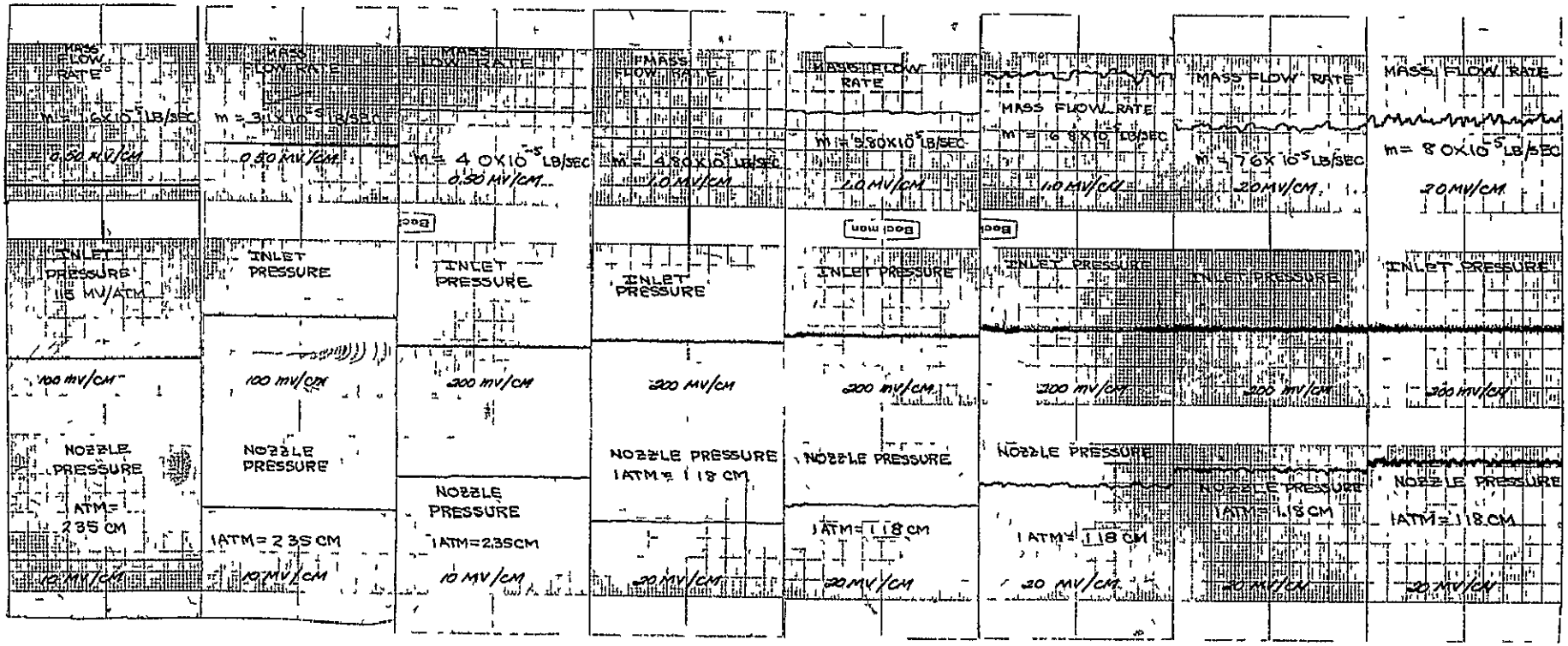

Fig 45 Preprototype Thruster Flow Instabilities

These instabilities can be explained as follows Consider the porous zirconia and feed tube to be a homogeneous body which has a uniformly distributed volumetric heat release rate ($\dot{Q}$) in that portion of body downstream of the end of feed tube as shown schematically in Fig. 46. Furthermore, let us assume that there are no losses from the sides of the body or from the downstream end while the upstream end of the tube is maintained at a constant temperature, T_o. The temperature distribution in that portion of the body downstream of the feed tube, i.e. region 1, in Fig. 46, is given as[13]

$$T-T_b = \frac{\dot{Q}L_1^2}{2k}\left\{1-\left(\frac{x}{L_1}\right)^2 - \frac{32}{\pi^3}\sum_{n=0}^{\infty}\frac{(-1)^n}{(2n+1)^3}\cos\left[\frac{(2n+1)\pi x}{2L_1}\right]\exp\left(-\frac{(2n+1)^2\pi^2}{4}\frac{\alpha t}{L_1^2}\right)\right\} \quad (102)$$

which at steady state yields

$$T-T_b = \frac{\dot{Q}L_1^2}{2k}\left\{1-\left(\frac{x}{L_1}\right)^2\right\} \quad (103)$$

The heat which is transferred from the reaction zone to the remaining portion of the body is simply

$$\dot{q} = QL_1 \quad (104)$$

This energy is absorbed by the propellant in the upstream area of the body in the process of vaporization or

$$QL_1 = \dot{m}\left\{C_p(T_b-T_o)+\Delta H_v\right\} \quad (105)$$

It is evident that at some flow rate the energy transferred down the tube is less than that required to vaporize the propellant since the maximum temperature which can be obtained in reaction region is the adiabatic flame temperature of the decomposition reaction. The maximum flow for which all the fluid is vaporized is then

$$m_M\left\{C_p(T_b-T_o)+\Delta H_v\right\} = \dot{Q}L_1 = \frac{2k(T_{af}-T_b)}{L_1} \quad (106)$$

or

$$m_M = \frac{2k(T_{af}-T_b)}{L_1\left\{C_p(T_b-T_o)+\Delta H_v\right\}} \quad (107)$$

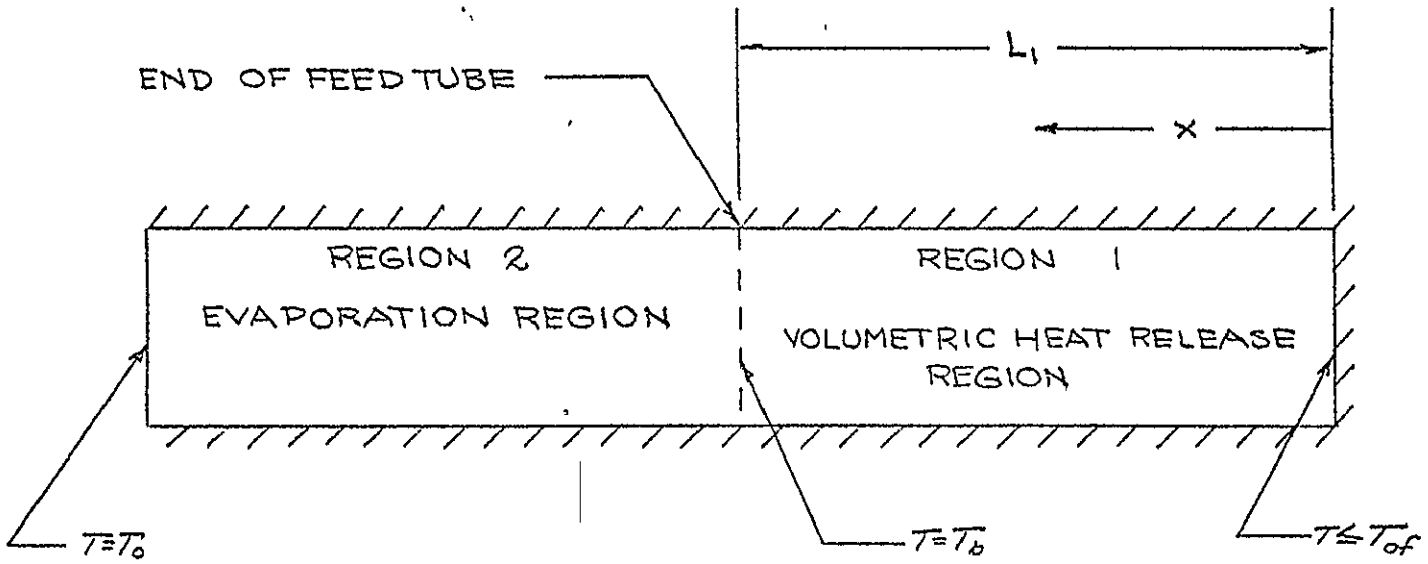

INDICATES INSULATED BOUNDARIES

FIG 46 SCHEMATIC DIAGRAM OF INJECTOR CONFIGURATION

At flow rates in excess of $\dot{m}_m$, the fluid will be only partially vaporized before it enters the reaction zone, while at lower flow rates, the propellant will be completely vaporized. Employing a thermal conductivity of 0 004 cal/cm-K-sec and the adiabatic flame temperature corresponding to an ammonia dissociation fraction of 0 40, the flow rate calculated from Equation (107) is 2.0×10^{-5} lb_m/sec

At low flow rates, we would expect the propellant flow to be completely vaporized in the upstream portion of the tube and hence, would have the characteristics of a gaseous feed system while at high flows it would behave as a liquid injection system This agrees well with what is observed experimentally as is shown by the following discussion At low flows, the propellant feed is directly proportional to the inlet pressure immediately downstream of the propellant control valve as shown in Fig 47, whereas at higher flow rates, the mass flow is nonlinear in the inlet pressure These data were also correlated with an expression of the form

$$\dot{m} = F P_1 \tag{108}$$

where the quantity F depends upon the ratio of inlet pressure to thruster chamber pressure

$$F = 1.0 \qquad \frac{P_2}{P_1} > 0\,56 \tag{109}$$

$$F = \frac{\left(\frac{\gamma}{\gamma-1}\right)^{1/2} \left(\frac{P_2}{P_1}\right)^{1/\gamma} \left(1-\left(\frac{P_2}{P_1}\right)^{\frac{\gamma-1}{\gamma}}\right)^{1/2}}{\left(\frac{2}{\gamma+1}\right)^{\frac{\gamma+1}{2(\gamma-1)}} \left(\frac{\gamma}{2}\right)^{1/2}} \qquad \frac{P_2}{P_1} < 0\,56 \tag{110}$$

for $\gamma = 1\,30$

These expressions are essentially the relationships which define the compressible gas flow through an orifice The correlation of the mass flow withethe inlet pressure is presented in Fig 48 At low flows, it is seen that

$$m = KFP_1 \tag{111}$$

as would be expected with a gaseous feed system while at high flow rates, the deviation in the observed flow from that obtained by extrapolation of the linear portion of the curve increases with increasing flow rate This deviation is believed to be the result of the propellant entering the reaction zone in a partially vaporized condition The instabilities inherent in a two-phase flow system are well documented[14, 15] and it is believed that

FIG 47. VARIATION OF PROPELLANT FLOW RATE WITH INLET PRESSURE

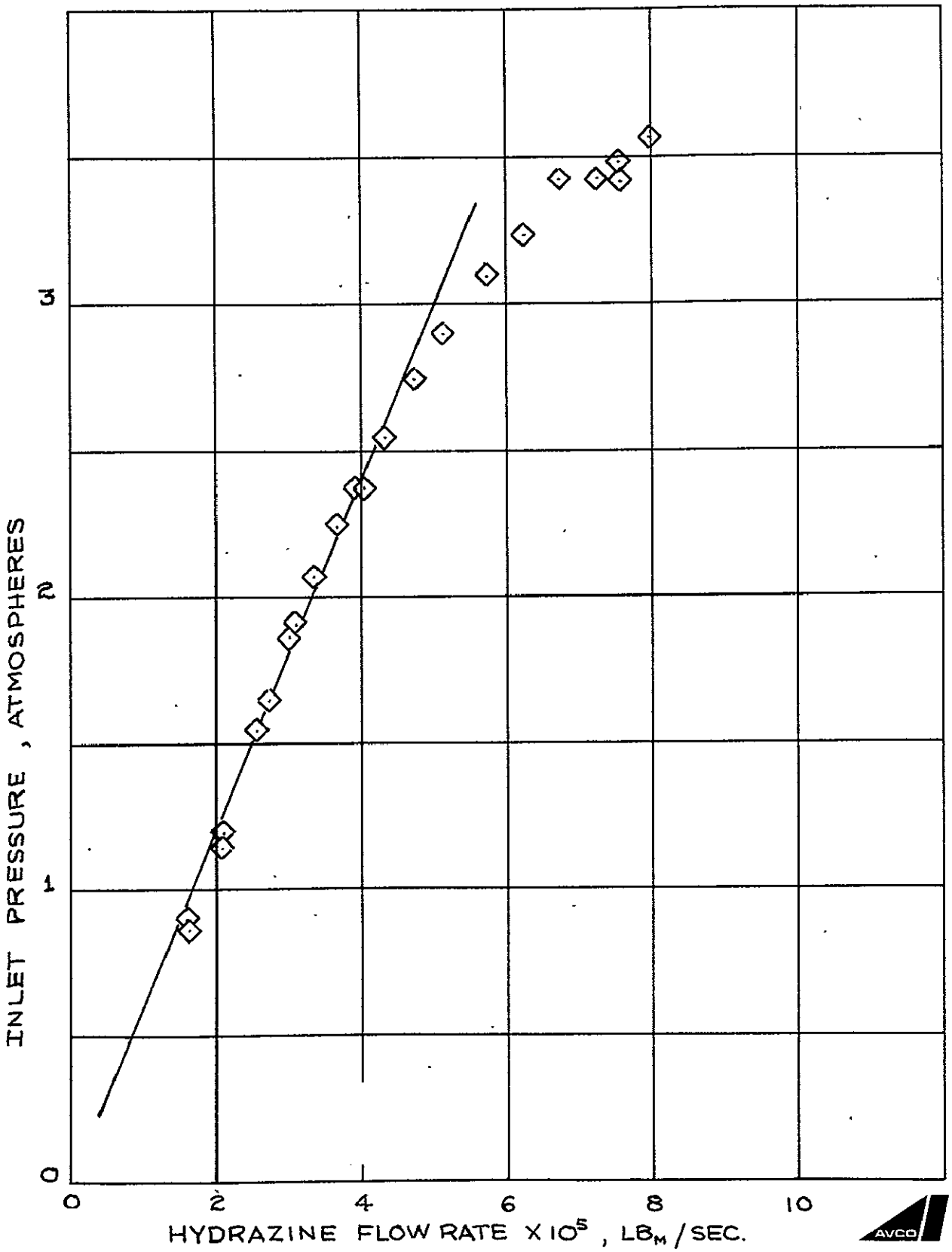

FIG 48 CORRELATION OF PROPELLANT FLOW RATES

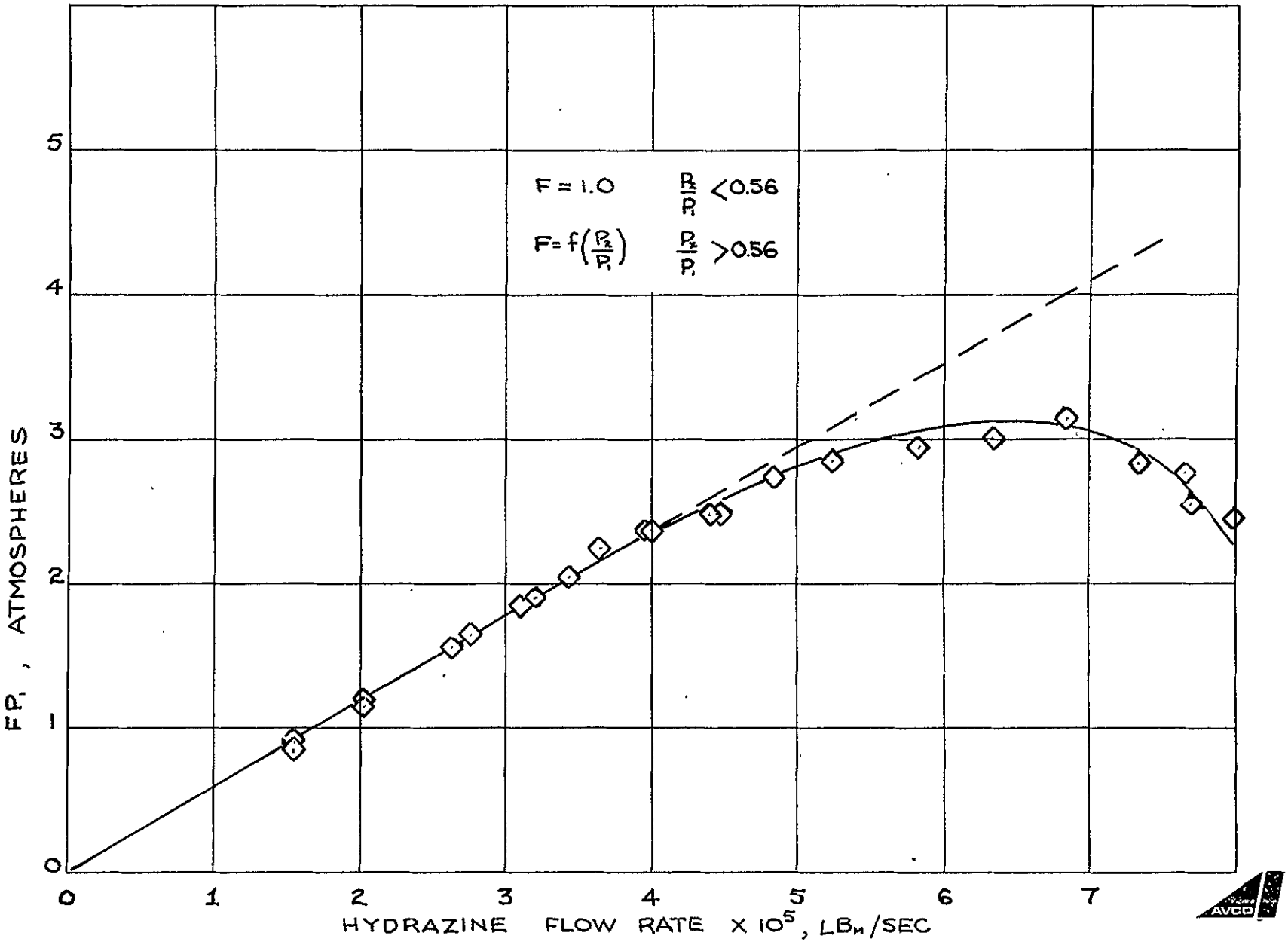

this is the cause of the pressure fluctuations observed in the preprototype thruster.

There is additional data which also supports this conclusion During operation of the preprototype thruster in the powered mode, it was observed that at any operating point where there were instabilities, increasing the power input to the heater coil decreases the magnitude of the fluctuations. Typical recorder traces which demonstrate this effect are shown in Fig 49 Obviously, some portion of the power applied to the coil is transferred to the zirconia and in turn results in an increase in the propellant flow rate at which two-phase flow first occurs

A second series of experiments were conducted with the preprototype thruster on a thrust and impulse measuring system The thrust and impulse measuring system consists of a "frictionless" inertial table whose angular velocity is measured by a rate gyro The table is suspended on a multi-filament steel cable. The wire is mounted to the inner race of a thrust bearing A servo-torque motor slaves the bearing position to the table position as a function of the error signal generated by the misalignment of a polarized light source (on the table) and sensor (on the bearing mount) Thus, the torque due to the angular deflection of the support wire may be maintained at a value less than that equivalent to 1×10^{-6} lb force acting at a two foot radius. An artist's representation of the thrust measuring system and its associated vacuum system are illustrated in Fig. 50

The application of Newton's second law to the table results in the following equation

$$\sum_{n=1}^{n} (Fr)_n = J\ddot{\Theta} \tag{112}$$

where

F=external tangential force (impulse thrust)
R=radius of tangential component of F
J=moment of inertia of the table
$\ddot{\Theta}$=rate of change of angular velocity

This measurement system may accommodate any number of torques, generally, a single torque is considered However, couples, as a pair of yaw thrusters, may be studied individualy or as a couple.

For impulse measurements of a single thruster, equation (112) is integrated once

$$\int_{t_1}^{t_2} F dt \equiv I = \frac{J}{r}(\dot{\Theta}_2 - \dot{\Theta}_1). \tag{113}$$

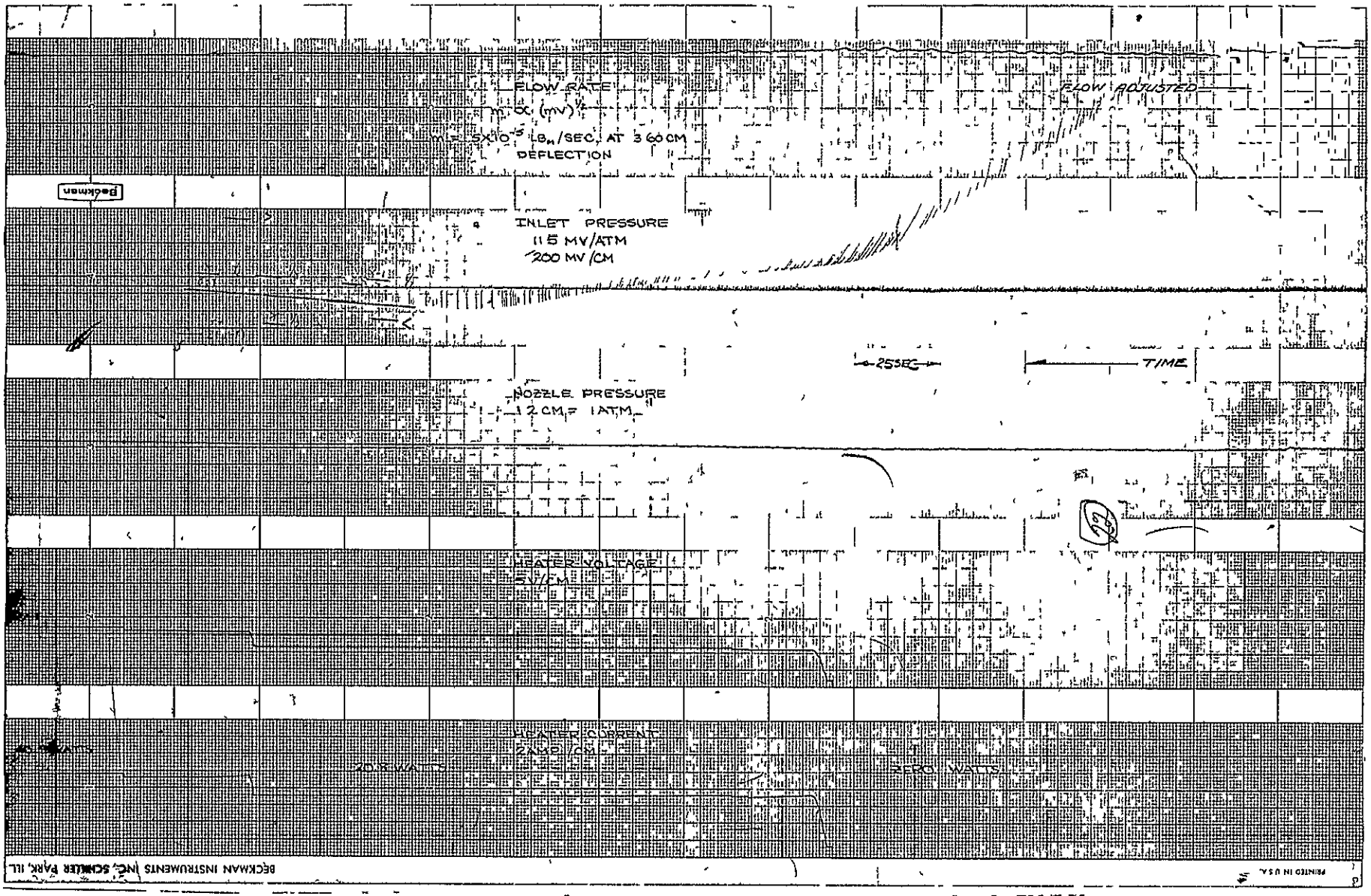

Fig 49 Effect of Power Addition on Thruster Instabilities ($\dot{m}$=5 0x10^{-5}lb$_m$/sec)

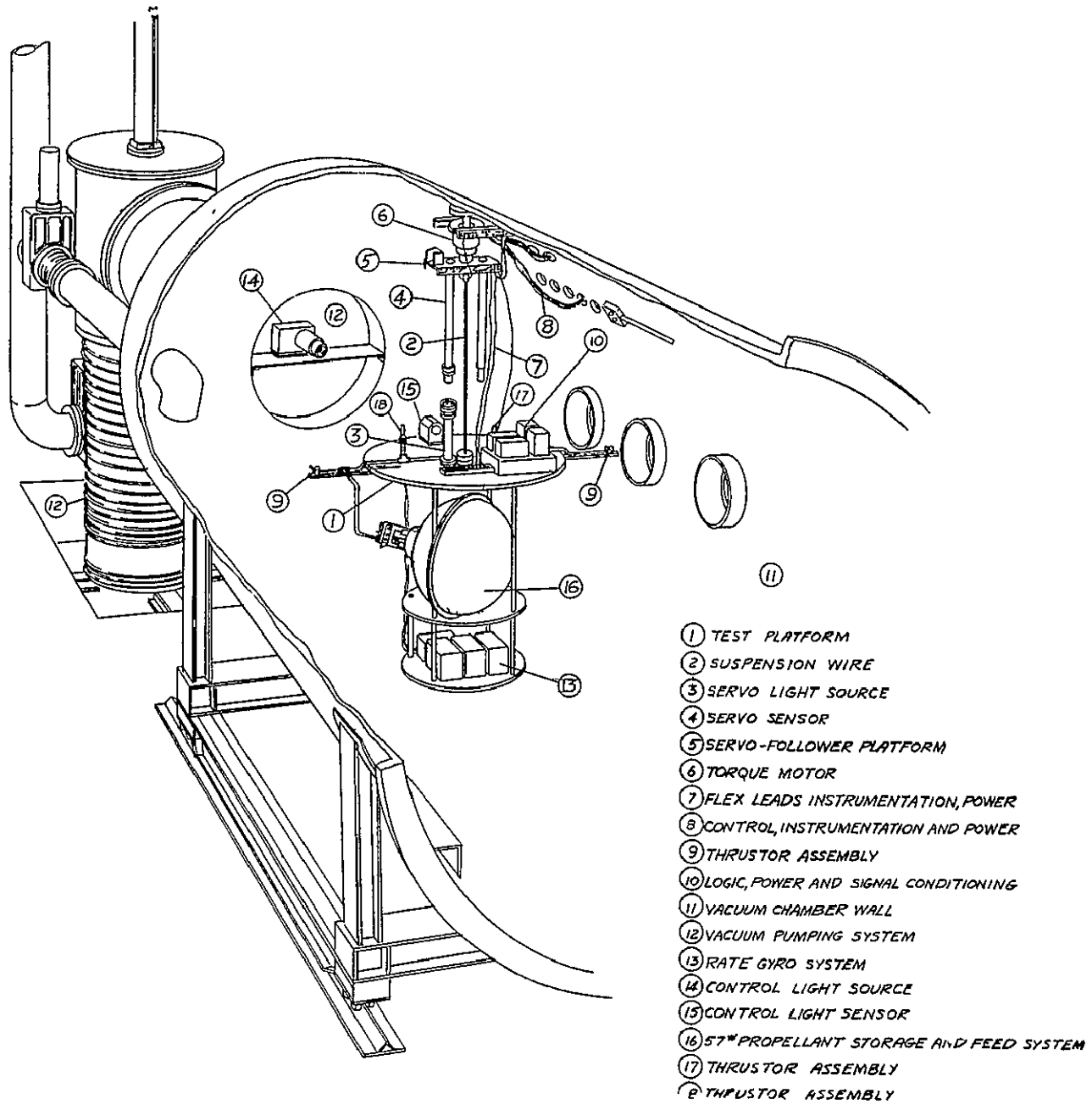

Fig 50. Auxiliary Propulsion Impulse and System Performance Measurement Facility

The gyro output is described by

$$\dot{\Theta} = K(E_{mv}) \tag{114}$$

where

E_{mv} = millivolt output signal

k = proportionality constants

Substitution of equation (114) into equation (113) results in the working equation for impulse measurements

$$I = \int_{t_1}^{t_2} F\,dt = \frac{JK}{r}\left(E_{mv_2} - E_{mv_1}\right) \tag{115}$$

The constant (Jk) is determined by calibration tests. The table is calibrated by applying known torques to the table and monitoring the gyro output during a calibration test. The applied force in equation (115) is constant so F may be brought outside the integral sign. Equation (116) describes the calibration test

$$F_c r_c = JK \frac{\Delta E_{mv}}{\Delta t} \tag{116}$$

where subscript c refers to calibration parameters

Rearrangement of equation (116) results in the working equation for evaluating (Jk) of equation (115)

$$C \equiv JK = F_c r_c \left(\frac{\Delta t}{\Delta E_{mv}}\right)_c \tag{117}$$

The total impulse delivered per flow valve pulse as calculated from equation (115) includes all losses due to pressure dependent, specific impulse, and nozzle viscous losses. If sufficient pulses are made, the total variation in impulse bits will include the variation in the plenum pressure within the deadband limits of the regulator.

It is noteworthy to point out some experimentally significant characteristics of equations (113) and (117). All the parameters of equation (117) are readily measurable and no compounding of inaccuracies result from its application to the calibration testing. The time different (Δt), and the millivolt difference (Δ mv), may be determined to within 5% The mass of the test weight and the moment arm may be determined to even greater accuracies. Thus, the evaluation of K should be within 1%. The application of equation (115) to the impulse mode of testing results in a direct measurement of impulse delivered as determined by a

voltage difference No further data analysis (as integration of force-time responses) are required. Thus, good resolution of the desired parameter, impulse bit, is obtained. Due to the nature of the rate gyro, frequency response is not a limiting factor The impulse measurement is dependent on resolving the difference in angular rate before and after the application of the impulsive thrust, and not on the ability of the gyro to faithfully tract the table velocity during the application of the impulsive force Thus, good integrated impulse resolution is obtained at the sacrifice of the detailed thrust-time history.

A schematic representation of a typical gyro output trace is shown in Fig. 51. Chronologically, the following sequence of events occur during a typical cycle of the gyro output signal At time t_0, the thrust delivered by the thruster is causing the table to accelerate in a counter-clockwise direction although the table is at rest. At time t_1, the table is moving at its maximum velocity and an auxiliary boom on the thruster engages an elastic bumper which changes the motion of the table from the counter-clockwise to the clockwise direction. This is accomplished during the period t_1 to t_2 During the time between t_2 and t_3, the table is being decelerated at a constant rate by the thruster The table comes to rest at time t_3 and is accelerated towards the bumper until time t_4 Referring to equation (115), the thrust is determined by the slope of the gyro output between times t_2 and t_4. It is noted, however, that this representation is idealized in that the gyro output is strictly a linear function of time In actual experiments, however, the output is not exactly linear as is shown by the experimental data illustrated in Fig. 52. These anomalies in the slope are caused by extraneous phenomena within the vacuum tank such as recirculation flow patterns, etc. Since most effects tend to produce a thrust decrement, it can be argued that the most logical slope of the gyro output curve to use in calculation of thrust is the maximum slope. For the example illustrated in Fig. 52, this amounts to a thrust obtained from the maximum slope which is 9 percent higher than that would be obtained from the average slope.

Steady state data obtained with the preprototype thruster are illustrated in Fig. 53. Data were reduced using both the maximum and average slope of the gyro output curve. It is seen that the deviation between the two methods amounts to approximately 9 percent. In order to provide a conservative evaluation of thruster performance, the average slope method has been adopted for representation of the experimental data

Characteristic velocity and thrust coefficients obtained from experimental data are depicted in Fig. 54. Characteristic velocity is in

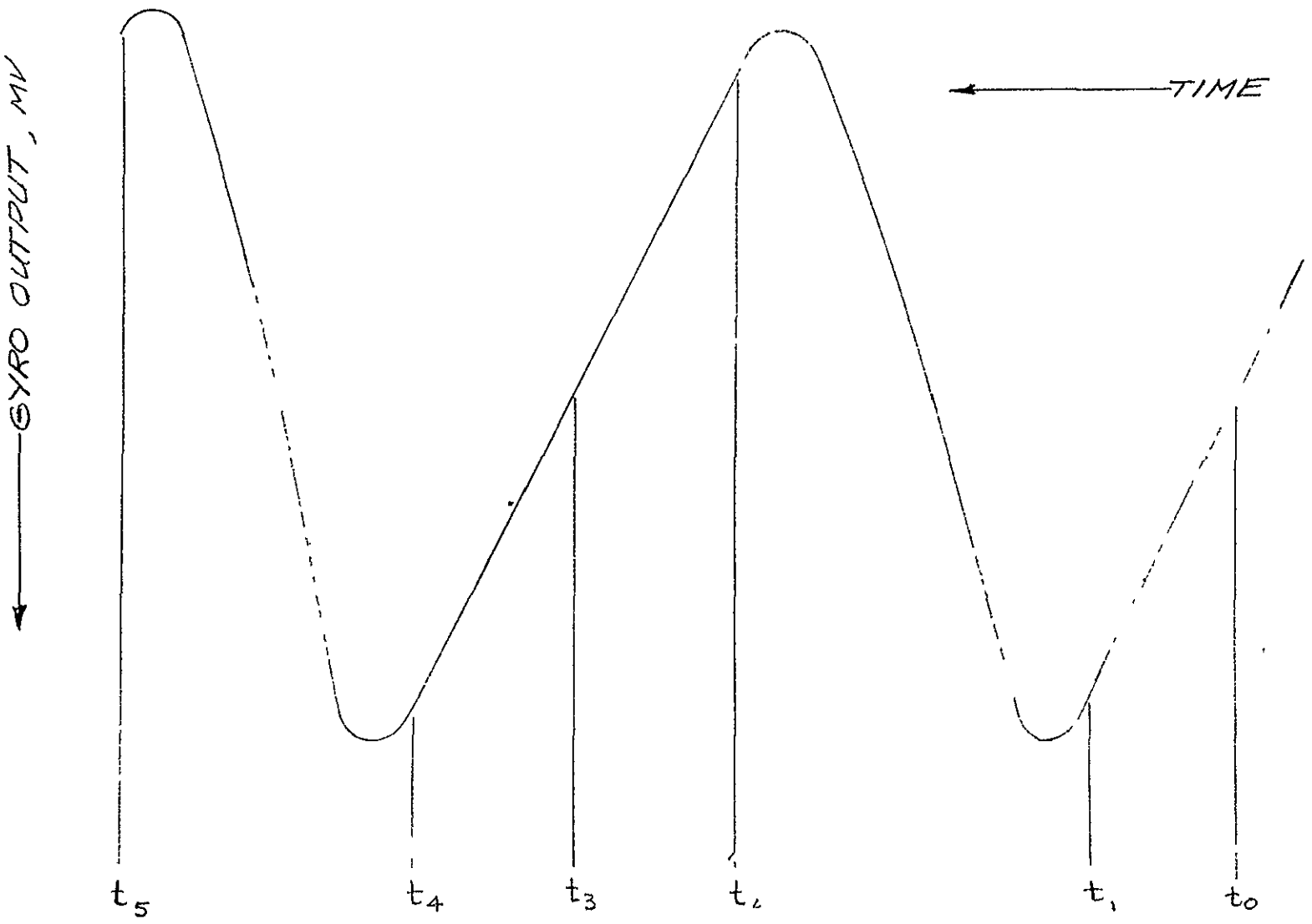

FIG 51 SCHEMATIC REPRESENTATION OF GYRO OUTPUT SIGNAL

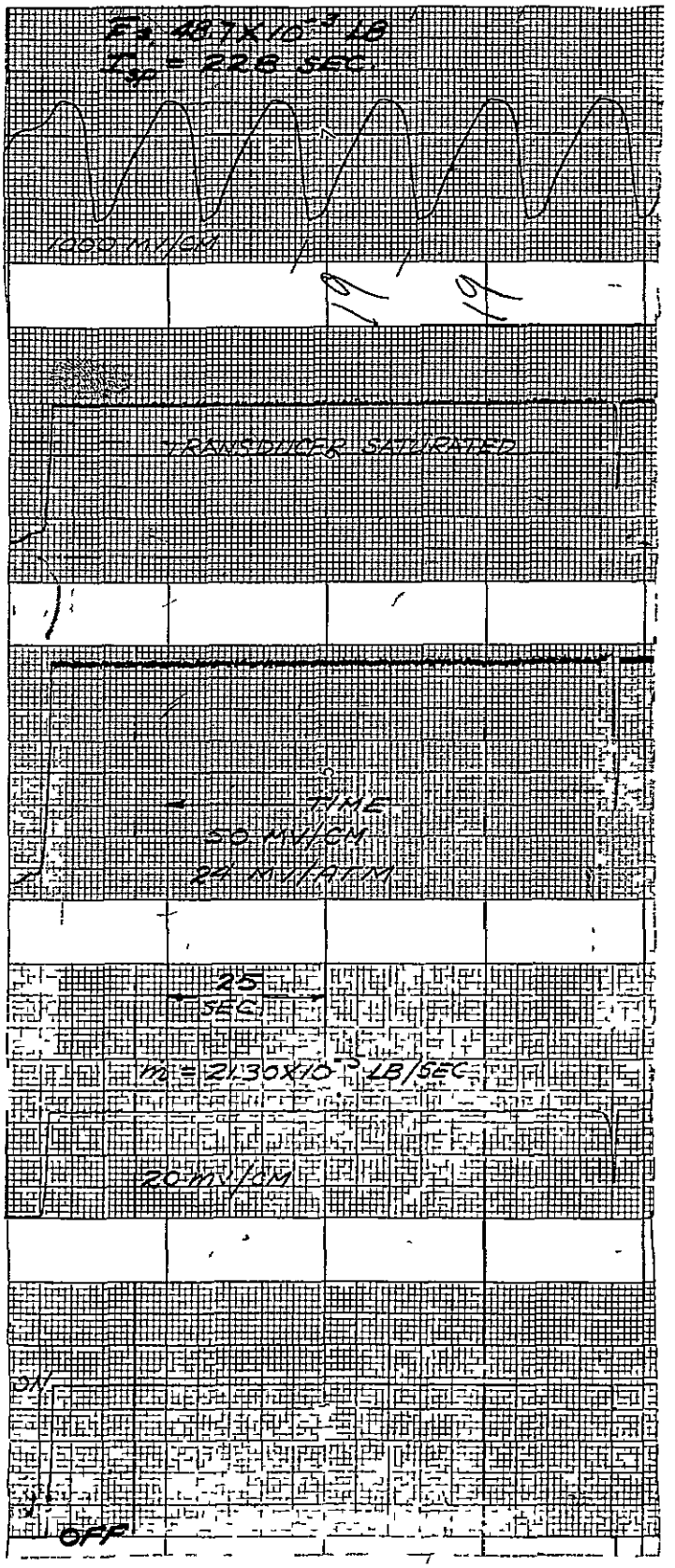

Fig.52 Typical Experimental Thrust Data

FIG 53 PREPROTOTYPE THRUSTER PERFORMANCE, STEADY STATE OPERATION

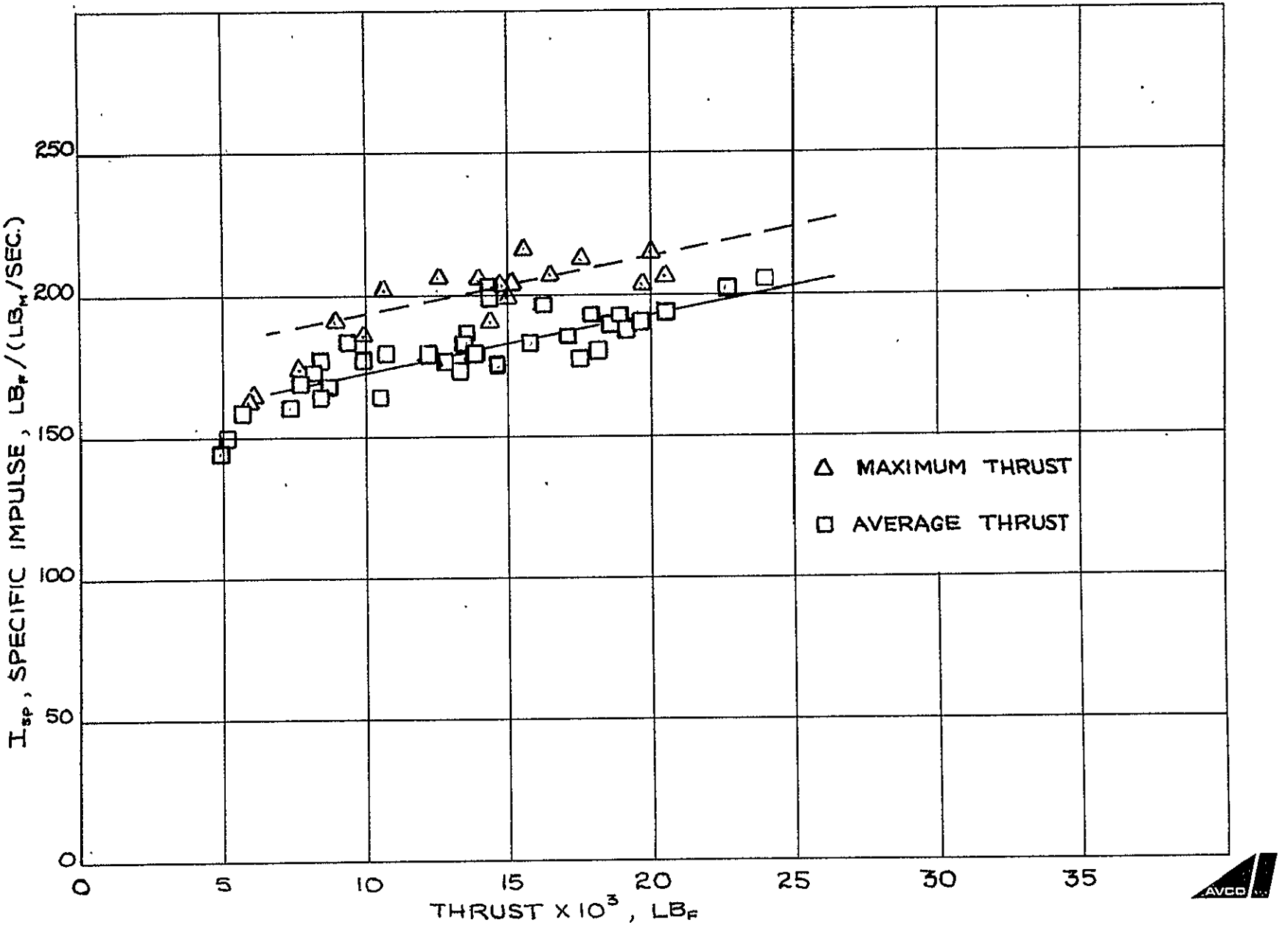

FIG 54 PREPROTOTYPE THRUSTER PERFORMANCE, STEADY STATE OPERATION

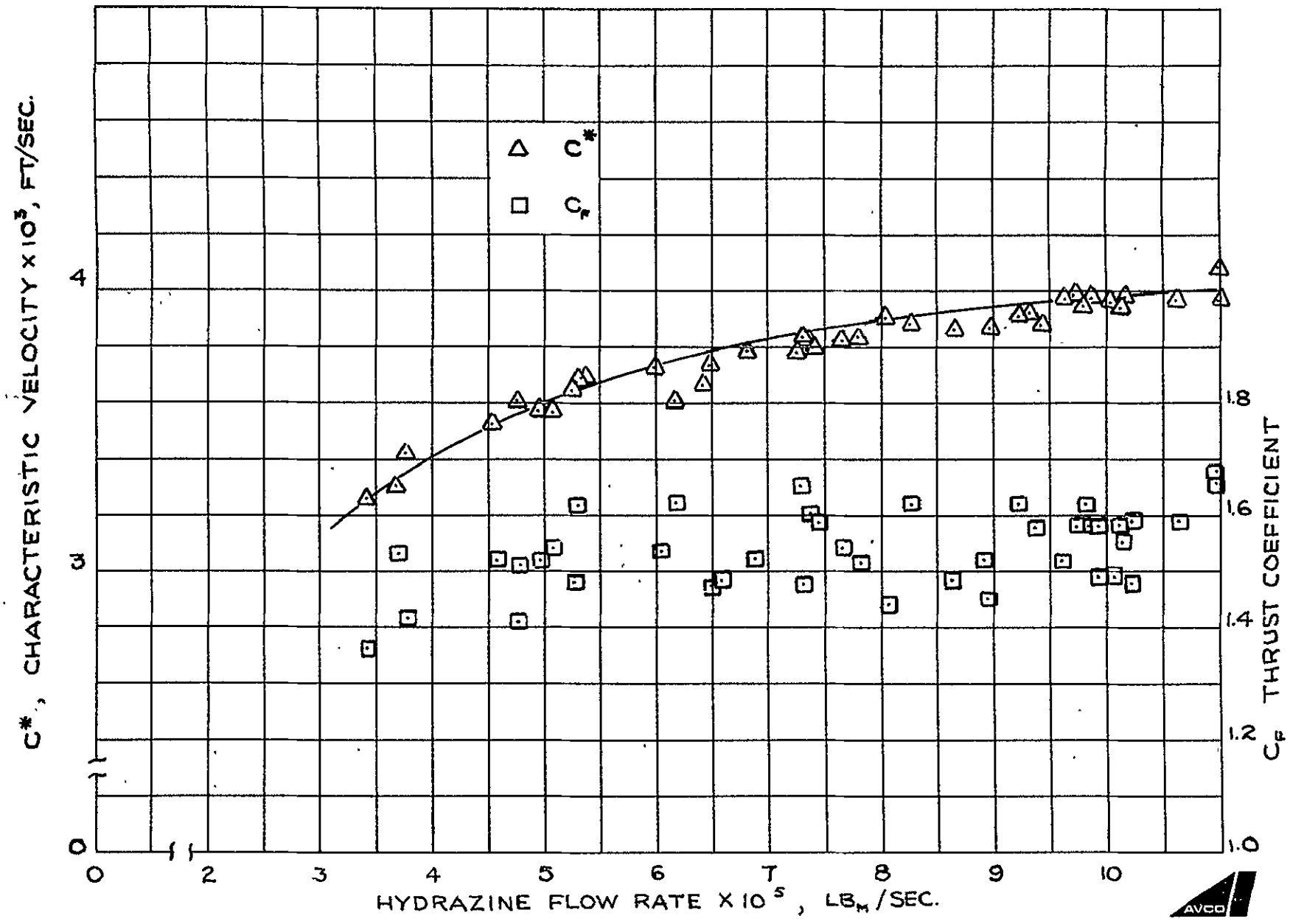

close agreement with similar data discussed previously Thrust coefficients were determined from the definition

$$C_F = \frac{F}{PA_t} \tag{118}$$

where the thrust employed was that obtained from the average slope of wire table gyro output curve The thrust coefficient was found to remain relatively constant with a mean value of 1 55 over the entire range of propellant flow rates investigated If the maximum slope of the gyro output curve were used to determine thrust, the average thrust coefficient would be increased to a value of 1 70.

A similar series of experiments were performed with a second preprototype thruster which had the porous insulator indicated in Fig 35 replaced with a solid refractory insulator (lava) such that the characteristic length of the thrust chamber was identical for the two devices. During operation of this unit on the thrust table, improvements were made to the propellant feed system which made it possible to increase the propellant supply pressure from the previous maximum value of 80 psid to 180 psid Hence, thrust data could be obtained over a wider range of propellant flow rates (3×10^{-5} to 25×10^{-5} lb/sec). Steady state thruster performance obtained with this unit is illustrated in Figs 55,56 Thrust was found to vary from 5 millipounds at the minimum flow rate to 59 millipounds at the highest propellant flow investigated using the average slope of gyro output signal The corresponding specific impulse increased monitonically from a value of 160 sec. to 238 sec when propellant feed from 3×10^{-5} lb/sec Comparison of the performance of the two preprototype thrusters indicate s that, as expected, the porous insulator was more effective in reducing energy losses from the thruster since the lava insulator has the higher thermal conductivity

Pulsed mode operational data were obtained with the preprototype thruster containing the lava insulator for duty cycles varying from 1 to 50 percent duty cycle with a 1 sec thrust period These investigations were performed with the unit operating in both the unpowered and powered modes The experiments were performed with this unit since it was expected that it would have a response time which would be considerably shorter than that of the preprototype containing the porous insulator. In the original preprototype, steady state nozzle pressure is achieved only after both the thrust chamber and the volume occupied by the porous insulator reach their steady state values, whereas, with the solid insulator only the thrust chamber needs to be brought up to pressure to attain steady state

Pulse data were gathered at nominal steady state thrust levels of 9×10^{-3} lb_f and 17 5 $\times 10^{-3}$ lb_f. In performing these experiments, the flow regulating valve was adjusted to give the steady state flow rate required to obtain the desired thrust level The flow regulating valve setting was main-

FIG 55 MODIFIED PREPROTOTYPE THRUSTER PERFORMANCE

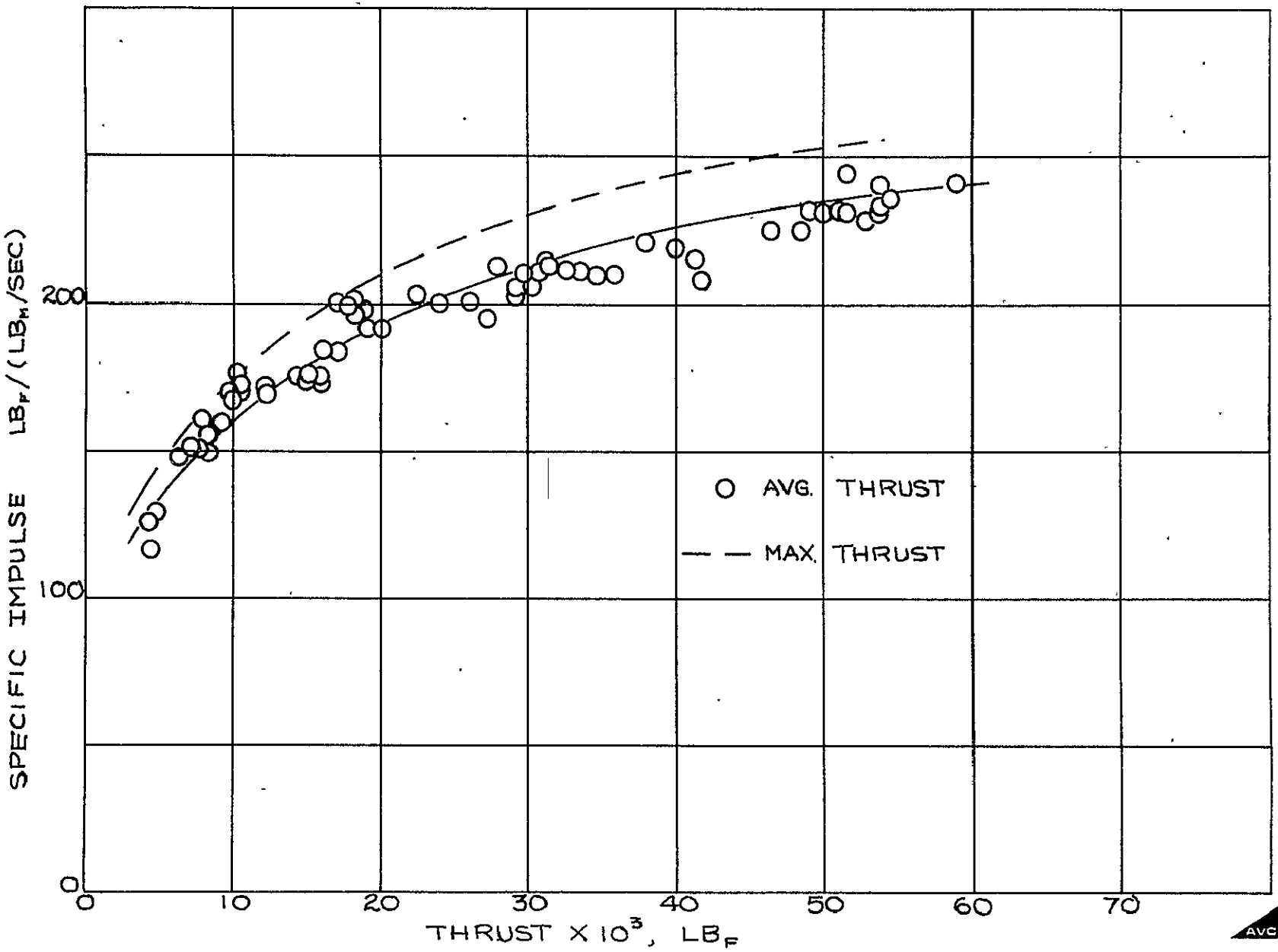

FIG. 56 MODIFIED PREPROTOTYPE THRUSTER PERFORMANCE , POWERED OPERATION

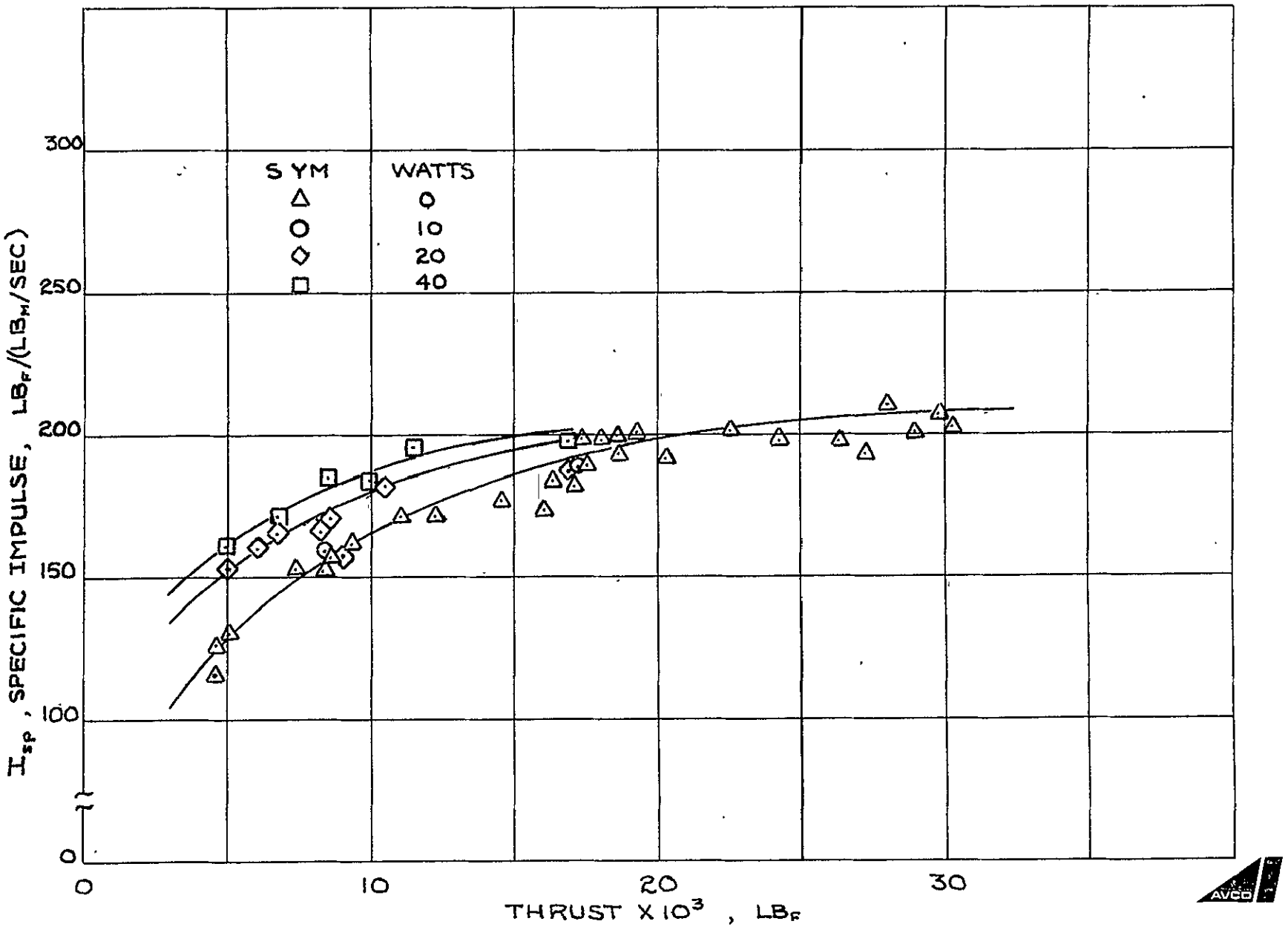

tained in this position during the pulsed mode of operation Typical recorder traces obtained in these experiments are illustrated in Figs. 57-59 Upon examination of these data several phenomena become apparent, namely.

a) There is a considerable lag in the output of the mass flow measuring system pressure transducer as demonstrated by the long period required for mass flow signal to return to zero after the propellant valve is shut

b) The time required for the thrust to decay to zero is on the order of 600 sec.

c) The maximum propellant flow rate during any pulse is in excess of that obtained during steady state operation.

Therefore, specific impulse obtained at any duty cycle could be obtained only after integration of the mass flow rate signal

$$\bar{\bar{I}}_{sp} = \frac{\int_t F\,dt}{\int_t \dot{m}\,dt} \tag{119}$$

where

$$\int_t F dt = \frac{JK}{r}\left(E_{mv_2} - E_{mv_1}\right) \tag{120}$$

Pulse mode operation data are illustrated in Figs. 60-62 for both powered and unpowered modes of operation in normalized with respect to parameters obtained at a 50 percent duty cycle. It is noted that at each thrust level the specific impulse obtained decreased quite rapidly with decreasing percent duty cycle to a value of 40-45 percent of the value obtained at a 50 percent duty cycle This was accompanied by an increasing integrated propellant flow rate and impulse bit as percent duty cycle was decreased from 50 percent to 1 percent. The observed drop in specific impulse is considerably greater than similar data obtained with catalytic hydrazine thrusters [16] For example, it is reported that with a nominal 5 pound thruster a degradation of specific impulse to 78 percent and 71 percent of steady state were observed when operating at conditions corresponding to 4 2 lb_f and 2 5 lb_f with a 0 4 percent duty cycle

A limited amount of data were obtained with the preprototype thruster ope rating with a pulse width of less than 1 sec. These results are listed in Table III, below

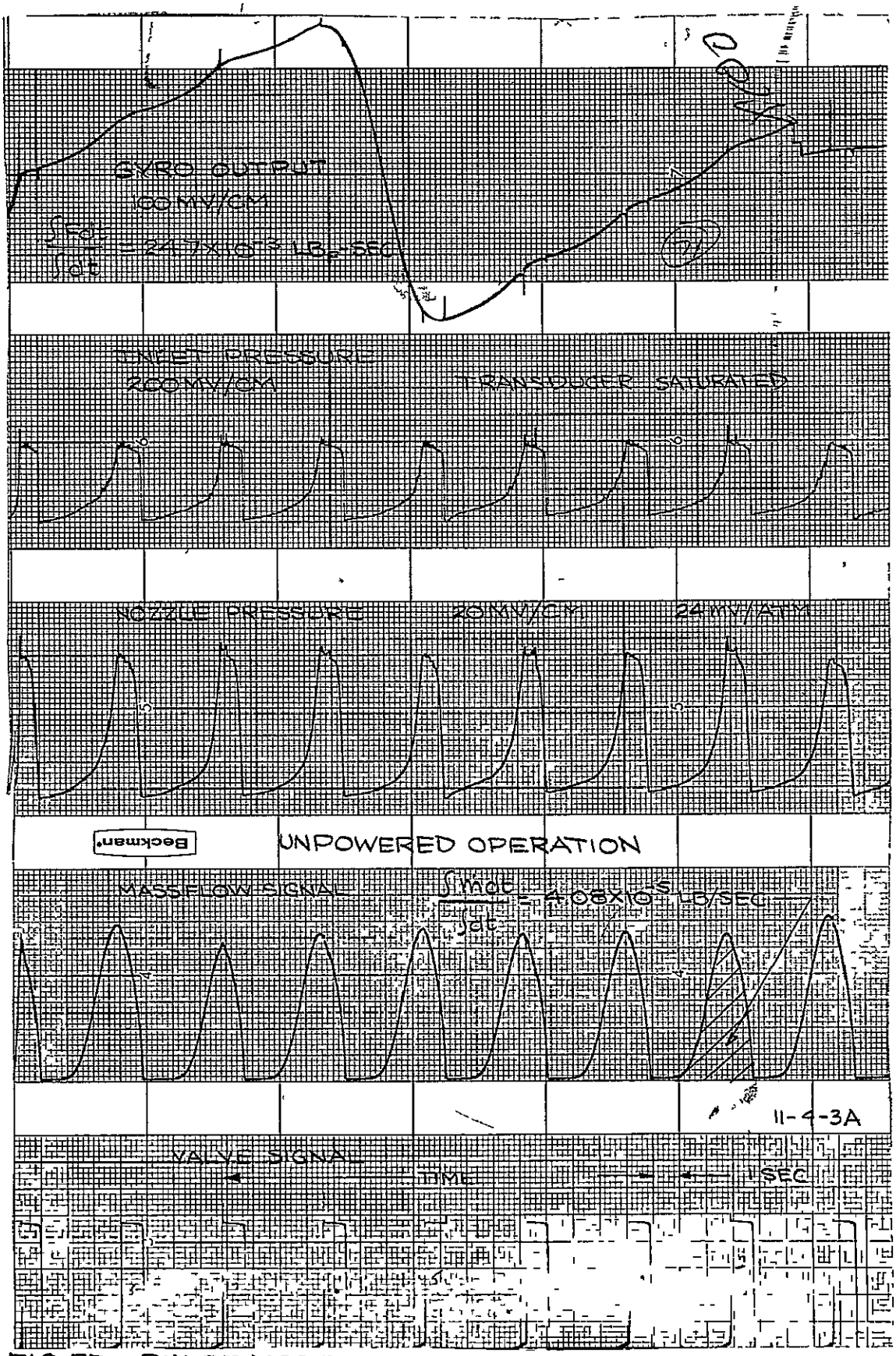

FIG 57 PULSE MODE RECORDER TRACES, MODIFIED PRE PROTOTYPE THRUSTER

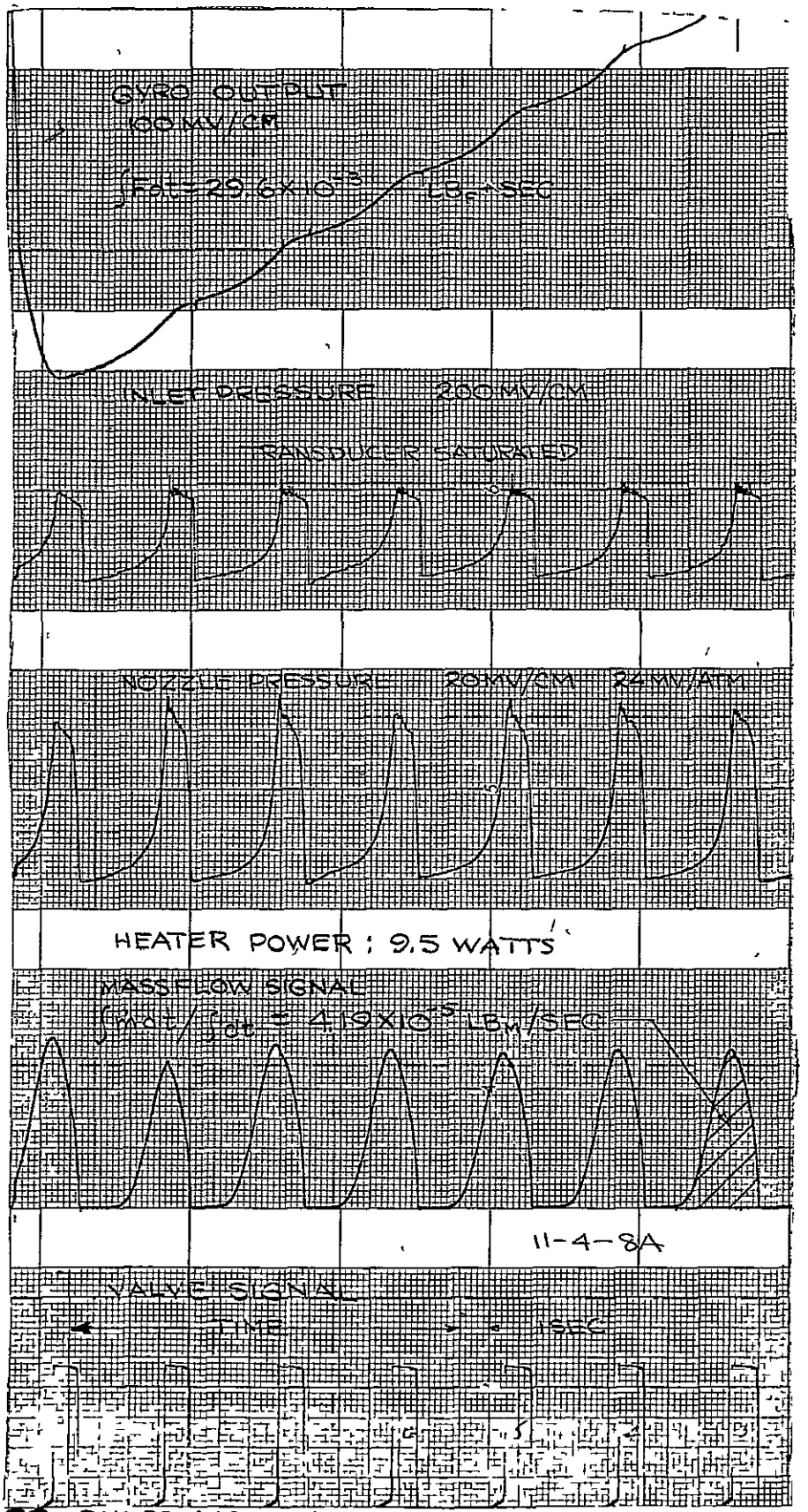

FIG 58 PULSE MODE RECORDER TRACES, MODIFIED PRE PROTOTYPE THRUSTER

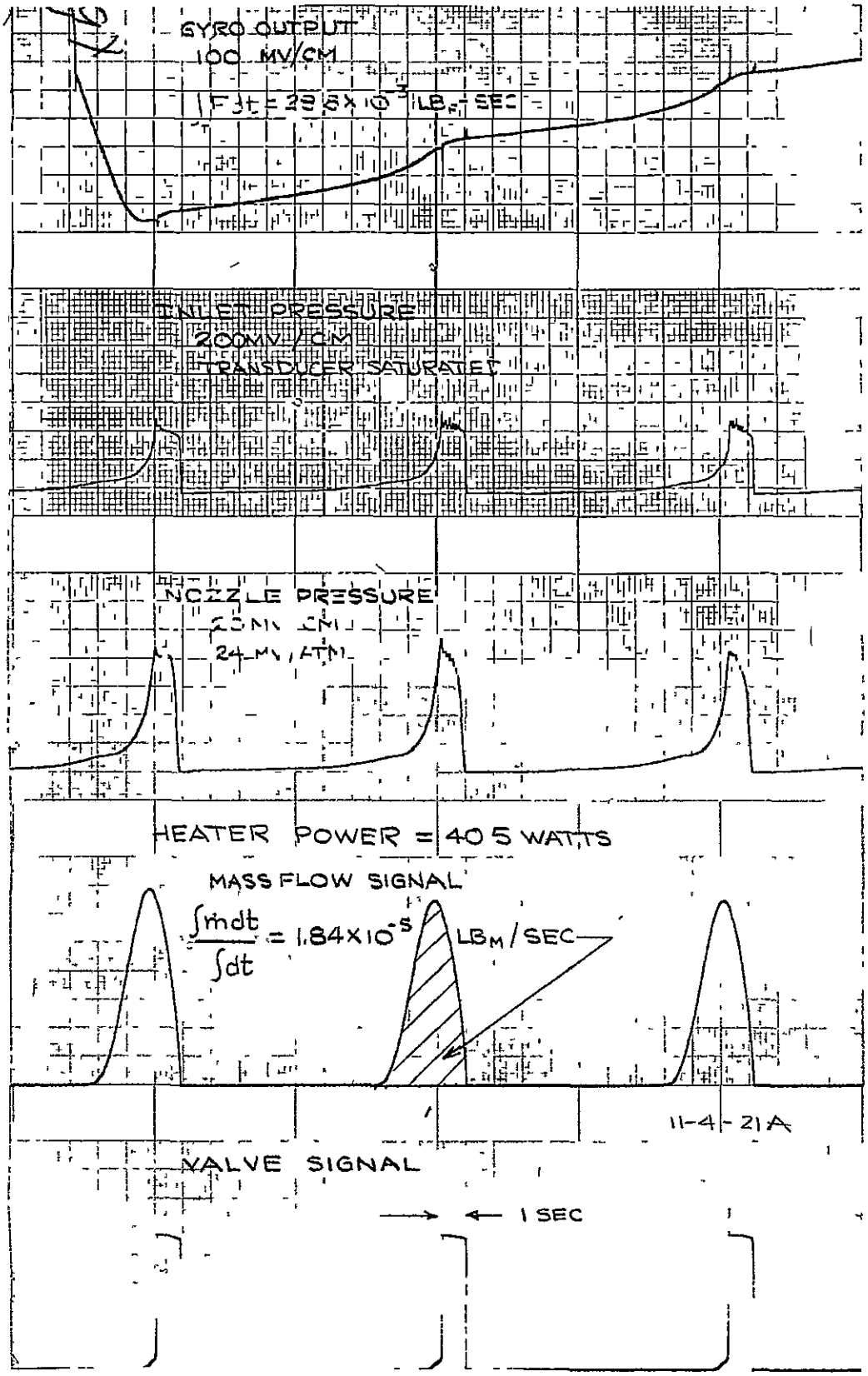

FIG 59 PULSE MODE RECORDER TRACES, MODIFIED PREPROTOTYPE THRUSTER

FIG. 60 MODIFIED PREPROTOTYPE THRUSTER PERFORMANCE AT 50% DUTY CYCLE (1 SECOND PULSE)

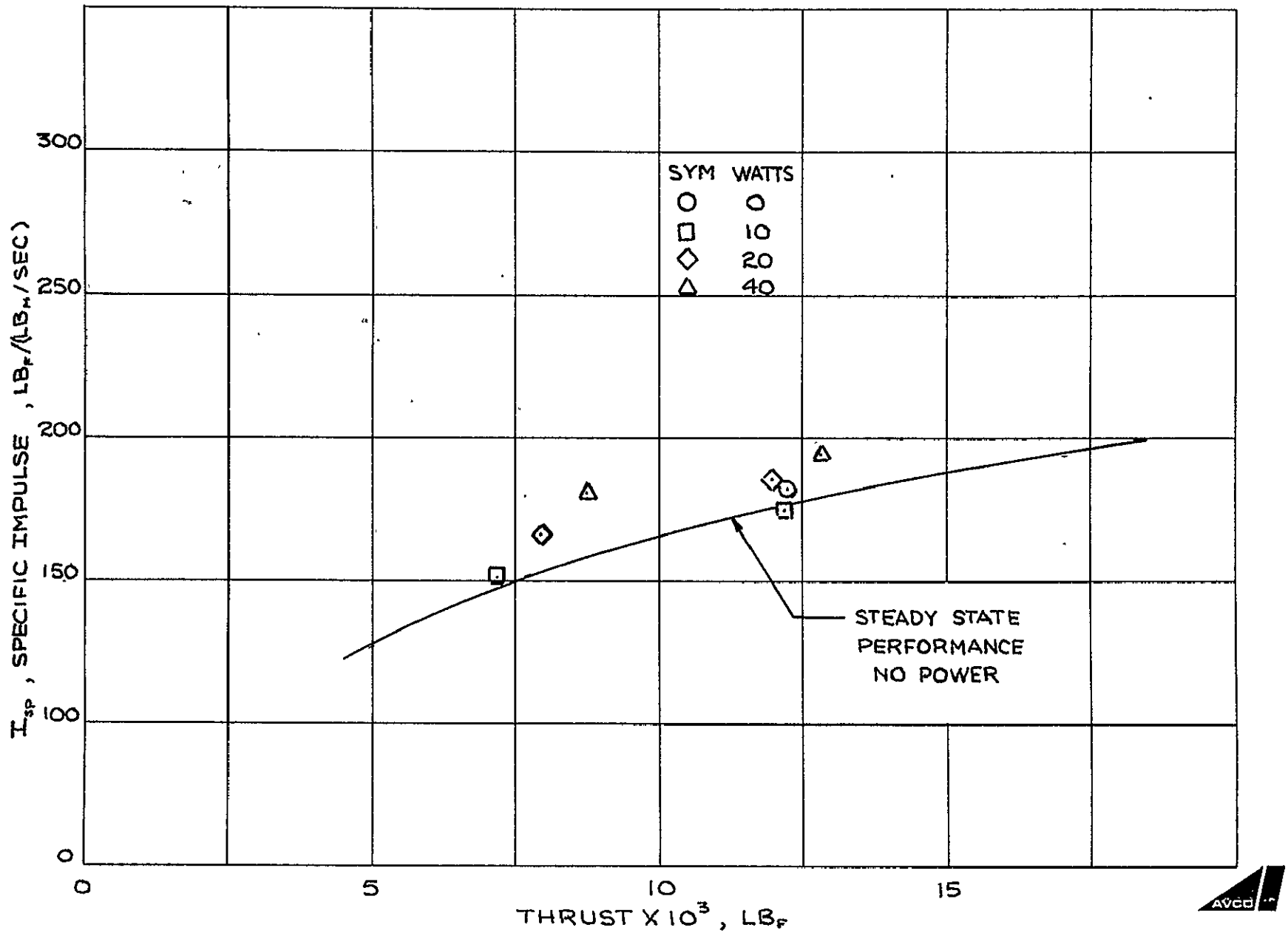

FIG. 61 EFFECT OF DUTY CYCLE ON MODIFIED PREPROTOTYPE THRUSTER PERFORMANCE

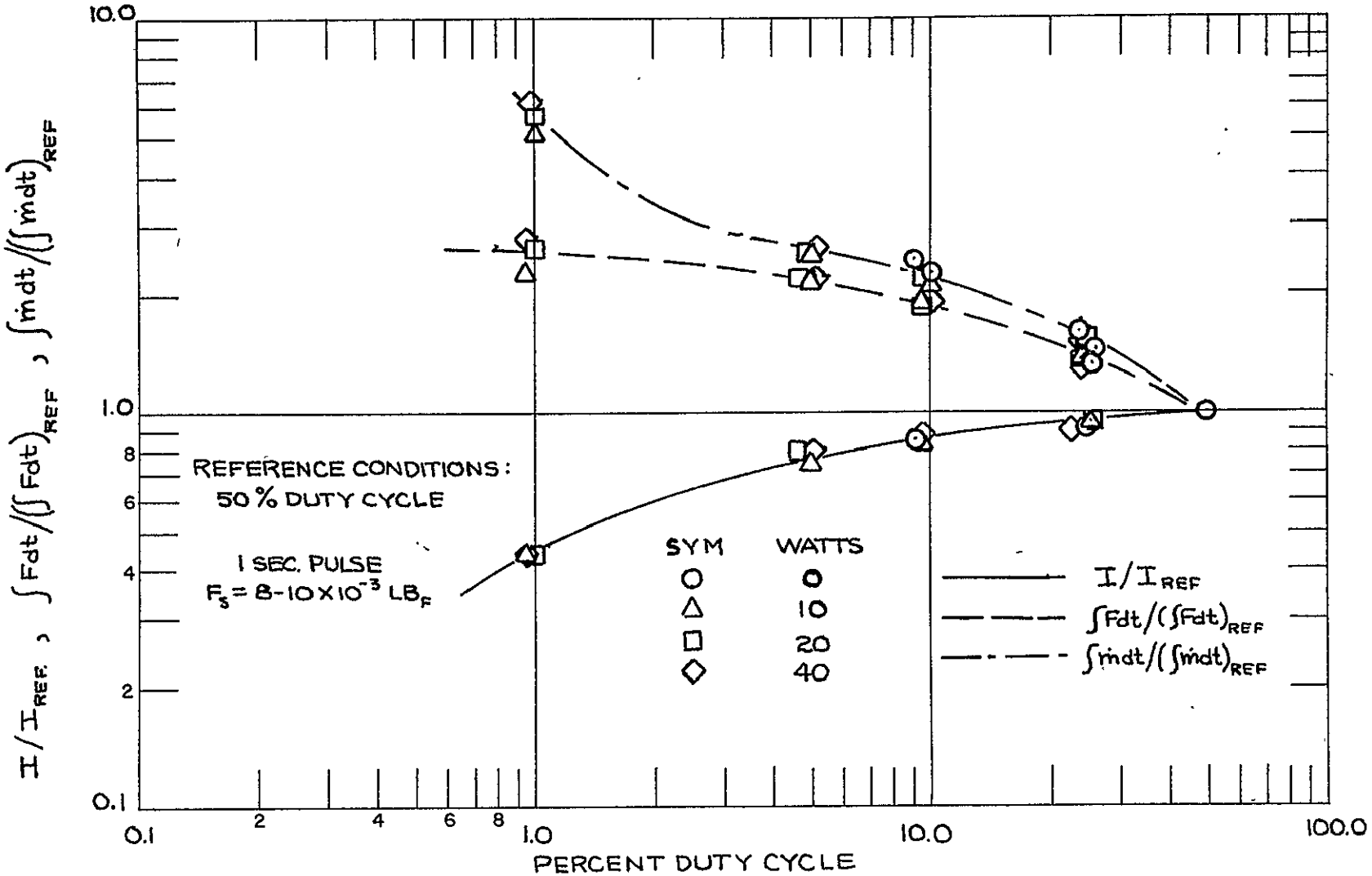

FIG 62 EFFECT OF DUTY CYCLE ON MODIFIED PREPROTOTYPE THRUSTER PERFORMANCE

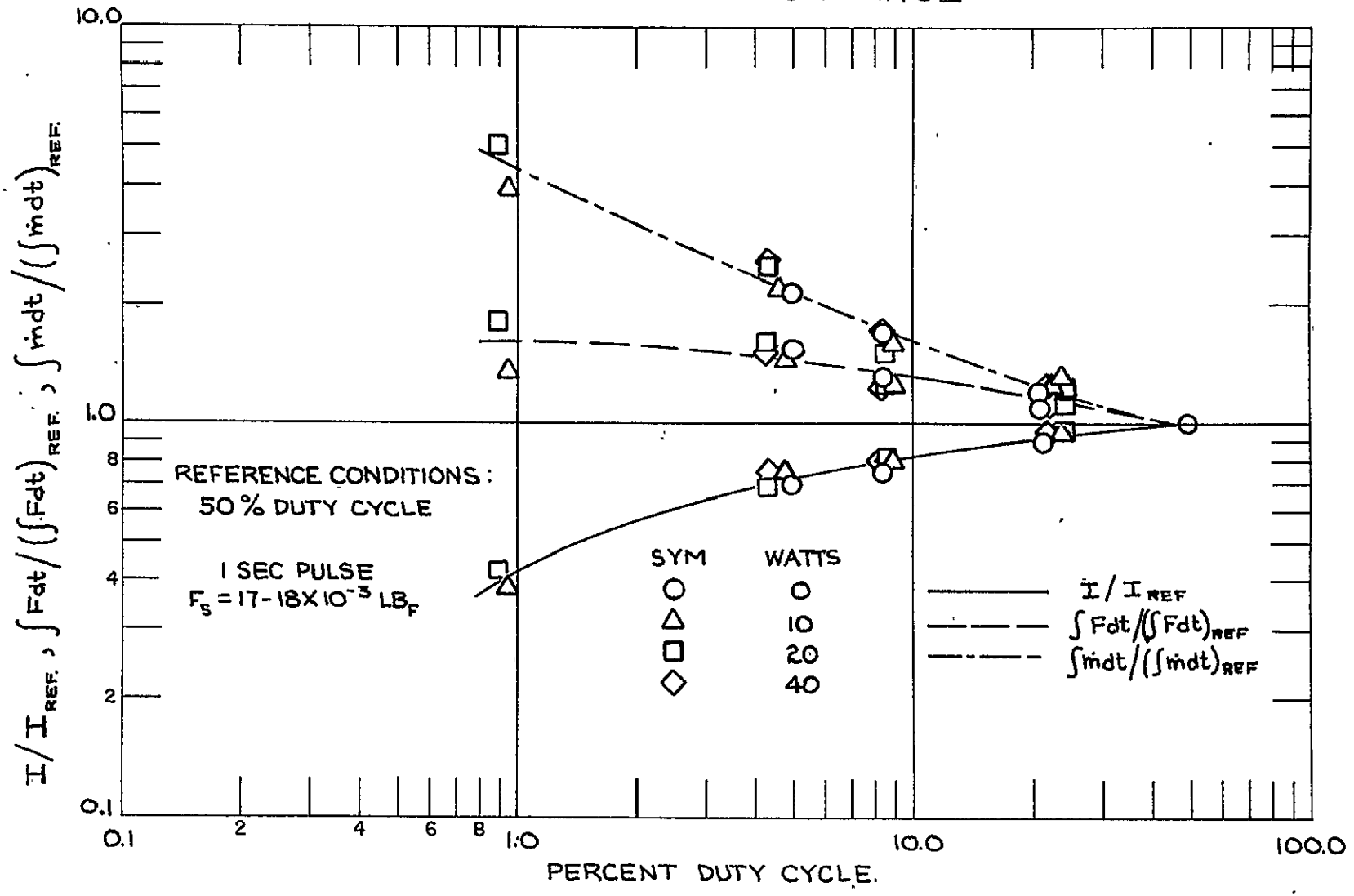

Table III
Summary of Short Pulse Data
Preprototype Thruster, Lava Insulator

Pulse Width sec.	% Duty Cycle	Specific Impulse sec	Impulse Bit $(lb_f - sec) \times 10^3$
∞	100	228	49×10^{-3}
0 10	10	200	21×10^{-3}
0.03	3	189	15×10^{-3}
∞	100	238	59×10^{-3}
0 10	1	180	41×10^{-3}

Although these data do not provide sufficient definition of performance with short pulses, the degradation in specific impulse is considerably less (I_{sp} =0 75 $I_{sp_{ss}}$) at a 1 percent duty cycle than that observed with the 1 sec. pulse.

It is believed that the reason for the discrepancy in the two sets of data can be explained by means of the following hypothesis as to the sequence of events occurring within the thruster after opening the propellant feed valve

1) At the time at which the propellant feed valve is opened, the propellant feed tube within the thruster has a temperature greater than the boiling point of the liquid propellant and the pressure within the thruster is low As propellant flows down the feed tube, it is partially vaporized and the propellant flow rate is relatively low (when compared to that obtained later in the operating period) since the pressure drop per unit mass flow is high for a two phase flow During this period, the temperature of the inlet tube is continuously decreasing until it drops to a value below the boiling point of the propellant In this part of the operating cycle, the specific impulse obtained is hypothesized to be close to that which would be achieved in steady state operation

2) During the second portion of the thrust period, propellant enters the thruster in the liquid state For given values of supply and thrust chamber pressure, the propellant feed rate achieved for liquid flow is considerably higher than with a two phase mixture. Hence, there is a rapid increase in propellant flow to values greater than that achieved in either the first portion of the pulse or during steady state operation The net effect of this high flow rate is to partially flood the thruster which results in thrust being delivered at specific impulses characteristic of partially reacted hydrazine These

hypotheses are supported by experimental pressure traces obtained for long pulses (see Figs 26, 27 and 28) which indicate that steady state behavior would be achieved only with pulses much longer than 1 sec duration.

3) Following shutting of the propellant feed valve at the end of the pulse, thrust and thrust chamber pressure decrease to a low value. However, thrust continues to be delivered as a fluid contained within the ullage volume between the valve seat and the thrust chamber vaporizes. During this period, the temperature of the propellant feed tube increases to attain values in excess of the propellant boiling point until the time at which the flow valve is opened at the start of the next pulse.

This hypothetical sequence of events would explain the difference between the observed behavior of the thruster when operated with short pulses (less than 0 10 sec.) and long pulses (1.0 sec.) However, it must remain strictly conjecture since the experimental data cannot be reduced to illustrate thrust as a function of time due to the lag in the mass flow measuring system signal and the inability of the thrust measuring system to accurately follow the variation of thrust with time

V Materials Compatibility

In the course of these investigations, several materials problem areas came to light, namely

a) The effects of hydrazine vapor and/or decomposition products on stainless steel at high temperatures

b) The effects of liquid hydrazine storage in stainless steel lines.

c) The anomalous behavior of stabilized zirconia when employed as a flow distributor in the hydrazine resistojet.

These problem areas are discussed below.

(1) During operation of the preprototype thruster in the pulsed mode, it was observed that it was impossible to remove the stainless steel feed line from the porous zirconia tube. The thruster was disassembled and the injector assembly was sectioned in the manner shown schematically in Fig 63, and photo micrographs were taken of the various cross-sections (Figs. 64-66). In the two photo micrographs, which include both the ceramic and the metal tube (Fig. 61), degradation of the tube by hydrazine is readily apparent with the amount of corrosion increasing with distance down the tube.

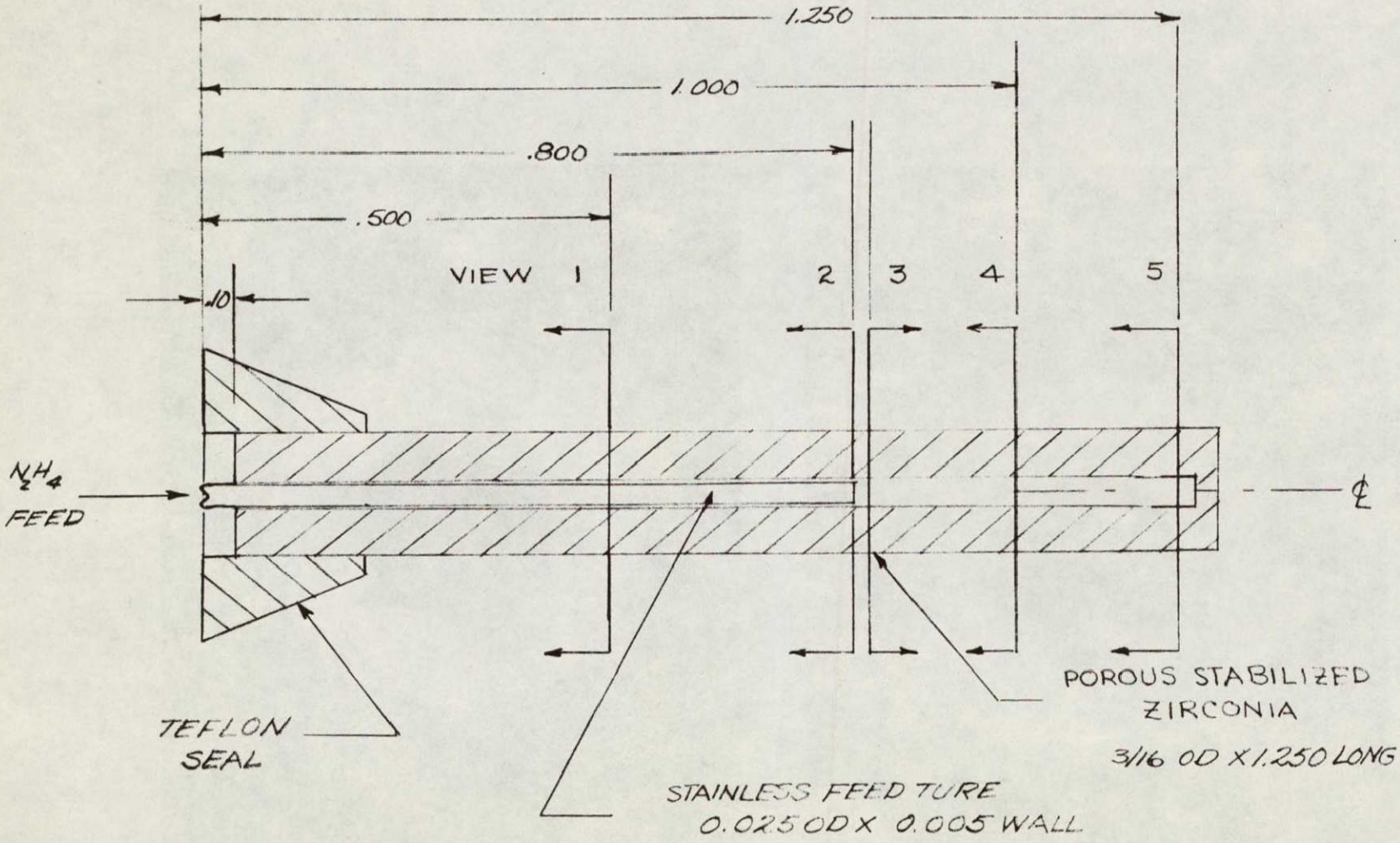

NOTE VIEWS 2 & 3 ARE SEPARATED BY THE WIDTH OF A SAW BLADE

FIG 63 SCHEMATIC OF PHOTOMICROGRAPH LOCATIONS

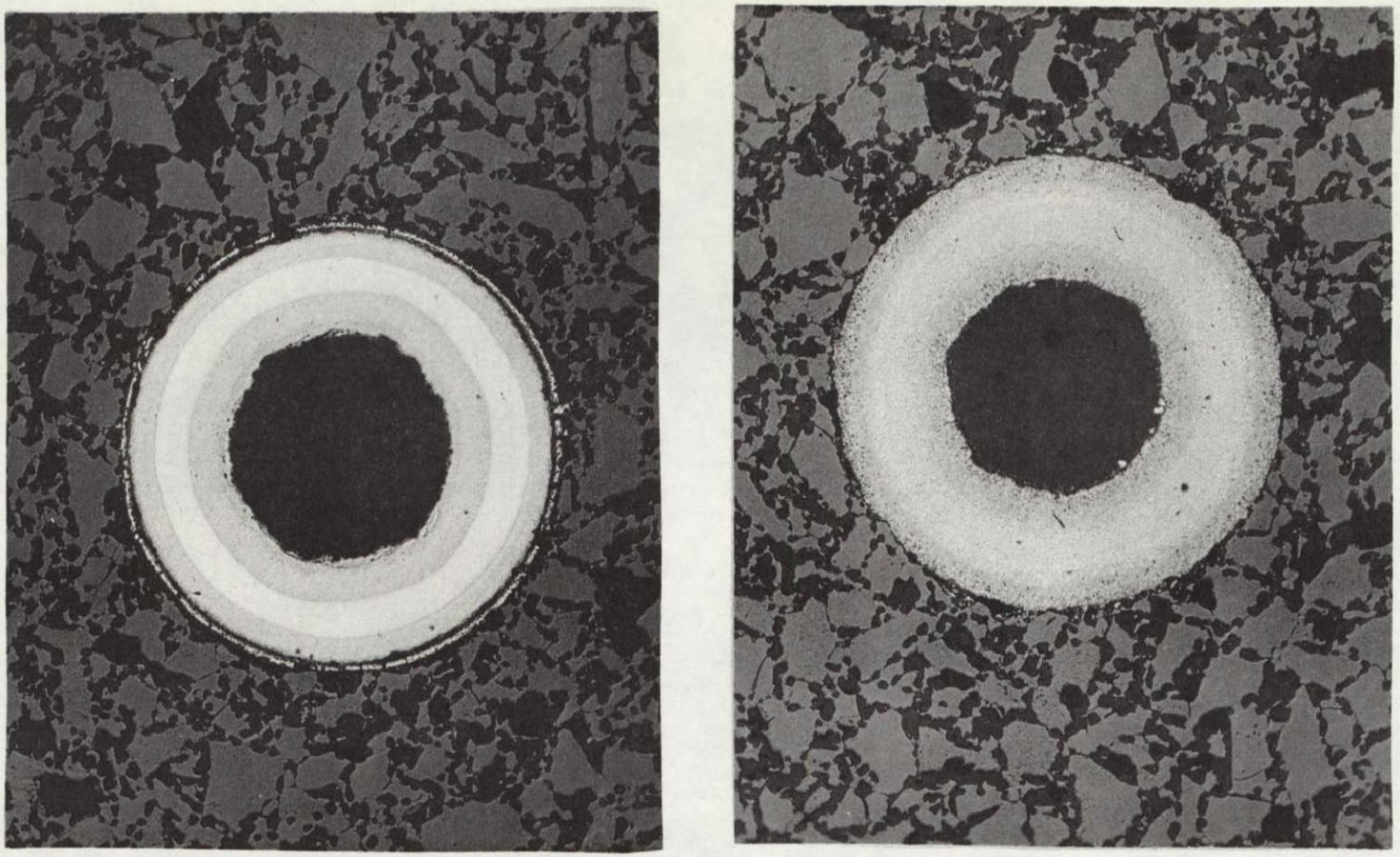

VIEW 1 VIEW 2

FIG. 64. PHOTOMICROGRAPHS OF SECTIONED INJECTOR ASSEMBLY (100X)

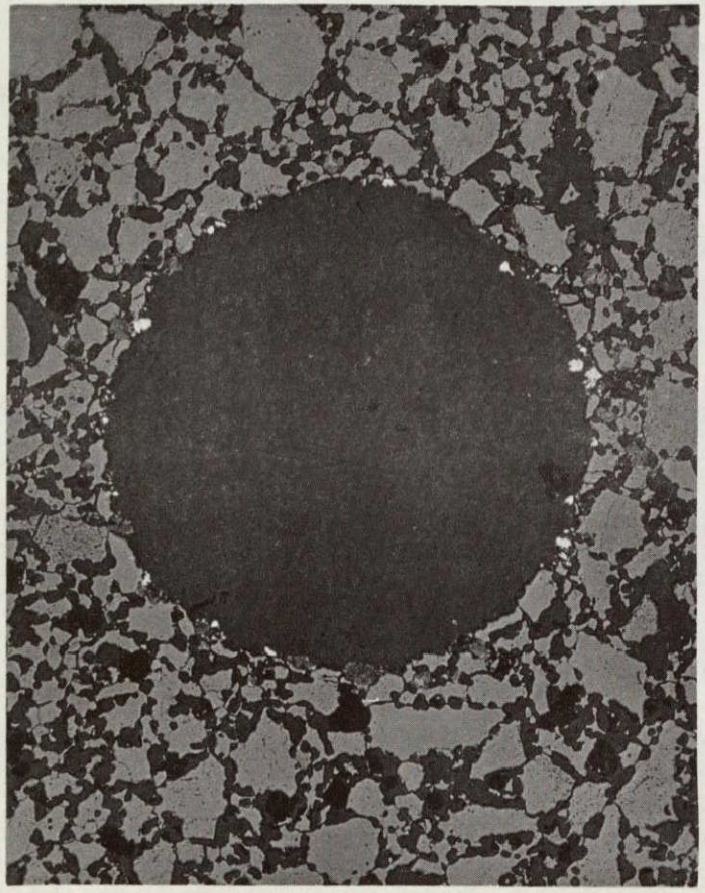

VIEW 3

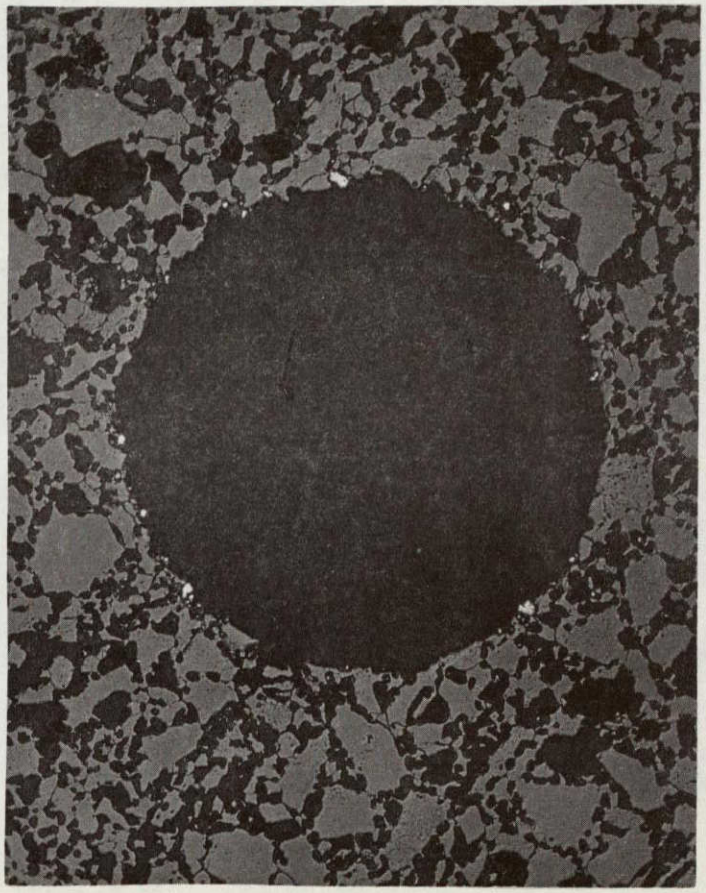

VIEW 4

FIG 65. PHOTOMICROGRAPHS OF SECTIONED INJECTOR ASSEMBLY (100X)

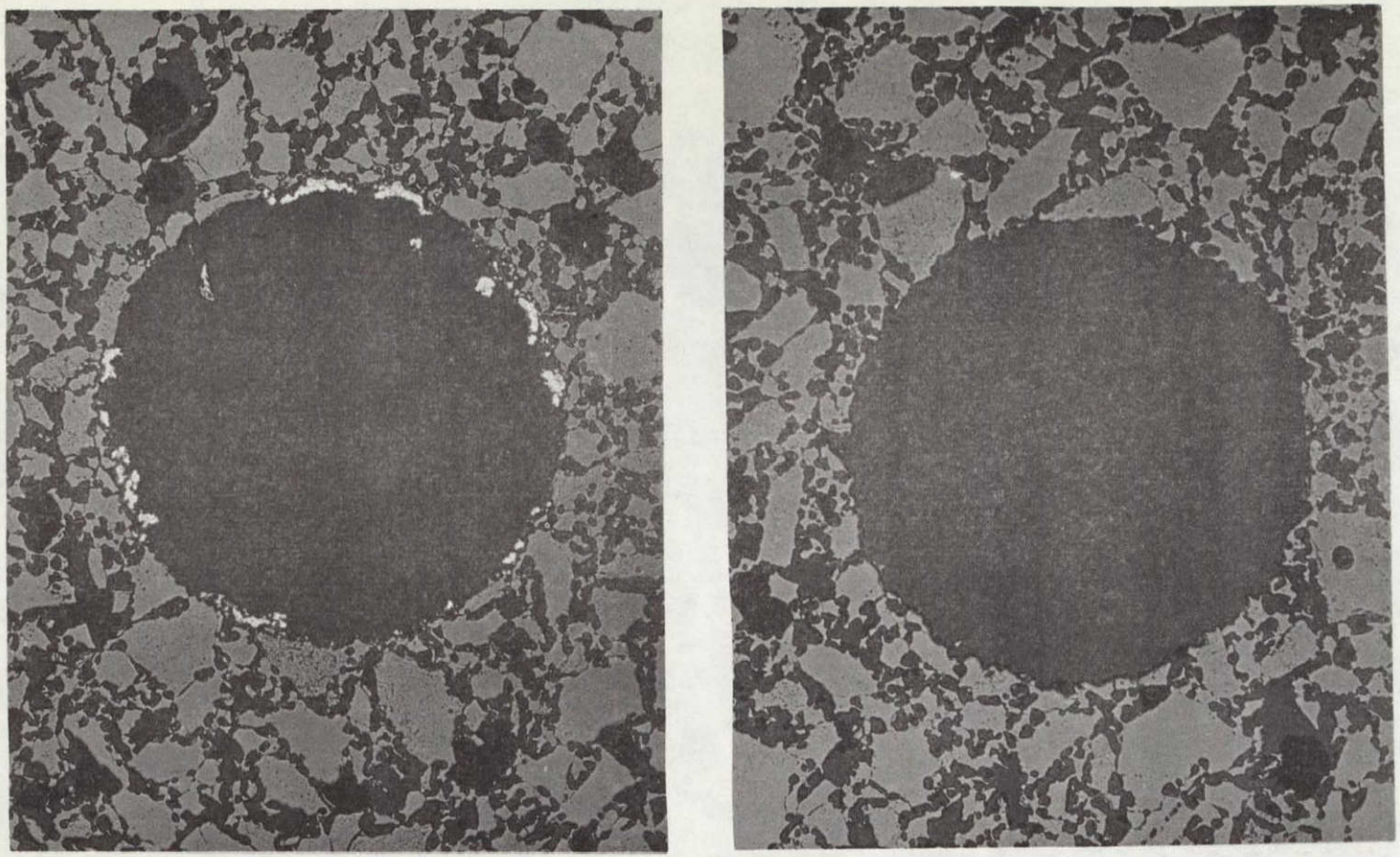

VIEW 5

VIRGIN ZIRCONIA

FIG 66. PHOTOMICROGRAPHS OF SECTIONED INJECTOR ASSEMBLY (100X)

At the downstream end of the tube, there is corrosion of some degree throughout the entire tube wall, this degradation was accompanied by a decrease in the inner diameter and an increase in the outer diameter of the tube This deformation has occurred to such an extent that the outer surface of the feed line has deformed in those regions where it is in contact with the sourrounding porous ceramic. Downstream of the end of the feed tube the porous zirconia appears to be physically similar to virgin material (see Fig. 66) with the exception of small pieces of metal in the passage down the axis of the ceramic It is not known whether these particles were a direct result of chemical attack on the stainless steel or were produced in the process of cross-sectioning the assembly Since the particular unit under discussion was used for a total run time in the vicinity of 10 hours, it is apparent that corrosion of stainless steel by hydrazine can be a serious problem

The mounted specimens shown in these photo micrographs and a sample of the stainless steel feed line have been forwarded to the NASA Goddard Space Flight Center for evaluation On the basis of metallographic examination and microhardness test results,[17] it was concluded that both the inside and outside surfaces of the stainless steel feed tube were nitrided during operation of the thruster On the basis of these investigations, it was recommended that Inconel or tantalum should be employed in fabrication of the feed tube or that the feed tube be plated to minimize nitriding with gold being the most likely candidate [17]

(2) Operation of the liquid hydrazine feed system in these investigations disclosed that there was a distinct possibility that liquid hydrazine is slowly decomposed on steel surfaces Evidence as to this phenomenon is as follows It was observed throughout the program that the response of the flow measuring was far removed from that which would be expected with a pure liquid system as demonstrated by lags in transient response of the differential pressure transducer across the flow metering orifice The slow transient response of the system can only be explained by compliance within the feed lines in the form of gas pockets. Direct experimental evidence of gas generation within the system was obtained from the necessity of periodic venting of the gas lines in the system However, after venting the lines it was observed that the compliance gradually increased with time.

(3) Anomalous behavior of the stabilized zirconia flow distributor was observed throughout the program. During steady state operation of both laboratory and preprototype thrusters, the use of stabilized zirconia was found to present little or no difficulty except when power addition at high levels (60-80 watts) was attempted. At the high power levels, the zirconia tube was found to be cracked upon disassembly of the thruster

This behavior was attributed to increases in radial temperature gradient in the thruster and hence, larger thermal stresses in the powered mode of operation. During pulsed mode of operation, the zirconia was found to crack with greater frequency probably due to high thermal stresses generated by the sudden surges in propellant flow rate Although this is the most likely reason for the observed behavior, the possibility of leaching of the calcia stabilizing agent by hydrazine should not be eliminated as the reason for the cracking. Experimental evaluation of a thruster with a cracked zirconia tube indicated that the cracks did not seriously effect thruster performance in that it produced only a 4 percent decrease in characteristic velocity However, the distinct possibility of ceramic particles lodging within the thruster nozzle throat with the accompanying decrease in performance due to nozzle inefficiencies leads to the conclusions that a porous metal structured be considered in place of the ceramic The most likely candidate materials for this flow distributor are Inconel and tantalum Although the presence of metal surfaces with the thruster will produce some dissociation of ammonia and hence, will result in lower specific impulses, it is felt that the dissociation can be minimized by decreasing the residence time within the structure.

References

1) Dow Chemical Company, "JANAF Thermochemical Data "

2) Michel, K W. and H G G. Wagner, "The Pyrolysis and Oxidation of Hydrazine Behind Shock Waves," Tenth Symposium (International) on Combustion, p.p 353, The Combustion Inst , 1965.

3) Eberstein, I J. and I Glassman, "The Gas Phase Decomposition of Hydrazine and Its Methyl Derivatives," ibid, p p 365-374

4) Gilbert, M , "The Hydrazine Flame," Combustion and Flame, p p. 137-147, (1958)

5) McHale, et al, "Determination of the Decomposition Kinetics of Hydrazine Using a Single Pulse Shock Tube," Tenth Symposium (International) on Combustion, p p. 341, The Combustion Inst., 1965

6) Gray, P , J.C. Lee and M Spencer, "Combustion, Flame and Explosion of Hydrazine and Ammonia, I-The Spontaneous Ignition of Pure Gaseous Hydrazine," Combustion and Flame 1, 315 (1963)

7) Bond, G. C., Catalysis by Metals, Academic Press, N Y 1962

8) Schreib, R.R., Pugmire, T. K., and Chapin, S G., "The Hybrid (Hydrazine) Resistojet," AIAA Paper 69-496

9) Adams, G.K, Stocks, G W., "The Combustion of Hydrazine," 4th Symposium on Combustion, p.p. 239, The Williams and Wilkins Co , 1953

10) Rocket Research Corp., "Monopropellant Hydrazine Design Data "

11) Gerstein, M., "Correlation and Prediction of Flame Properties with Special Reference to Liquid Hydrazine," ARS Journal, July 1959, p p 514-516.

12) Cass, L A., "Improved Radiant Heat Source, "Avco Space Systems Division, AVSSD-0133-68-RR, Technical Report AFFDL-TR-68-93, 15 June 1968.

13) Carslaw, H. S., and Jaeger, J. C., "Conduction of Heat in S lids," 2nd Edition, p p 130

References
(concl'd)

14) Smith, R.V., "Some Idealized Solutions for Choking, Two-Phase Flow of Hydrogen, Nitrogen, and Oxygen," Advanced in Cryogenic Engineering, Vol. 1, p p 563-573, Plenum Press, N.Y., N.Y., 1963

15) Rogers, J.D., "Oscillations in Flowing and Heated Subcritical Hydrogen," Advanced in Cryogenic Engineering, Vol. 10, p.p 223-231, Plenum Press, N Y , N.Y., 1965

16) Hamilton Standard, "Hydrazine Engine Development Five Pound Thrust Performance, "Report No. SLS 6514

17) Grimsley, John and Jellison, Jane, "Metallographic Investigations of a Hydrazine Engine Thruster Tube," Memorandum to R. A Callens, Auxiliary Propulsion Branch, NASA/GSFC, 19 August 1970